Czech Technical University in Prague

Faculty of Electrical Engineering
Department of Electrical Drives and Traction

Design and Implementation of Hybrid Magnetic Bearing Control Part

Doctoral thesis

Ing. Tomáš Kupka

Prague, October 2017

Ph.D. Program: P2612 – Electrical Engineering and Information Technology
Branch of study: 2642V004 – Electrical Machinery and Drives

Supervisor: prof. Ing. Jiří Pavelka, DrSc.

Statement of originality

I hereby declare that this document is my own work. To the best of my knowledge and belief, the thesis contains no material previously published except where due references are made.

CTU has my permission to publish an electronic copy of my doctoral thesis.

Place and date

Signed by Ing. Tomáš Kupka

Acknowledgements

My greatest thanks go to my supervisor prof. Jiří Pavelka for his advises, support and help all the time of my doctoral study and for his leading of my doctoral thesis.

The real electrical device described in this thesis couldn't be designed and constructed without support of managers and colleagues in my employing company Finepower GmbH. I'm very grateful for their help.

I would also like to thank Mr. Zdeněk Šabat for his effort in the CTU laboratory.

List of publications of the candidate

Publications related to the doctoral thesis:

Conferences:

T. KUPKA and J. PAVELKA: *Realization of Hybrid Magnetic Bearing*; In: Proceedings of the 15th International Power Electronics and Motion Control Conference and Exposition, EPE-PEMC 2012 ECCE Europe; University of Novi Sad, Faculty of Technical Sciences; (100%)

Reviewed papers:

T. KUPKA: "*Vibrace točivých strojů s magnetickými ložisky*"; In: Elektro – Magazine for Electrical Engineering, 05/2017; (100%)

Other publications:

Conferences:

T. KUPKA and M. PATT: *Hybrid Photovoltaic Inverter for Smart Grids*; In: The 4th International Symposium on Sustainable Development, ISSD 2013; International Burch University, Sarajevo, Bosnia and Herzegovina; (100%)

Patents:

K. JÄGER, T. KUPKA and G. HEILAND: "*Verfahren zum Betrieb eines Resonanzkreises*"; German National Patent DE102015004742; (15%)

M. TAUER, T. KUPKA and G. HEILAND: "*Verfahren zum Betrieb zumindest zwei elektrisch miteinander verbundener Umrichter*"; German National Patent DE102015006210; (45%)

M. TAUER and T. KUPKA: "*Verfahren zum Betrieb eines Buck-Boost-Konverters*"; German National Patent DE102016000207; (50%)

Abstract (EN)

Experiments with magnetic levitation for stabilization of rotating parts of electrical machines started in the middle of 20th century, but first practical application started with powerful digital microprocessors. Recently, price and quality of micro-controllers and other supporting circuits allow to design a number of magnetic bearings in all power classes.

However, more complicated construction (and higher price) classifies magnetic bearings to be used in special applications of high speed and power drives or aggressive ambient or vacuum. There are just a few companies producing magnetic bearings on the worldwide market (e.g. Synchrony Magnetic Bearings, Waukesha Magnetic Bearings, Calnetix Technologies or Levitronix).

Industrial using of active magnetic bearings is defined by international standard ISO 14839. The standard describes technical terms, measurement and diagnostic of machine equipped by active magnetic bearings and evaluation criteria.

Worldwide there are a few patents and technical papers describing the theory of hybrid magnetic bearings, but a real product still does not take a significant place on the market. Also the industrial standard doesn't describe any flux-combined type of the magnetic bearing.

The aim of this doctoral thesis is to analyse capability of the permanent-magnet-based active magnetic bearing with three-phase stator winding. Diagnostic by the international standard for the active magnetic bearing was used as a method of the bearing evaluation features. For this purpose a new electrical part of the hybrid magnetic bearing was designed and constructed. It was driven together with a three-phase magnetic part and tests and diagnostics of the complete system according to the actual international standard were made. It was found that the hybrid magnetic bearings are able to fulfil all requirements of the standard ISO 14839, which proves that they could be used in the same application as active bearings, since the standard defines only the active ones. The practical outcome of this paper is a description of a perspective way how to develop the hybrid magnetic bearing for real industrial applications.

Abstrakt (CZ)

S využitím magnetické levitace ke stabilizaci rotoru strojů se začalo experimentovat již v první polovině dvacátého století. První praktické aplikace se ale začaly uplatňovat až s nástupem výkonných digitálních procesorů. Důvodem byla složitost metod řízení magnetických ložisek, kterou dokázal obsloužit až vysoký výpočetní výkon signálových procesorů. Jejich klesající cena pak počátkem jednadvacátého století umožnila rozvoj magnetických ložisek v mnohých aplikacích všech výkonových tříd.

Komplikovanost konstrukce a z ní vycházející vyšší cena přesto odkázala magnetická ložiska pouze do specifických aplikací, ať už vysokootáčkových a výkonových pohonů nebo zařízení pro kontaminované, citlivé anebo agresivní prostředí či vakuum. Na trhu dnes existuje omezený počet výrobců s celosvětovou působností. Jedná se například o společnosti Synchrony Magnetic Bearings, Waukesha Magnetic Bearings, Calnetix Technologies nebo Levitronix.

Použití aktivních magnetických ložisek v průmyslové praxi upravuje norma ISO 14839 „Vibrace – Vibrace točivých strojů vybavených aktivními magnetickými ložisky“. Norma definuje technické termíny, měření a diagnostiku strojů s aktivními magnetickými ložisky a jejich dělení do tříd použitelnosti.

Úkolem této disertační práce je analyzovat vlastnosti hybridního magnetického ložiska s permanentním pomocným polem a třífázovým vinutím statoru. Jako ověřovací metoda byla použita diagnostika podle normy ISO 14839 pro aktivní ložiska. Pro tento účel byla vyvinuta nová elektronická a řídicí část k již existující magnetické části ložiska. Celý systém byl poté zprovozněn a odladěn, aby mohla být provedena samotná diagnostika. Výsledná měření ověřila schopnost hybridního magnetického ložiska s třífázovým vinutím statoru plnit požadavky mezinárodní normy, příslušné pouze pro aktivní ložiska. Mohou proto být použity ve stejných aplikacích. Praktický výsledek této práce je pak popis optimální vývojové procedury hybridního magnetického ložiska pro reálné průmyslové aplikace.

Notations and abbreviations

Notation	Details
B_r, B_{PM}, $B_{\delta 0}$	[T]; Flux Density
BH_{max}	[J/m^3]; Magnetic Energy Product
d	[m]; Diameter
δ	[m]; Length Difference
f	[Hz]; Frequency
F_m	[N]; Mechanical Force
F_W, F_{PM}	[A-t]; Magneto Motive Force
Φ	[Wb]; Magnetic Flux
$G_O(s)$	Open-loop Transfer Function
$G_C(s)$	Closed-loop Transfer Function
$G_S(s)$	Sensitivity Transfer Function
${}_BH_C$	[A/m]; Coercivity
I, i	[A]; Electric Current
l	[m]; Length
m	[kg]; Mass
N	[-]; Number of Windings
R_i, R_{mi}, R_g	[H^{-1}]; Magnetic Reluctance
R_{DS}, R_T, R_N, R_{win}	[Ω]; Resistance
W_m	[J]; Magnetic Energy
P	[W]; Power
Q	[m^2]; Cross-section of wires in one slot
q	[m^2]; Cross-section of single wire
σ	[A/m^2]; Current Density
Ψ	[Wb]; Magnetic Flux Leakage
S	[m^2]; Surface
μ	[H/m]; Permeability
μ_0	$4\pi 10^{-7}$ H/m; Permeability of Vacuum
T	[K]; Temperature
U, u	[V]; Voltage

Abbreviation	Details
ADC	Analog to Digital Converter
AMB	Active Magnetic Bearing
CTU	Czech Technical University
ČSN	České Technické Normy
DSP	Digital Signal Processor
EEPROM	Electrically Erasable Programmable Read Only Memory
FEE	Faculty of Electrical Engineering
GND	Ground
GUI	Graphical User Interphase
HMB	Hybrid Magnetic Bearing
IGBT	Insulated Gate Bipolar Transistor
INV	Inverter
ISO	International Organization for Standardization
MCU	Microcontroller Unite
MMF	Magneto Motive Force

MOSFET	Metal-Oxide-Semiconductor Field-Effect Transistor
PC	Personal Computer
PCB	Printed Circuit Board
PM	Permanent Magnet
PMB	Passive Magnetic Bearing
PMSM	Permanent Magnet Synchronous Motor
PTC	Positive Thermistor
PWM	Pulse Width Modulation
RAM	Random Access Memory
SC2	Subcommittee
SMD	Surface-Mount Device
TC 108	Technical Committee
UART	Universal Asynchronous Receiver-Transmitter
WG7	Working Group

Table of contents

Introduction

Experiments with magnetic levitation for stabilization of rotating parts of electrical machines started in the middle of the 20th century, but first practical application started with powerful digital microprocessors. Actually, more complicated construction (and higher price) classifies magnetic bearings to be used in special applications of high speed and power drives or in aggressive ambient or vacuum.

Actual industrial market of magnetic bearings contains almost only active magnetic bearings. Industrial using of active magnetic bearings is defined by international standard ISO 14839. The standard describes technical terms, measurement and diagnostic of machine equipped by active magnetic bearings and evaluation criteria. Worldwide there are a few patents and technical papers describing the theory of the permanent-magnet-based active magnetic bearings, but a real product still did not take a significant place on the market. Also the industrial standard doesn't describe any flux-combined type of magnetic bearing.

The first study of magnetic bearings in Czech Republic (resp. Czechoslovakia) was made at the Czechoslovak Academy of Science in 1989 and the Department of Electrical Drives and Traction CTU has continued the research in 1992. The research project began with various types of active magnetic bearings. The first mechanical part of the permanent-magnet-based active magnetic bearing at the CTU was intuitively designed in 2001 and its construction began in the following year. The type with three-phase stator winding was chosen for the first prototype, but the functionality was never proven by technical research. However, this magnetic bearing type provides promising opportunities in the field of power consumption and space optimization.

This doctoral thesis continues in the research of the field of magnetic bearings at the CTU, it proves the functionality of the permanent-magnet-based active magnetic bearing with three-phase stator winding and it explores capability of bearing features. The system diagnostic of international standard for active bearings is used as proving method. If there were any doubts about functionality of the construction, control system or capability of our type of magnetic bearing, my doctor thesis answers all these important question.

1 State of the Art

Many applications of rotating systems use features of magnetic bearings. Especially the ability of contact-less working allows magnetic bearings to be used in extreme ambient or high speed systems. [1]

Technology of magnetic bearings is known several decades, but their practical use was limited by control the system unable to provide complex calculation fast enough. Recently, price and quality of micro-controllers and other supporting circuits allow to develop a number of magnetically stabilized machines. Actually there are just a few companies producing magnetic bearings on worldwide market (e.g. Synchrony Magnetic Bearings [2], Waukesha Magnetic Bearings [3], Calnetix Technologies [4], Levitronix [5] or Mecos [6]).

The state of magnetic bearings development allowed to form ISO/TC 108/SC 5/WG 7 (ISO – International Organization for Standardization, TC 108 - Technical Committee "Mechanical vibration and shock", SC2 - Subcommittee "Measurement and evaluation of mechanical vibration and shock as applied to machines, vehicles and structures", WG7 - working group "Vibration of rotating machinery equipped with active magnetic bearings"). This WG7 elaborated and published the ISO standard series ISO 14839 with four parts. First part was published in the year 2002. All four parts of this series are translated in the Czech language as ČSN ISO 14839. [7]

International Symposiums on Magnetic Bearings are organized from the year 1988 with period of two year. Next symposium ISMB 16 will be held in Beijing in the year 2018. The Symposium proceedings are published from each Symposium.

Last book about magnetic bearings [8] was edited in the year 2013. This publication contains last theoretical and practical knowledge about magnetic bearings.

1.1 Magnetic bearing classification

1.1.1 Classification by force producing principal

The standard ISO 14839 – 1 – The vocabulary distinguishes the following types of magnetic bearings from the point of view of the principle that they create the bearing force on the rotor. [7]

1.1.1.1 Passive magnetic bearing

Passive magnetic bearing (PMB) uses uncontrolled force of permanent magnets for stabilization in axial or radial rotor axis. One of the axes have to be hold by the fixing system based on different technology (active magnetic bearing, hydraulic or mechanical bearing).

Fig. 1: Example of passive magnetic bearing

Obvious advantage is absence of any supplying and control parts and simplicity of construction. On the other hand, passive magnetic bearings have low stiffness and damping. However, there are applications which could use passive bearings apart from those disadvantages (e.g. accumulators of kinetic energy, vertical compressor or toys – Fig. 1). [9]

1.1.1.2 Active magnetic bearing

Active magnetic bearing (AMB) consist of electromagnets (at least two opposite located magnets per axis) on stator and ferromagnetic or permanent magnet on the rotor. Attractive (or detachment) forces between the stator and rotor are used for position displacement. Real-time controlling of the magnetic flux by current flowing in the electromagnets provides the stabilization. In contrast to the passive bearing, both axes could be controlled by one device. Permanent supplying is a disadvantage of the active bearings. [9]

A principle of active magnetic bearing is clear from Fig. 2 where displacement sensor is 6, electromagnet is 3, power amplifier is 2, power supply is 4 and controller is 6.

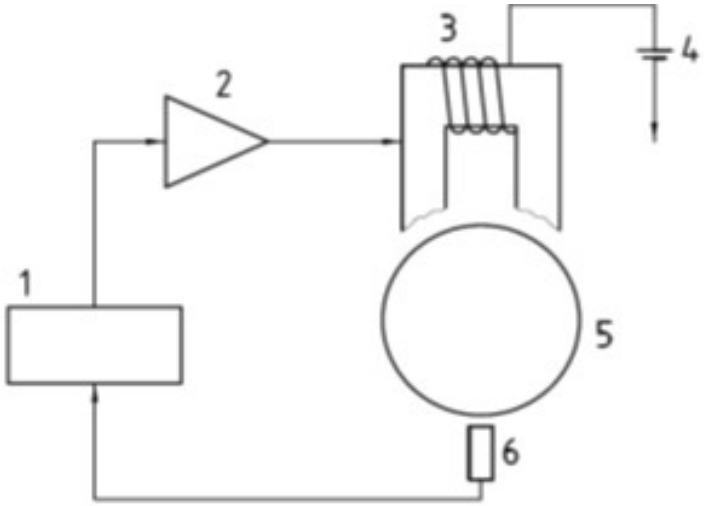

Fig. 2: The principle of active magnetic bearing [7]

1.1.1.3 Special and combined types

Hybrid magnetic bearing (HMB) consists of any combination of active magnetic bearing and passive magnetic bearing.

A special HMB type is **Permanent-Magnet-based AMB**, representing the active magnetic bearing in which the nominal (nonzero) or bias air gap fluxes are established by one or more permanent magnets. It uses advantages of both types. The basic magnetic flux is excited by the permanent magnet and currents in the stator winding are used just for dynamic stabilization. Advantages are good stiffness and damping as in the active bearing, but lower power consumption. More complicated construction and supplying necessity could be a disadvantage.

Worldwide there are a few patents and research projects describing the theory of hybrid magnetic bearings, but a real product still does not take a significant place on the market. Also the industrial standard doesn't describe any combined magnetic bearing type. The reason could be that the actual state of development of the hybrid magnetic bearing is not focused to practical application. This doctoral thesis tries to fill this gap as its targets define a in chapter 2.

This thesis works with the radial permanent-magnet-based AMB. It is especially focused to analysing problems of electrical and control part, since the magnetic one is already present in the CTU laboratories. A detailed description of our type of hybrid magnetic bearing is in the chapter 3.

1.1.2 Classification by force direction

The standard ISO 14839 – 1 – The vocabulary distinguishes also the following types of the active magnetic bearings from the point of view the bearing force direction on the rotor. [7]

Radial AMB is an active magnetic bearing which levitates a rotor against gravity and/or supports it against disturbance forces in the radial direction such as unbalance forces or fluid forces.

Axial or Thrust AMB is an active magnetic bearing which supports a rotor against disturbance forces in the axial direction, such as fluid forces, and/or levitates a vertical rotor against gravity, etc.

1.1.3 Classification by poles polarity

The standard ISO 14839 – 1 – The vocabulary distinguishes also the following types of active magnetic bearings from the point of view the bearing poles magnetic polarity. [7]

Heteropolar type of AMB means a radial AMB in which the cross-section has magnetic poles of different polarity, and the magnetic poles may have different polarity arrangements ((N, S, N, S,...) or (N, S, S, N,...)). An example in Fig. 3, where 1 is radial core, 2 radial sensor, 3 radial sensor target, 4 radial rotor core, 5 axial center of radial AMB, 6 radial stator core and 7 is shaft.

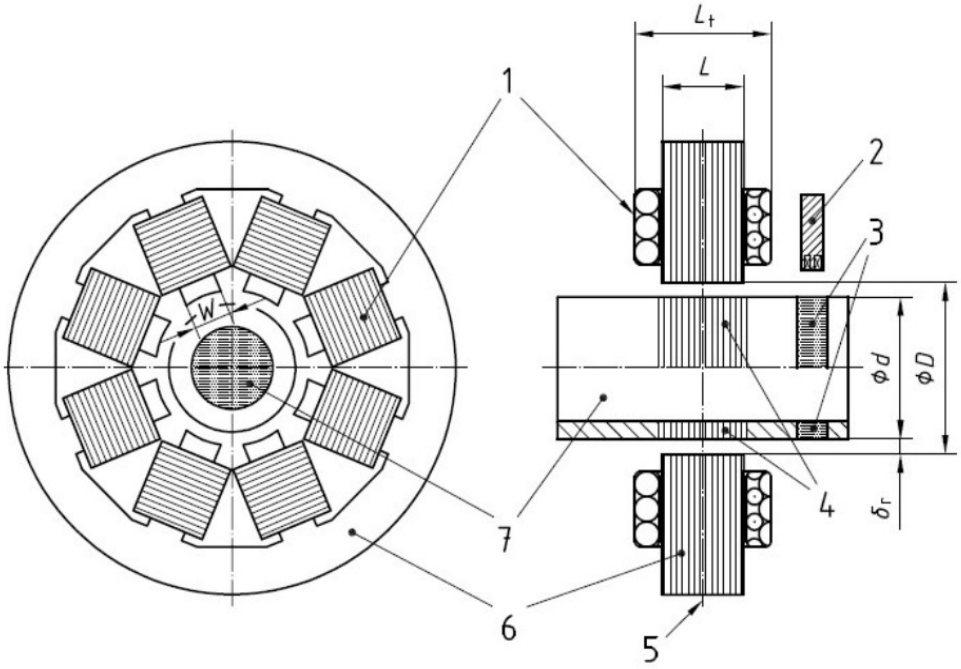

Fig. 3: Heteropolar type radial AMB [7]

Homopolar type of AMB means radial AMB which has more than one cross-section having poles of the same polarity, and all poles in each cross section have the same polarity. An example is in Fig. 4, where X_1, Y_1 are control axis.

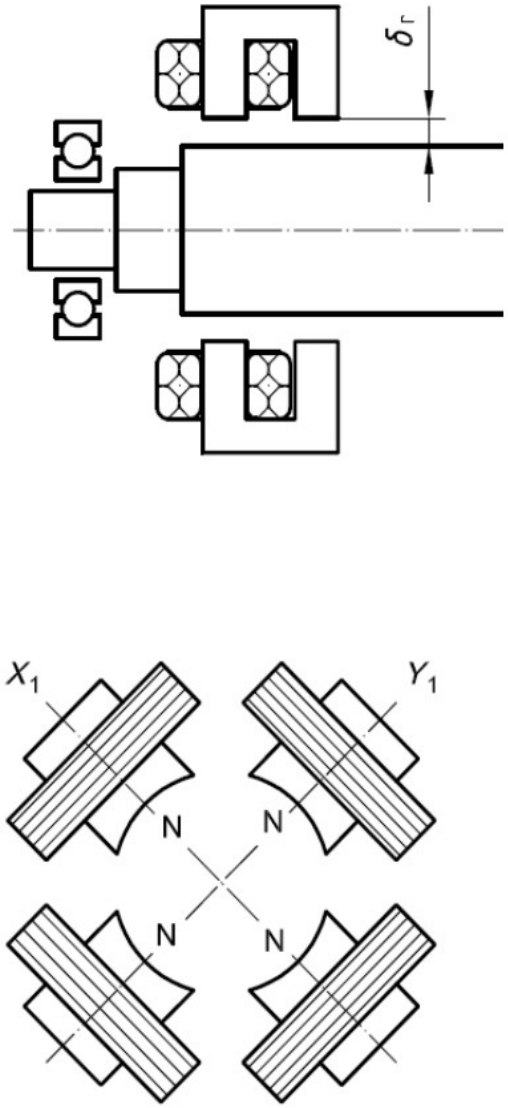

Fig. 4: Homopolar type radial AMB [7]

1.2 Electric machines with magnetic bearings

Figure 5 shows the typical structure of an electric machine that is equipped with magnetic bearings. The main electric motor is located between the two radial magnetic bearings. Each radial magnetic bearing generates radial forces in two perpendicular radial axes x_1, y_1, resp. x_2, y_2. These radial forces are controlled by negative feedback control systems so that the radial shaft position is regulated to the center of the stator core. Similarly shaft position in the axial axis z is controlled by the trust magnetic bearing.

All types of active magnetic bearings mentioned in the previous part have a magnetic circuit and can be used in different types of machines with rotating part. Using of active magnetic bearings in rotary electric machines allows to combine a magnetic circuit of an electric machine and magnetic circuit of a magnetic bearing into a common magnetic circuit. More information about different types of these electric machines is given in [10]. Small motors can be designed with a slide permanent magnet on the rotor and with two windings (turning and stabilization) on the stator. [11] An example of this machine for a blood pump is in Fig. 6. The passive axial force of the slide permanent magnet in the air gap of the stator magnetic circuit is used for the stabilization of the rotor position in the axial axes. Two pole stabilization stator winding is used for active radial stabilization of the slide permanent magnet rotor in the air gap and four pole turning stator winding

is used for production of an electromagnetic torque in the air gap.

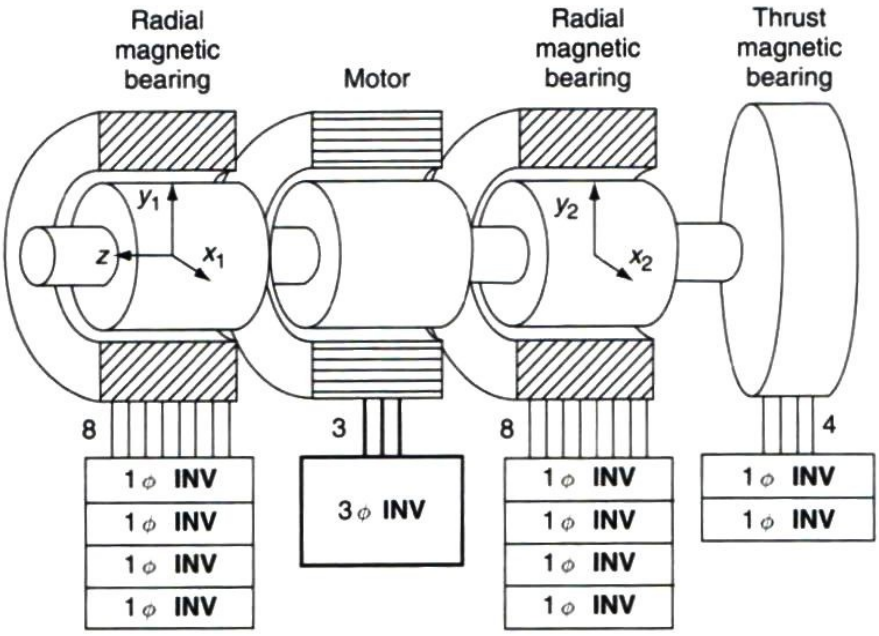

Fig. 5: Typical structure of motor drive with separated magnetic bearings [8]

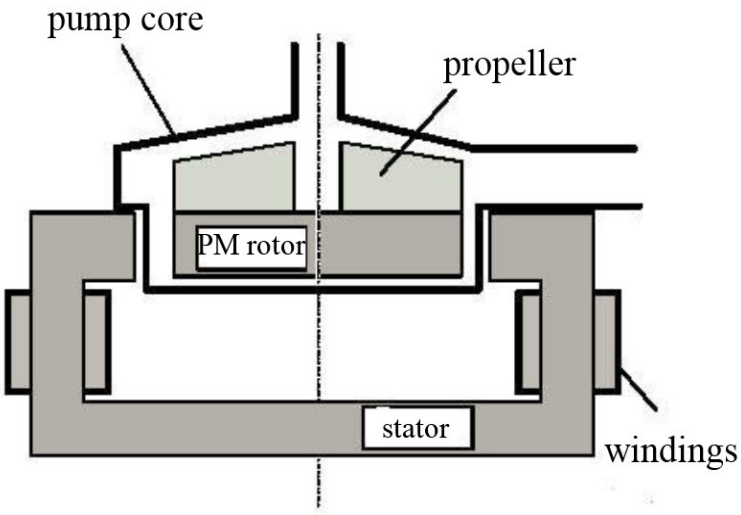

Fig. 6: Small motor with disc permanent magnet on the rotor and with two - turning and stabilization – windings on the stator

An example of a hybrid bearing-less motor is in Fig. 7. The flux path of magnetizing flux is the same as that of a homopolar magnetic bearing. Each stator core has one separated 2 – pole three phase suspension winding. These two windings produce four radial forces in four air gaps so that four radial rotor positions can be magnetically separately controlled. Both cores have also common 4 – pole three phase winding that produces the rotated magnetic flux. The rotor has four salient poles and it is without winding. The electromagnetic torque is generated by the interaction of the rotating magnetic field of 4-pole stator winding and the salient poles of the rotor. Several other variations and modifications are possible.

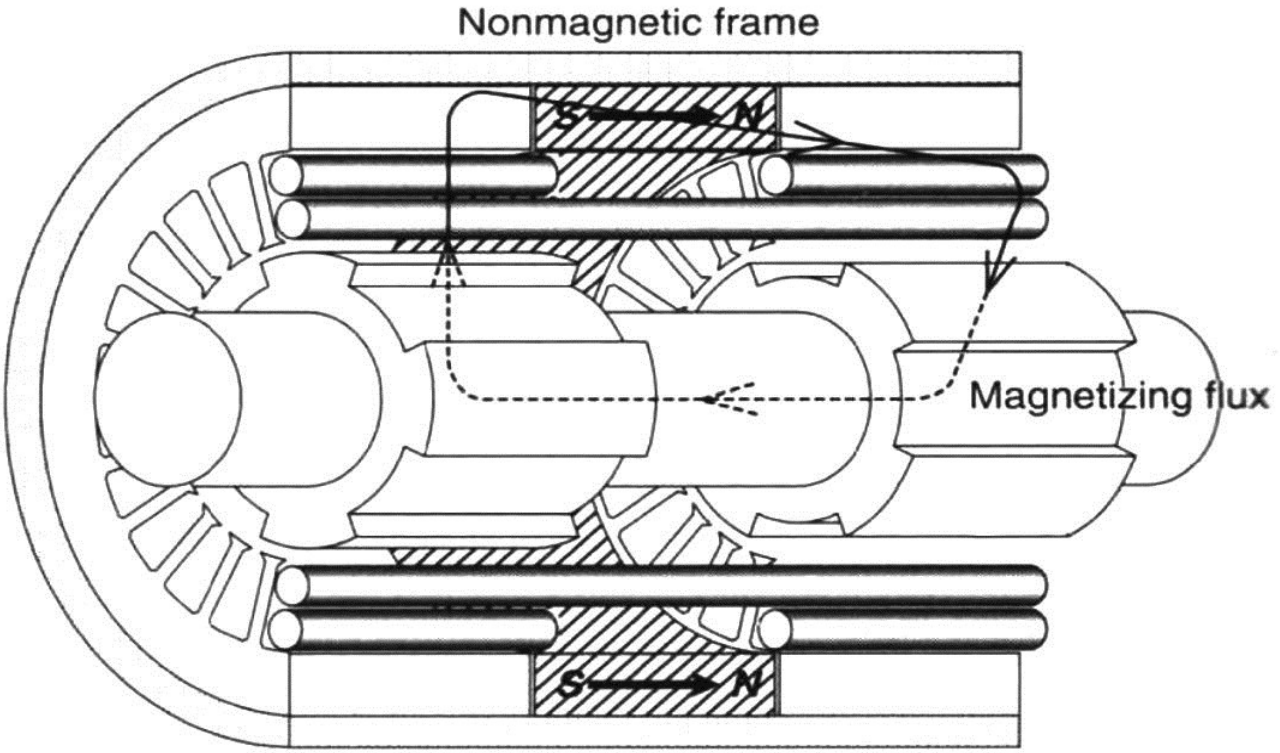

Fig. 7: An example of a hybrid bearing-less motor with PM [8]

1.3 History of magnetic bearing development on CTU

The first study of magnetic bearing in the Czech Republic (resp. Czechoslovakia) was made by the Czechoslovak Academy of Science in 1989. Department of Electrical Drives and Traction of CTU has continued the research since 1992. First thesis was focused to define the actual situation in the magnetic bearing development and to start the realization of a magnetic bearing workstation. A part of development work was cooperated CTU – FI – Department of Designing and Machine Components and external research organization or industrial companies. [1] The first radial heteropolar magnetic bearing was finished in the year 1993. (see Fig. 8).

Doctoral thesis "Identification of Magnetic Bearing", made by Ing. Jan Jára was finished in the year 1997. The aim of this thesis was mathematical description of an active magnetic bearing system. The base of a new system identification method was real-time measurement and digital mathematical description. [13]

Ing. Pavel Komárek defended his doctoral thesis "High-speed bearing-less motor with slide rotor" in the year 2004. A synchronous motor with permanent magnets slide rotor (PMSM) and only with one stator winding was the result of this thesis. This simple hardware configuration requires complicated control system, because one control current that flows in one winding must not only stabilize the rotor but also to produce the torque for the rotor rotation. The search of proper position sensor was described in a special chapter of the thesis. Several types as Hall Effect sensors, capacitive sensors or HF bridge sensors were tested. [12]

The first doctoral thesis, which includes bearing diagnostic according to standard ISO 14839 3 was called "Active magnetic bearing with adaptive control" and was defended by Ing. Luděk Synek in the year 2010. The thesis object was to prove the actual control method, to optimize the controller and power inverter diagnostic and to measure the system stability according to the ISO standard. [14]

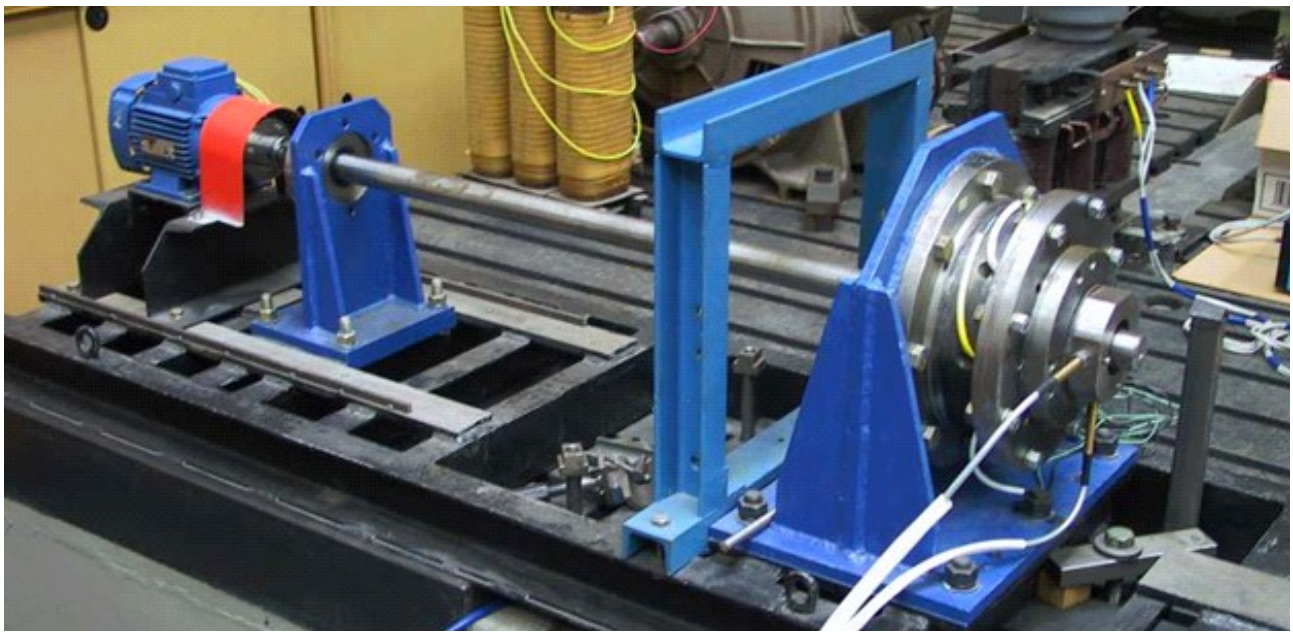

Fig. 8: Radial hetero-polar magnetic bearing in lab of CTU in Prague, FEE, Department of electric drives and traction

The meeting of ISO/TC108/SC2/ working group WG7 – "Vibration of rotating machinery equipped with active magnetic bearings" was held in CTU – FEL in the year 2005. Members of WG7 group visited working place of magnetic bearings at the Department K13114 and Ing. Luděk Synek presented results of his research works to the group members during their visit. (see Fig. 9)

Fig. 9: Ing. Luděk Synek presented results of his research works to the group WG7 members during their visit in CTU-FEE. The persons are listed in Tab. 1.

First-name	Surname	Country	Institution
Jiří	Pavelka	Czech Rep.	CTU-FEE
Richard	Marker	Germany	TU Darmstadt
Takao	Azuma	Japan	Japan University
Eric	Maslen	USA	Virginia University
Patrick	Keogh	U.K.	TU in Bath
Michel	Lacour	France	S2M company
René	Larsonneur	Switzerland	Mecos company

Tab. 1: List of names and basic information about persons shown in Fig. 9. The list starts on first left position.

First mechanical part of the hybrid magnetic bearing at the CTU was designed intuitively in the year 2001 and its production finished in the year 2003. The photo of the radial PM active magnetic bearing in lab of the CTU in Prague, FEE is in Fig. 10. The same other parts of AMB sets as the main power converter, a main processor for controller, current and position sensors were used for both types of the magnetic bearings.

Actually there are two doctoral theses in elaboration with objects of hybrid magnetic bearings at the CTU in Prague - FEE. Both theses use the same magnetic part, but the electrical power parts and control parts are different.

The aim of Ing. Vitner thesis is to analyze, to design and to measure the method of unbalance force counteracting control. Ing. Vitner uses the same main power converter, main processor for controller, current and position sensors as they are used for the heteropolar radial AMB shown in Fig. 8.

Fig. 10: Radial PM active magnetic bearing in lab of CTU in Prague, FEE

The aim of my thesis is to use the new main power converter, the main processor for controller, current and position sensors and to prove, among other things, that the PM active magnetic bearing can be used for industrial applications as well as a conventional heteropolar active

magnetic bearing.

2 The object of this doctoral thesis

The object of this doctoral thesis is to analyse capability of hybrid magnetic bearing with three-phase stator winding. It should also define possible functional or construction problems, describe the solutions and suggest the direction for further research. All problems found during the development should be summarized together with optimal solutions or suggestions in the conclusion.

The thesis should further design, construct, run and test power and control electronic for the existing magnetic part of the hybrid magnetic bearing. New electronic and software tools should be developed, different semiconductors will be used, control will run on different frequencies and on different platforms. The final system of magnetic bearing should be diagnosed according to the actual standard.

The mechanical and magnetic part of hybrid magnetic bearing with three-phase stator winding is already present in the CTU laboratory. It was designed intuitively in 2001, but the functionality was never proved by technical research. New design method of magnetic part, new electrical and control systems has to be designed for finalizing functional analysis described in following chapters. Detailed targets are listed below.

2.1 Theoretical analysis of hybrid magnetic bearing

Theoretical analysis of the defined hybrid magnetic bearing with three-phase stator winding should be made as well as features comparison with a corresponding active magnetic bearing. All functional and construction advantages of our hybrid magnetic bearing should be described. The target of the thesis is to define a new design method.

2.2 New power electronic development

A new power electronic should be designed as a replacement of universal inverters used on a previous tests of the hybrid magnetic bearing mechanical part at the CTU laboratory. The purpose is to design an optimum power inverter for this application, maximize features for real operation, but minimize dimensions and price.

Original inverters used external laboratory power supplies, a number of intermediate capacitors wired together and the slow IGBT bridge. My dissertation thesis combines the input power rectifier, DC-link circuit and 3-phase power inverter into one PCB. The input part will be able to be supplied by standard power grid and the output bridge will use faster MOSFET transistors.

2.3 New control electronic development

Additionally to new power electronic, the control system has to be replaced and integrated to the power part. Then, the final device will be a complex and small driving unit and it could be easily used as a base for industrial applications.

The universal DSP evaluation board produced by Freescale Semiconductor was used for the previous tests on the magnetic bearing. During the time Freescale company was merged with NXP Semiconductors, so the original producer does not exist any more. The microcontroller DSP56F805 was assembled on the board. It runs with the 40MIPS at 80MHz. One of the objects of this doctoral thesis is to use a faster controller (TMS320F2801 produced by Texas Instruments) and to design specific measurement, control and communication circuits on the PCB together with the power electronic part. New control electronics also need a new control software based on a different platform.

2.4 Construction of the hardware

The next object of this project is to design the printed circuit board layout, assemble it by correct components and test the basic functionality of the whole electrical part. Each functional part or circuit should be at first tested separately step by step to minimize possible damages of other components. Searching for mistakes on the board and fixing them is the main point of this chapter.

2.5 Running and tuning the system

After the electronic is finished, both parts of the hybrid magnetic bearing will be assembled together and final functionality development will take part. The hardware topology requires designing, testing and tuning a complex control system. Development of the microcontroller and PC software and theoretical background will be described in this document as well as unexpected troubles and their solution.

2.6 Diagnostic of magnetic bearing according to the actual standard

The result of the points above should be a fully operational hybrid magnetic bearing. This chapter requires functional tests according to the international standard ISO 14839. Final diagnostic is the best way to show real capability of the designed bearing.

2.7 Evaluation of hybrid magnetic bearing features

The diagnostic result, described in previous chapter, will provide a base for final evaluation of the hybrid magnetic bearing features. Successful result would prove that our bearing is capable to be used in the same applications as active magnetic bearings.

3 Theoretical analysis of radial PM active magnetic bearing

Basic information about different types of magnetic bearings are given in [8] and [10]. Both books contain only small parts about PM active magnetic bearings.

3.1 Magnetic part

A very simple biased electromagnet in Fig. 11 is used for the explanation of electromagnet function. The moving part of this electromagnet is called “Flotor” and is located between four poles. Four bias magnetic fluxes are the results of two PM Magneto Motive Forces (MMFs). As it is seen in Fig. 11 (a) each bias magnetic flux flows through two air gaps. If the control coils are not energized then magnetic fluxes in contiguously disposed opposite air gaps are identical and therefore the resulted magnetic force is equal to zero.

If the control coils on vertical poles are energized then there are sources of the same MMFs, These MMFs excite the same magnetic flux in both air gaps. As is seen in Fig. 11 (b) the resulted magnetic force is also equal to zero.

It is seen from Fig. 11 (c) that both types of magnetic fluxes are added together in the upper vertical air gap and there are subtracted together in the lower vertical air gap. The direction of the resulted magnetic force in the vertical direction is therefore up.

A cross-section sketch of a realistic PM biased radial AMB magnet set is depicted in Fig. 12. This magnetic bearing is composed from one or two stator pole pieces, the axially polarized ring shaped permanent magnet and eight control coils. Some more detailed descriptions or details of the proposal design procedure are not given in [8].

The PM active magnetic bearing in Fig. 10 was designed intuitively on the base of knowledge from the theory of electrical machines. The intuitive design started in November 2001 and the production of the PM radial AMB was finished in the year 2003.

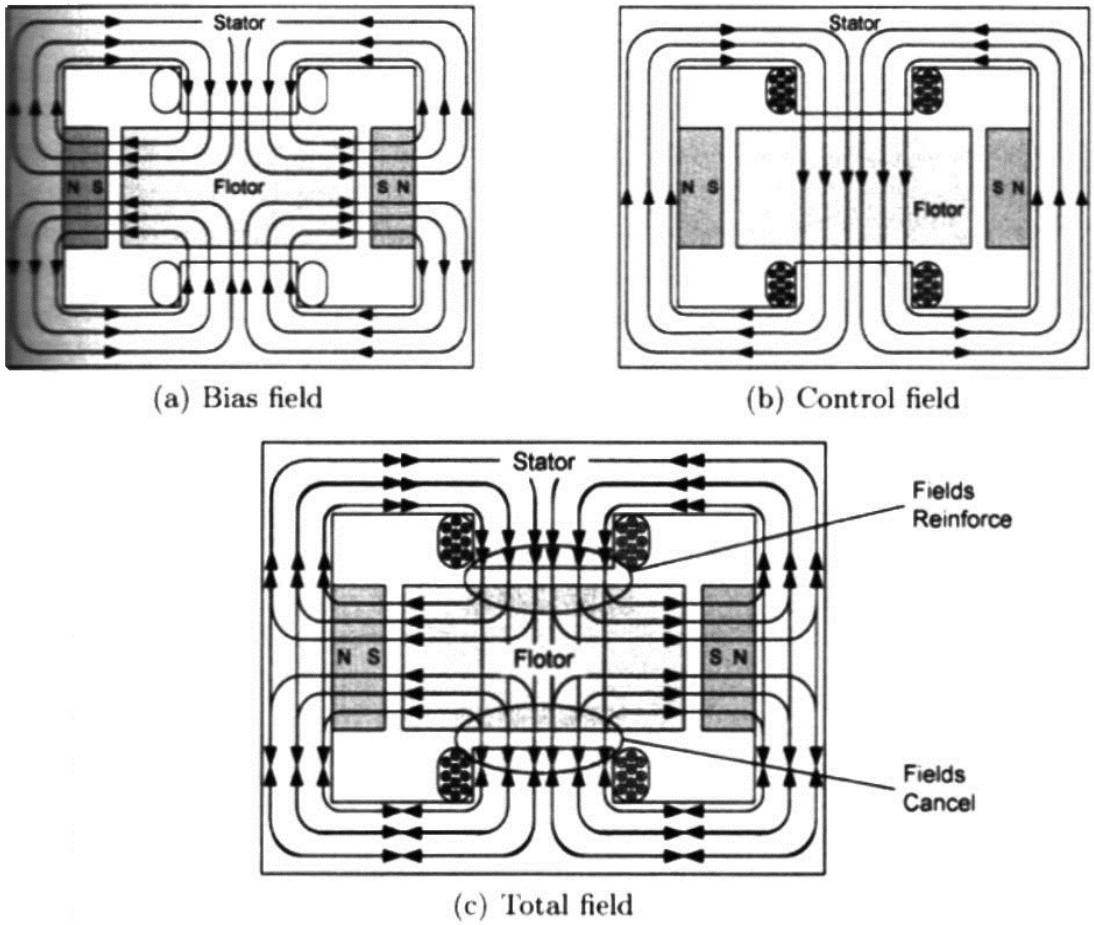

Fig. 11: Schematic diagram of very simple PM biased electromagnet [8]

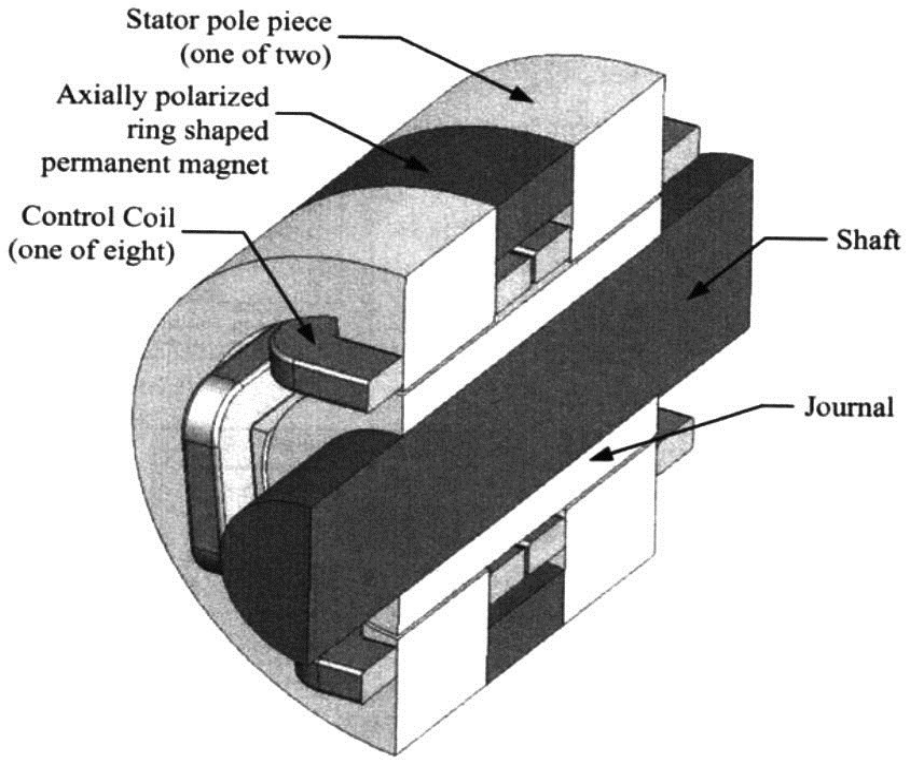

Fig. 12: Schematic diagram of very simple PM biased electromagnet [8]

The theoretical analysis of a radial PM active magnetic bearing was elaborated later during the last year of my PhD study (in the year 2017). It allowed comparing the intuitive design from years 2001 – 2003 with results of the systematic design on the base of above mentioned theoretical analysis.

Following theoretical analysis of the radial permanent magnet active magnetic bearing starts from the conventional homopolar radial magnetic bearing.

3.1.1 Theoretical analysis of conventional homo-polar active magnetic bearing

Cross section of the conventional radial homo-polar active magnetic bearing is depicted in Fig. 4. Four C – cores are located around of the rotor shaft and they represent four electromagnets. The angle between axes of the neighboring electromagnets is 90º. The main close flux path of each electromagnet is composed from its C-core, two air gaps and a part of the rotor shaft. Each flux path part has a reluctance R_i shown in Eq. (1).

$$R_i = \frac{l_i}{\mu_r * \mu_0 * S_i} \tag{1}$$

where l_i is the flux path length
S_i is the cross-section area of the flux path
μ_r is the relative permeability of flux path material
μ_0 is the permeability of vacuum ($\mu_0 = 4\pi*10^{-7}$ H/m)

The C-core and the shaft material is an iron with the relative permeability μ_{rFe} in the range of 1000 – 10000. In opposite the relative permeability of air μ_{rair} is approximately equal to 1. Therefore the air gap reluctance is significantly larger than the reluctance of iron parts. Therefore the reluctance of the iron parts are negligible and only the air gap reluctance R_g can be used in the following calculations. Its value can be calculated from Eq. (2).

$$R_g = \frac{\delta_g}{\mu_0 * S_g} \tag{2}$$

where δ_g is length of the air gap
S_g is air gap area

The magnetic flux Φ in the magnetic path is shown in Eq. (3):

$$\Phi = \frac{2 * N * i}{2 * R_g} = \frac{N * i}{R_g} \tag{3}$$

where Φ is the magnetic flux in the flux path
I is the instantaneous current in the winding
N is the number of winding turns

The flux linkage Ψ of the winding coil is defined as the number of winding turns N multiplied by the flux Φ passing through the winding coil (see Eq. (4)).

$$\Psi = \frac{N^2 * i * \mu_0 * S_g}{\delta_{g0}} = L_0 * i \tag{4}$$

where L_0 is the nominal coil inductance for the nominal air gap length δ_{g0}.

The magnetic energy W_m in the air gap with the nominal length δ_{g0} for the unsaturated magnetic circuit is equal to Eq (5).

$$W_m = \frac{1}{2} * \Psi * i = \frac{N^2 * i^2 * \mu_0 * S_g}{4 * \delta_{g0}} = \frac{1}{2} * L_0 * i^2 \tag{5}$$

A mechanic force can be calculated from the Eq.(6).

$$F_m = \frac{\partial W_m}{\partial \delta_g} = \frac{\partial L_0}{\partial \delta_{g0}} * \frac{i^2}{2} = \frac{L_0}{\delta_{g0}} * \frac{i^2}{2} = \frac{N^2 * \mu_0 * S_g}{4} * \frac{i^2}{\delta_{g0}^2} \tag{6}$$

If the value of the air gap δ_{g0} is constant, as the result of the rotor position control, then the mechanic force F of the active magnetic bearing is in square proportion to the coil current i.

This magnetic force in the air gap of the C-core can be only attractive for both polarities of the coil current i.

Two electromagnets located in the opposite position to the rotor form one couple. A resulted mechanic force F_m of this couple is given by Eq. (7)

$$F_m = F_1 - F_2 = \frac{N^2 * \mu_0 * S_g}{4 * \delta_{g0}^2} * \left(i_1^2 - i_2^2\right) \tag{7}$$

It is supposed that outputs of the current controllers fulfil following relation – Eq. (8):

$$i_1 = I_0 + \Delta i \qquad i_2 = I_0 - \Delta i \tag{8}$$

where I_0 is the bias current
Δi is control current.

The resulted mechanic force F_m is in linear proportion to Δi as following Eq. (9):

$$F_m = \frac{N^2 * \mu_0 * S_g}{4 * \delta_0^2} * \left(\left(I_0 + \Delta i\right)^2 - \left(I_0 - \Delta i\right)^2\right) = \frac{N^2 * \mu_0 * S_g}{\delta_0^2} * I_0 * \Delta i \tag{9}$$

It is seen that the resulted mechanic force F_R can be in both polarities.

3.1.2 Energy consummation of the homopolar active magnetic bearing couple

We will suppose that the value of the control current Δi changes from $-I_0$ to $+I_0$. The losses in all four coils of magnet couple are defined by Eq. (10).

$$\Delta P_{loss} = 2 * R_{win} * \left(\left(I_0 + \Delta i\right)^2 + \left(I_0 - \Delta i\right)^2\right) = 4 * R_{win} * \left(I_0^2 + \Delta i^2\right) \tag{10}$$

Minimum losses are for $\Delta i = 0$ and its value is $4*R_{win}*I_0^2$, maximum losses are for $\Delta i = \pm I_0$ and their values are $8*R_{win}*I_0^2$.

The replacement of the bias current I_0 by a permanent magnet allows to reduce losses in coils of the active magnetic bearing to one half or even more.

3.1.3 Replacement MMF of bias current I_0 by MMF of permanent magnet

A bias current I_0 that flows in two magnet coils each with N turns produces MMF that is

equal to $2*N*I_0$. This MMF is the cause of the magnetic flux Φ_0. The value of this magnetic flux Φ_0 can be calculated from Eq (11):

$$\Phi_0 = \frac{2*N*I_0}{2*R_g} = \frac{N*I_0}{R_g} \tag{11}$$

Simplified magnetizing characteristic shape of a quality permanent magnet material is in Fig. 13. A prism from the permanent magnet material with the length l_{PM} and with the cross-section area S_{PM} can be replaced by the MMF that is equal to $({}_BH_C*l_{PM})$ and by the equivalent PM inner reluctance R_{PM} in Eq. (12).

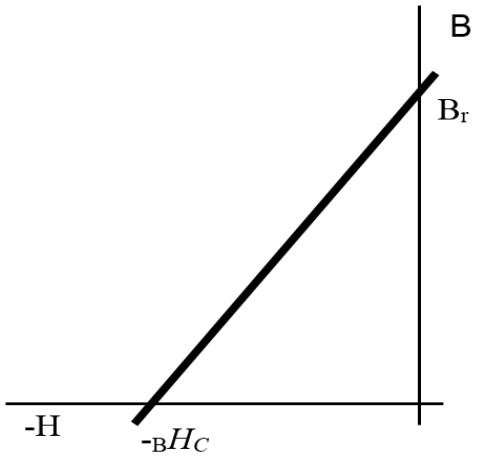

Fig. 13: PM magnetizing characteristic

$$R_{PM} = \frac{{}_BH_C*l_{PM}}{B_r*S_{PM}} = \frac{l_{PM}}{\mu_{PM}*S_{PM}} \tag{12}$$

where μ_{PM} is relative permeability of the permanent magnet material $\mu_{PM} = B_r / {}_BH_C$.

The equivalent diagram of a closed magnetic circuit is drowning in Fig. 14. The magnetic flux Φ_0 can be calculated on the base of this equivalent circuit, as shown in Eq. (13).

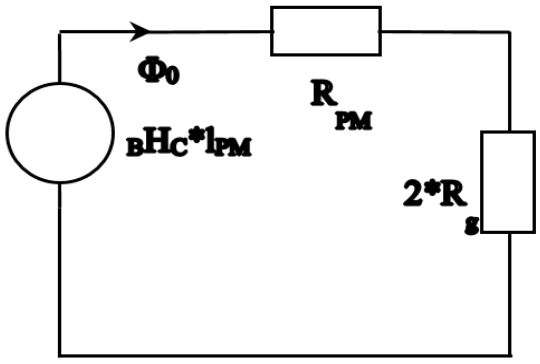

Fig. 14: Equivalent diagram of closed magnetic circuit with PM

$$\Phi_0 = \frac{{}_BH_C*l_{PM}}{R_{PM}+2*R_g} \tag{13}$$

Dividing of the PM MMF ${}_BH_C{*}l_{PM}$ between the PM inner reluctance R_{PM} and the air gap reluctance $2{*}R_g$ can be calculated from Eq. (14) that was developed on the base of Fig. 15.

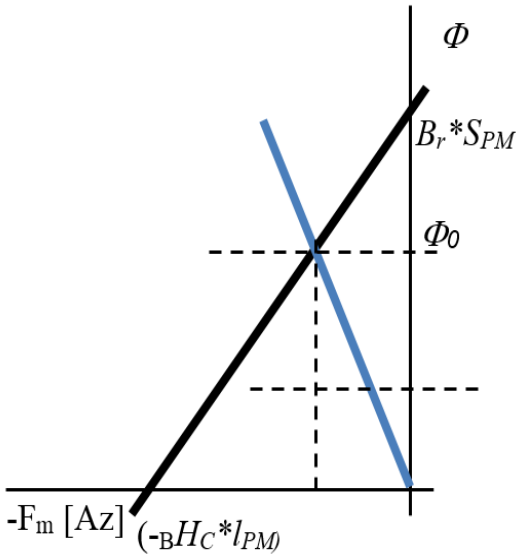

Fig. 15: Dividing of PM MMF between the PM inner reluctance and the air gap reluctance

$$\frac{\Phi_0}{B_r * S_{PM}} = \frac{B_{PM}}{B_r} = \frac{R_{PM}}{R_{PM} + 2 * R_g} = \frac{1}{1 + \frac{2 * R_g}{R_{PM}}} = \frac{1}{1 + \frac{\mu_{PM}}{\mu_0} * \frac{2 * \delta_{g0}}{l_{PM}} * \frac{B_{\delta 0}}{B_{PM}}} \tag{14}$$

Last Eq. (14) can be rewritten to the following form:

$$\frac{B_{PM}}{B_r} = 1 - \frac{\mu_{PM}}{\mu_0} * \frac{2 * \delta_{g0}}{l_{PM}} * \frac{B_{\delta 0}}{B_{PM}} \tag{15}$$

We suppose that all values in the Eq. (15) are constants expect variables B_{PM+} and l_{PM}. When the value of one variable B_{PM+} or l_{PM} is known then Eq. (15) allows to calculate the value of the second variable. The value of B_{PM} has to be lower than the value of B_r .

3.1.4 Location of permanent magnets in C-cores of electromagnets

A location of the PM is depicted in Fig. 16. PMs are located in centers of the C-core magnet yokes. The coils are located symmetrically on both ends of the C-core magnet.

PMs of all four C-core magnets have the same magnetic polarity. Therefore all four yokes of the C-core magnets can be jointed to one tube and four permanent magnets can be replaced with one PM ring.

Basic magnetic force of one homo-polar magnet end is equal to Eq. (16)

$$F_{m1} = \frac{B_{0\delta}^2}{2 * \mu_0} * S_{m1} = \frac{B_{0\delta}^2}{2 * \mu_0} * l_m * k_m * \frac{\pi}{4} * d_{shaft} \tag{16}$$

where l_m is the length of ,the magnet C-core

$$S_{m1} = l_m * k_m * \frac{\pi}{4} * d_{shaft}$$

k_m is the ratio of the magnet width to the pole pitch τ_p ($\tau_p = \frac{\pi}{4} * d_{shaft}$)

d_{shaft} is the shaft diameter

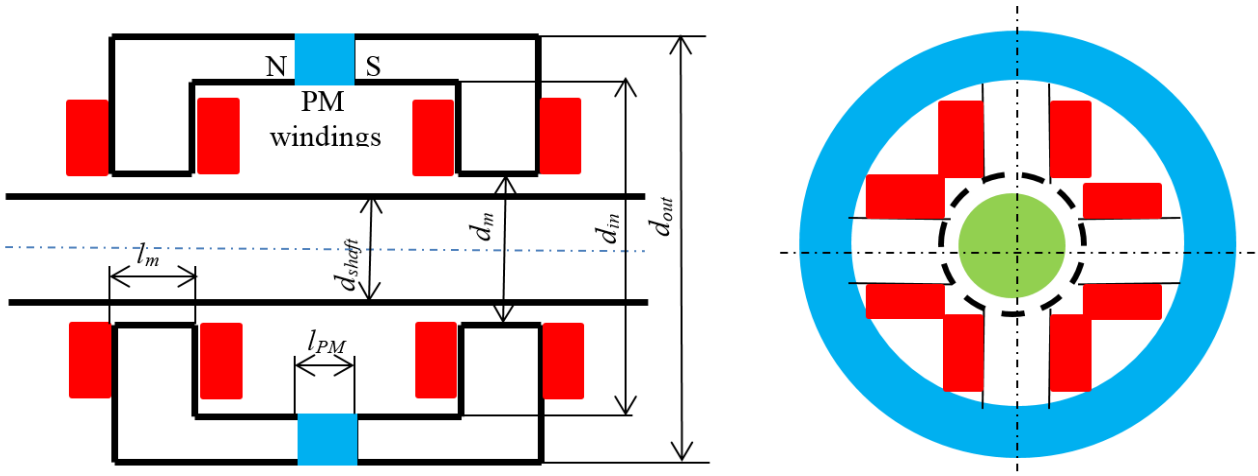

Fig. 16: Location of PM in the C-core of electromagnet

The area of the PM ring can be calculated from following Eq.(17):

$$S_{PM} = \frac{\pi}{4} * (d_{out}^2 - d_{in}^2) = \frac{\pi}{4} * (d_{out} + d_{in}) * (d_{out} - d_{in}) = \frac{\pi}{4} * 2 * (d_{in} + h_{PM}) * 2 * h_{PM} = \\ = \pi * (d_{in} + h_{PM}) * h_{PM} \quad (17)$$

where $h_{PM} = (d_{out} - d_{in})/2$ is the height of the PM ring

The area of the PM ring for one magnet pole:

$$S_{PM1} = \frac{S_{PM}}{4} = \frac{\pi}{4} * (d_{in} + h_{PM}) * h_{PM} \quad (18)$$

Equation (18) can be rewritten to Eq. (19).

$$h_{PM}^2 + d_{in} * h_{PM} - \frac{4 * S_{PM1}}{\pi} = 0 \quad (19)$$

We define the ratio k_B as Eq. (20):

$$\frac{1}{k_B} = \frac{S_{PM1}}{S_{m1}} = \frac{B_{\delta 0}}{B_{PM}} = \frac{\left(h_{PM}^2 + d_m * h_{PM}\right)}{l_m * k_m * d_{shaft}} \quad (20)$$

Equation (20) can be rewritten as quadratic relation for h_{PM}

$$h_{PM}^2 + d_m * h_{PM} - l_m * \frac{k_m}{k_B} * d_{shaft} = 0 \quad (21)$$

Positive solution of the quadratic equation (21) is:

$$h_{PM} = -\frac{d_m}{2} + \sqrt{\left(\frac{d_m}{2}\right)^2 + l_m * \frac{k_m}{k_B} * d_{shaft}} \tag{22}$$

3.1.5 The mechanical force generated by conventional homopolar magnetic bearing couple

The mechanical force in air gaps of one homopolar AMB can be calculated from the following equation (23)

$$F_m = \frac{1}{2} * S_g * \left(B_{g1}^2 - B_{g2}^2\right) = \frac{1}{2} * S_g * \mu_0 * \left(\frac{(NI)_1^2}{\delta_1^2} - \frac{(NI)_2^2}{\delta_2^2}\right) \tag{23}$$

It is seen from Eq. (23) that mechanical force F_m of the homopolar AMB in a one direction is one linear function.

For the magnet couple is possible to write:

$$\begin{aligned} (NI)_1 &= NI_0 + \Delta Ni \qquad (NI)_2 = NI_0 - \Delta Ni \\ \delta_1 &= \delta_0 - \Delta\delta \qquad\qquad \delta_2 = \delta_0 + \Delta\delta \end{aligned} \tag{24}$$

After application of Eq. (24) in Eq. (21), linearisation and adjustment we obtain following equation (25). The mechanical force F_m is a linear function of both variables now (ΔNi and $\Delta\delta$).

$$F_m = \frac{2 * S_g * \mu_0 * (NI_0)^2}{\delta_0^2} * \left(\frac{\Delta Ni}{NI_0} + \frac{\Delta\delta}{\delta_0}\right) \tag{25}$$

3.1.6 Mechanical force generated by radial PM magnetic bearing couple

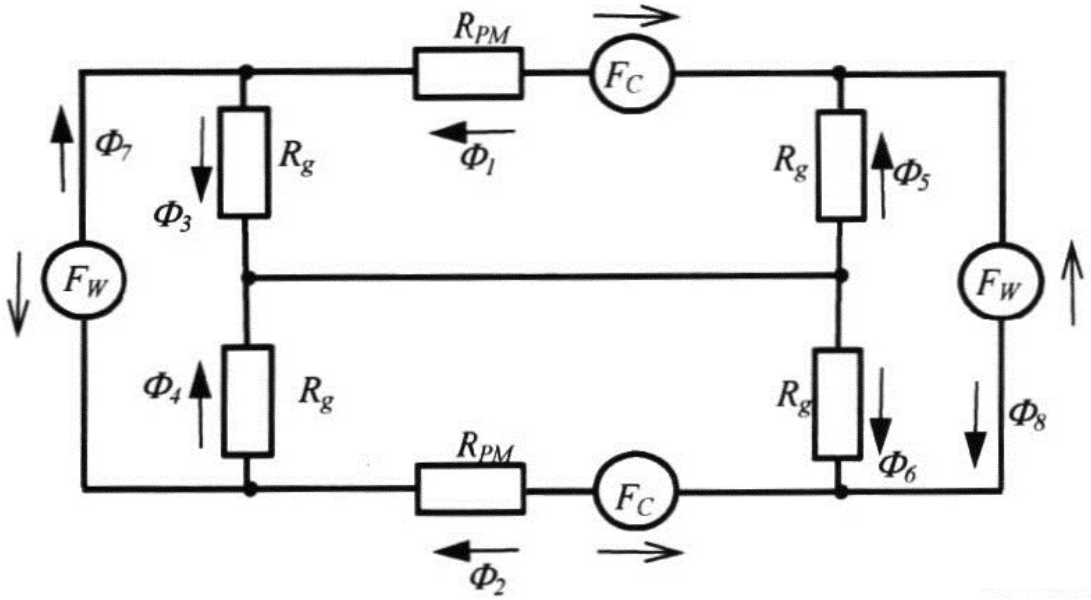

Fig. 17: Equivalent diagram of one couple PM radial AMB

It is supposed that a controller of conventional homopolar magnetic bearing couple operates with the constant bias MMF NI_0. If this bias MMF is replaced by MMF of a permanent magnet then

the MMF of the PM changes with ΔNi of an active magnet bearing control system. Equivalent diagram of the homopolar PM radial AMB is in Fig. 17.

The equivalent diagram can be described by following 8 equations:

$$F_C = R_{PM} * \Phi_1 + R_g * (\Phi_3 + \Phi_5) \tag{26}$$

$$F_C = R_{PM} * \Phi_2 + R_g * (\Phi_4 + \Phi_6) \tag{27}$$

$$F_W = R_g * (\Phi_3 - \Phi_4) \tag{28}$$

$$F_W = R_g * (\Phi_5 - \Phi_6) \tag{29}$$

$$\Phi_3 = (\Phi_7 + \Phi_1) \tag{30}$$

$$\Phi_4 = (\Phi_2 - \Phi_7) \tag{31}$$

$$\Phi_5 = (\Phi_1 - \Phi_8) \tag{32}$$

$$\Phi_6 = (\Phi_2 - \Phi_8) \tag{33}$$

The system of Eq. (26) – (33) has 10 variables: Φ_1, Φ_2, Φ_3, Φ_4, Φ_5, Φ_6, Φ_7, Φ_8, F_W, F_C. For unambiguous solution, two variables must be selected as independent. We select F_W and F_C.

Then the solution of equation system is:

$$\Phi_3 = \frac{K_5 - K_6}{K_5^2 - K_6^2} * (F_W + K_4 * F_C) \tag{34}$$

$$\Phi_5 = \frac{1}{K_5} * (F_W + K_4 * F_C) - \frac{K_6}{K_5} * \Phi_3 \tag{35}$$

$$\Phi_2 = \frac{K_2}{K_1} * F_C - \frac{K_3}{K_1} * (\Phi_3 + \Phi_5) \tag{36}$$

$$\Phi_1 = \frac{1}{R_{PM}} * F_C - \frac{R_g}{R_{PM}} * (\Phi_3 + \Phi_5) \tag{37}$$

$$\Phi_6 = \Phi_2 - \Phi_5 + \Phi_1 \tag{38}$$

$$\Phi_4 = \Phi_2 - \Phi_3 + \Phi_1 \tag{39}$$

$$\Phi_8 = \Phi_5 - \Phi_1 \tag{40}$$

$$\Phi_7 = \Phi_3 - \Phi_1 \tag{41}$$

Where $K_1 = 1 + \frac{2 * R_g}{R_{PM}}$ $K_2 = \frac{1}{R_{PM}} + \frac{2 * R_g}{R_{PM}^2}$ $K_3 = \frac{R_g}{R_{PM}} + \frac{2 * R_g^2}{R_{PM}^2}$

$$K_4 = \frac{R_g}{R_{PM}} + R_g * \frac{K_2}{K_1} \qquad K_5 = 2 * R_g + \frac{R_g^2}{R_{PM}} + R_g * \frac{K_3}{K_1}$$

The mechanical force F_{m1} of one side of the homopolar PM radial AMB couple can be changed by a change of F_W. Its value can be calculated from following equation (42).

$$F_{m1} = \frac{1}{2} * S_g * \left(B_{g1}^2 - B_{g2}^2\right) = \frac{1}{2 * S_g} * \left(\Phi_3^2 - \Phi_4^2\right) \tag{42}$$

We will suppose that the value F_C is constant and the value F_W changes in the range $\pm F_{Wmax}$. Then is it possible to determine not only a dependence of the mechanical force F_{m1} on F_W, but also a dependence of the permanent magnet magnetic fluxes Φ_1 and Φ_2 on F_W.

3.2 Power electric part

Simplified connection of a power electronic converter for AMB is in Fig. 2. It is clear from Eq. (6) that magnetic force is in quadratic proportion to the control current and therefore only positive mechanic force can be controlled. It is sufficient to use a two quadrant power electronic DC- DC converter with one polarity output current and both polarity output voltage. Two and four quadrant converters are shown in Figs. (18), (19).

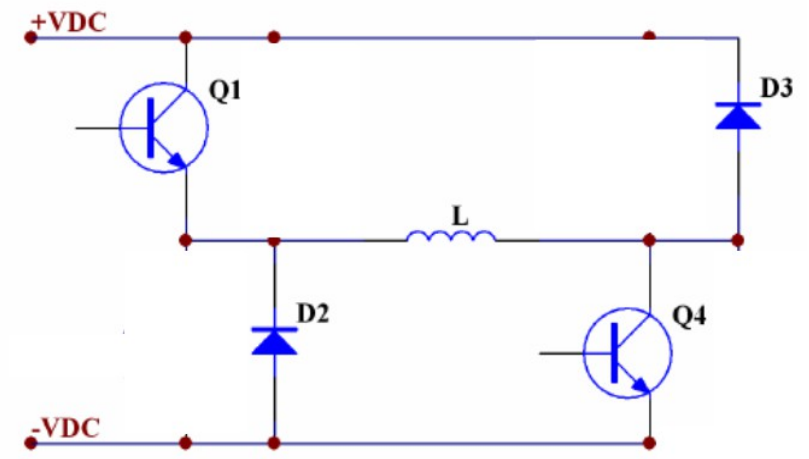

Fig. 18: Two quadrant DC-DC converter

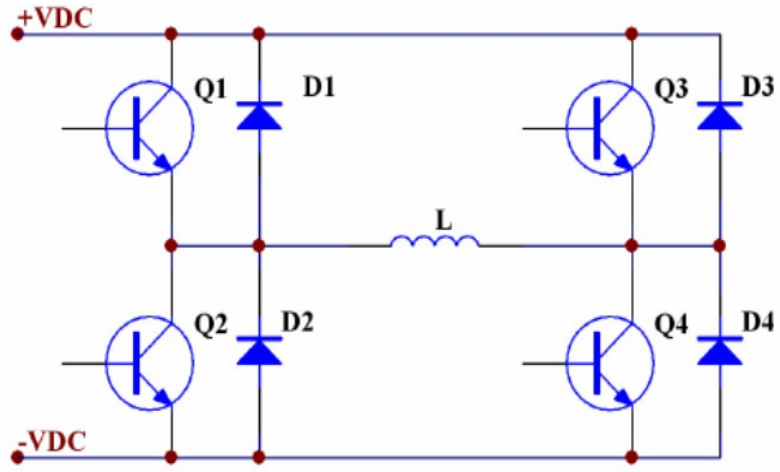

Fig. 19: Four quadrant DC-DC converter

In our case, the active stator winding, which is responsible for dynamic stabilization, is constructed in the three-phase configuration as shown in Fig. 21. Therefore, the supplying electric energy has to have three-phase character. The target is to design a device close to industrial use, so the final magnetic bearing, should be complex, small and simple to use. It should also work without any special supplying or any other connections, excluding service situations. One of the advantages to use three-phase configuration is lower number of active electronic parts (described at Tab. 2).

Homopolar radial Active Magnetic Bearing			
Type of AMB	conventional	with Permanent Magnets	with three-phase windings
Number of excitation windings	4	2	3
Type of converter	two quadrant	four quadrant	three phase
Number of active electronic parts (transistors)	8	8	6

Tab. 2: Homopolar radial Active Magnetic Bearing power supply comparison

Generally the power electric part consists of the passive rectifier, intermediate DC-link circuit and current controlled three-phase voltage inverter (Fig. 20). Moreover we should consider gate-drivers, output current sensors and low voltage internal supply as a part of the power circuit.

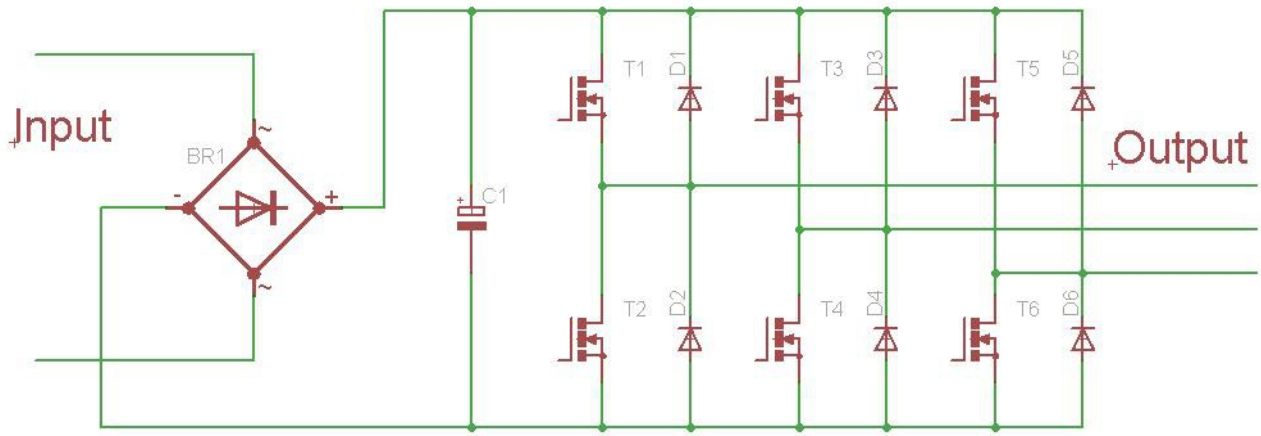

Fig. 20: Power electronic [15]

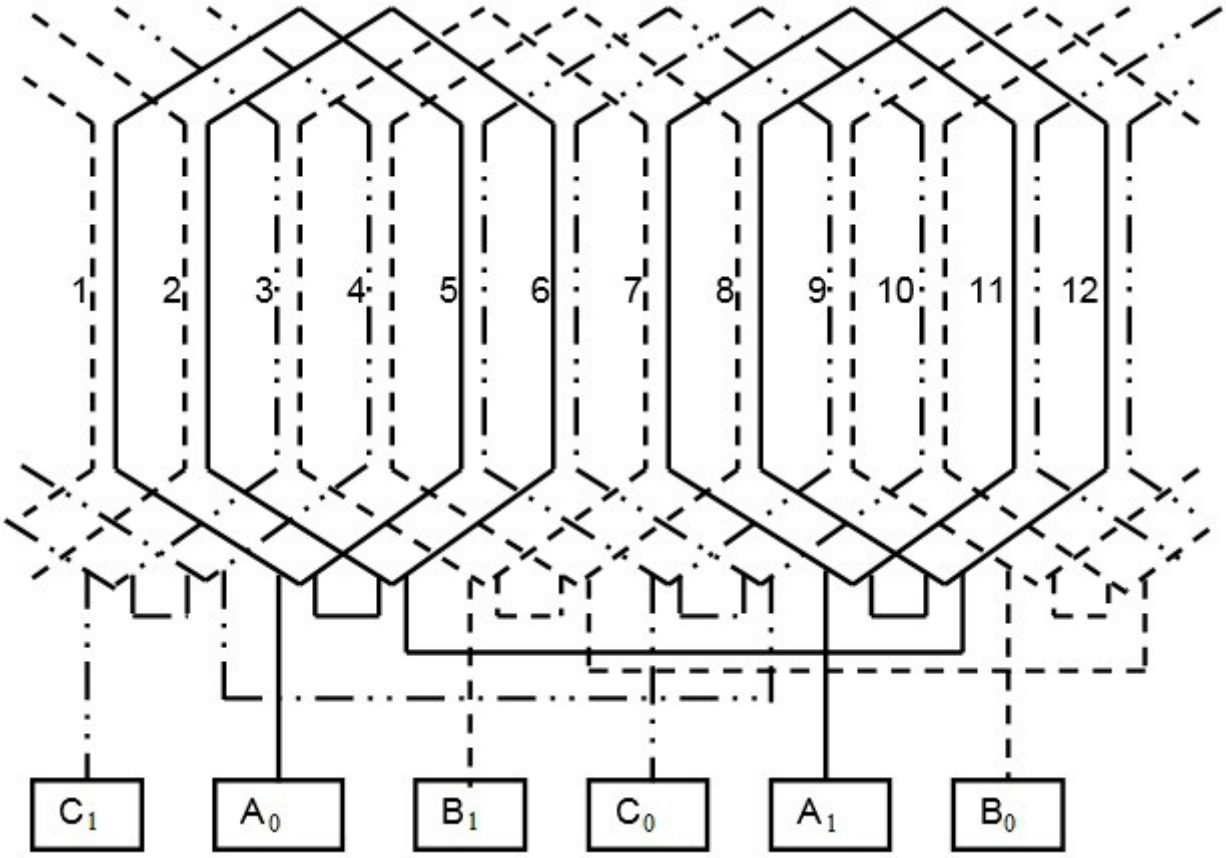

Fig. 21: Three-phase stator winding [9]

According to the requirements above, only input connection will represent standard grid plug. Net sinuous voltage will be rectified and DC energy will be stored in the intermediate capacitor. The DC-link voltage level will be used like a source for the output power generation and internal bias supply. The magnetic bearing starts to work just after the power grid is connected by the operator or superior system.

3.3 Control part

The control part in Fig. 2 is marked as 1. Its input is a signal from the position sensor and its output is an estimated value of a control current *i*.

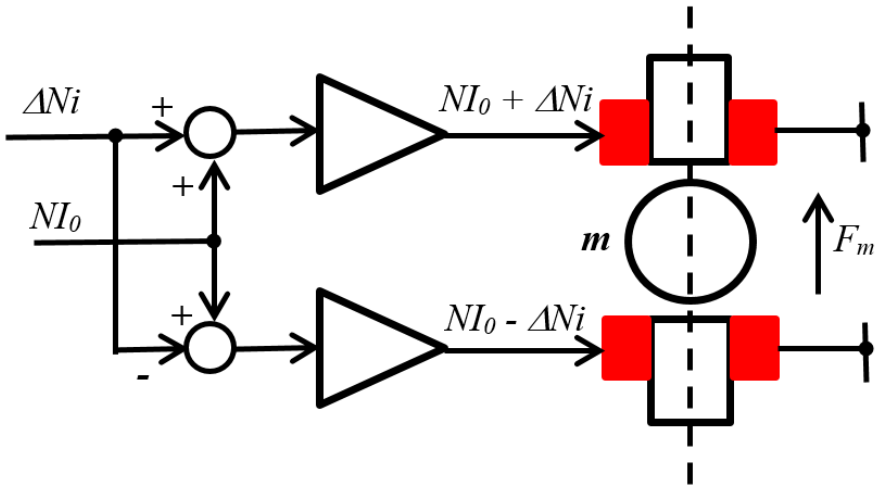

Fig. 22: Control diagram for one couple of homopolar conventional radial AMB

One couple of the conventional homopolar radial AMB contains two excitation winding that are energized from two two-quadrant converters.

In part 3.1.5 is was developed equation (25), after linearisation of the Eq. (23). It defines the mechanical force F_m that is generated by conventional homopolar magnetic bearing couple. This force is a linear function of inputs ΔNi and $\Delta\delta$. A control diagram for this couple for the input ΔNi is in Fig. 22.

It is seen that bias NI_0 *is* constant and therefore the result mechanical force F_m is a linear dependence on ΔNi.

When the bias NI_0 *is* replaced by the permanent magnet then the control diagram will be simplified to the diagram in Fig. 23.

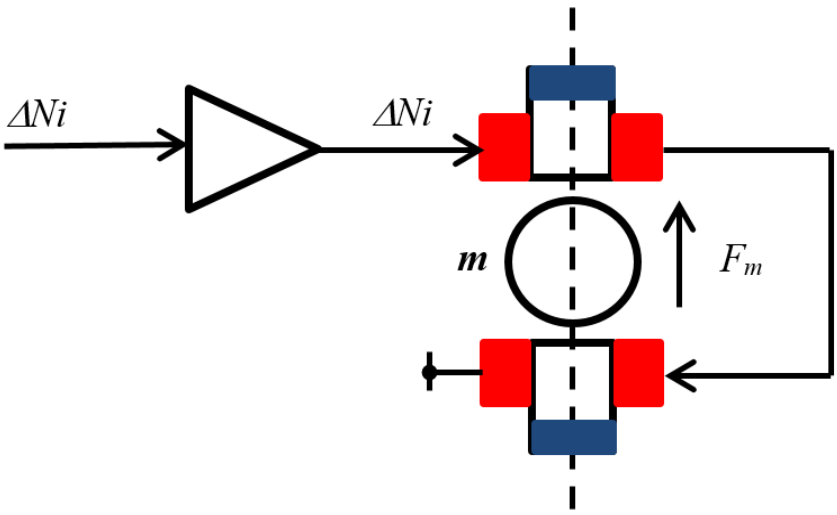

Fig. 23: Control diagram for one couple of homopolar conventional radial AMB

In part 3.1.6 it was developed the equivalent diagram for calculation of magnetic fluxes in different places of the PM radial AMB magnetic circuits. This equivalent diagram in Fig. 17 can be described by the system of eight linear equations (34) – (41) for eight magnetic fluxes in eight different places of the magnetic circuit. The knowledge of the magnetic flux in air gap allows to calculate the resulted mechanical force F_m using the equation (42).

The dependence of the mechanical force F_m as the function of control MMF F_W was calculated for the following constant parameters:

$\delta_0 = 0{,}5$ mm $\quad \mu_0 = 1{,}26*10^{-6}$ H/m $\quad S_{g1} = 679$ mm^2

$\mu_{PM} = 1{,}43*10^{-6}$ H/m $\quad S_{PM1} = 618$ mm^2

and for two lengths PM ring: 4 mm and 8 mm.

The result of calculation is in Fig. 24 as two curves. The blue curve is for $l_{PM} = 4$ *mm* and the red curve is for $l_{PM} = 8$ *mm*.

It is seen that the dependence $F_m = f(F_W)$ is a linear function. Its gradient is a function of the PM ring length. The gradient increases with the length of the PM ring.

It is seen from Fig. 2, that an active magnetic bearing system consists of five components. They are described bellow as points a) – b). Each component has its input and output. The relationship between an output and an input after Laplace's transformation is called in the control technique as a transfer function $G(s)$, where s is Laplace's operator.

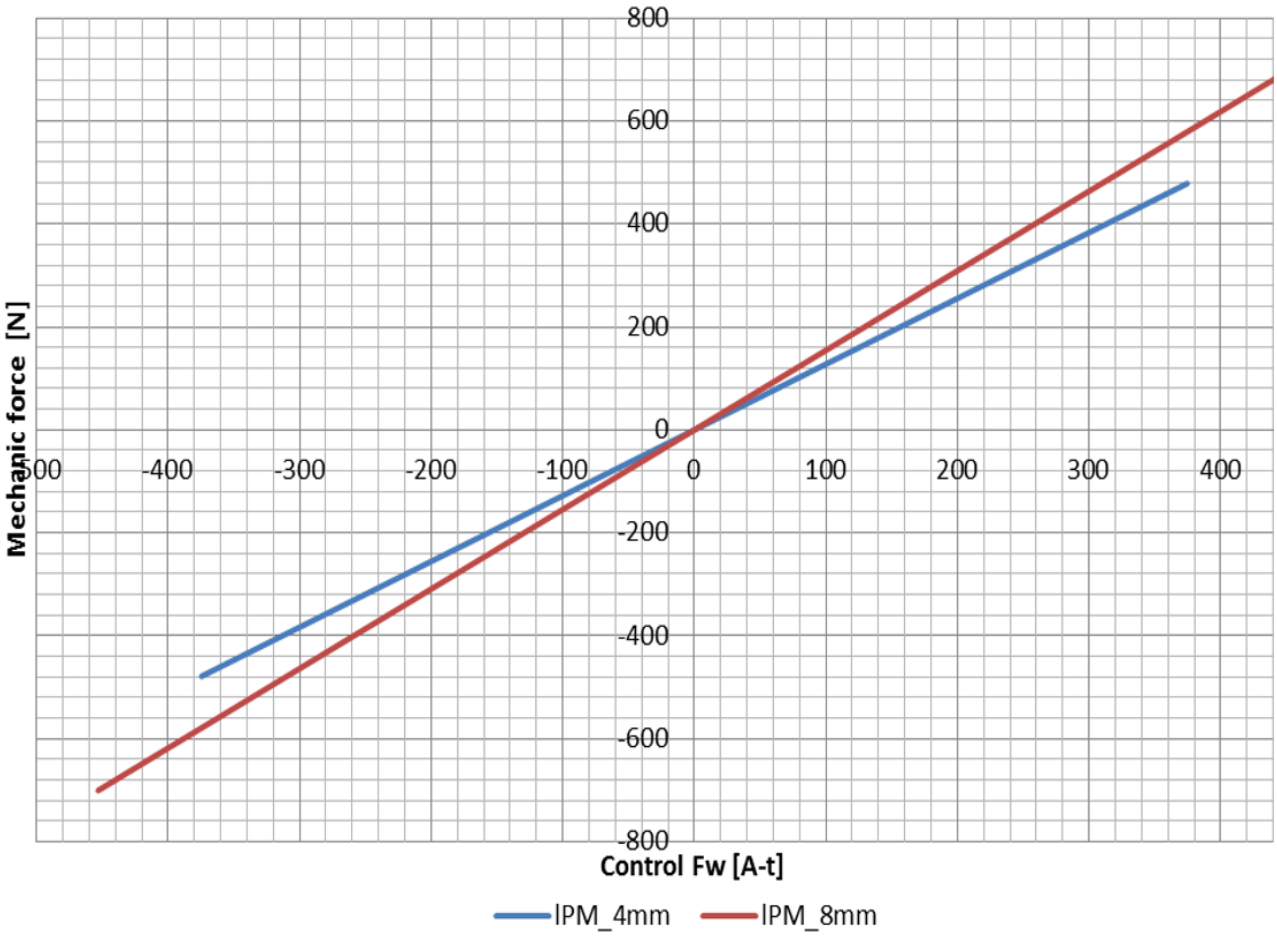

Fig. 24: Dependences F_m on F_W for two lengths of PM ring

a) **Rotor mass**.

The output is a position in the rotor shaft x and the input is a mechanical force F_m . The relation between input and output is described by following Eq. (43).

$$F_m(t) = m_{shaft} * \frac{d^2x(t)}{dt^2} \quad \Rightarrow \quad F_m(s) = m_{shaft} * s^2 * X(s)$$
$$G_m(s) = \frac{X(s)}{F_m(s)} = \frac{1}{m_{shaft} * s^2} \tag{43}$$

The relation between two inputs and one output was developed as Eq. (25) in the part 3.1.5. Equation (25) can be modified to following Eq. (44).

$$F_m(t) = K_{Fi} * \Delta i + K_{Fx} * \Delta x \quad \Rightarrow \quad F_m(s) = K_{Fi} * \Delta i(s) + K_{Fx} * \Delta x(s)$$
$$G_{Fi} = \frac{F_{mi}(s)}{\Delta i(s)} = K_{Fi} \qquad G_{Fx} = \frac{F_{mx}(s)}{\Delta x(s)} = K_{Fx} \tag{44}$$

It is seen that the mechanical force is in linear proportion to the excitation current Δi and the rotor position Δx.

b) Electromagnet with excitation winding.

The winding of electromagnet can be described as an electric circuit with a voltage source u, a resistance R_w and an inductance L_w. This electric circuit can be described by following Eq. (45).

$$\Delta u(t) = R_W * \Delta i + L_W * \frac{d\Delta i}{dt} \quad \Rightarrow \quad \Delta u(s) = R_W * \left(1 + \frac{L_W}{R_W} * s\right) * \Delta i(s)$$

$$G_{em}(s) = \frac{\Delta i(s)}{\Delta u(s)} = \frac{1}{R_W * \left(1 + \frac{L_W}{R_W} * s\right)} \tag{45}$$

c) Power electronic amplifier

It is supposed that power electronic amplifier has the linear relation between the output voltage u and the control input signal u_{coni} Therefore the power electronic amplifier can be described by following Eq. (46).

$$\Delta u(t) = K_U * u_{coni}(t) \quad \Rightarrow \quad \Delta u(s) = K_U * u_{coni}(s)$$

$$G_{amp}(s) = \frac{\Delta u(s)}{u_{coni}(s)} = K_U \tag{46}$$

d) Current controller

We suppose to use standard PI controller. Its input is the deviation of the current $e_i = (\Delta i^* - \Delta i)$ and its output is the value of voltage u_{coni} Therefore the current controller can be described by following Eq. (47).

$$u_{coni}(t) = K_{Pi} * e_i(t) + K_{Ii} * \int e_i(t) * dt \quad \Rightarrow \quad u_{coni}(s) = \left(K_{Pi} + \frac{K_{Ii}}{s}\right) * e_i(s)$$

$$G_{coni}(s) = \frac{u_{coni}(s)}{e_i(s)} = \left(K_{Pi} + \frac{K_{Ii}}{s}\right) \tag{47}$$

e) Position controller

We suppose to use standard PD controller. Its input is a position signal deviation e_x and its output is the estimated value of the current i^*. Therefore the position controller can be described by following Eq. (48).

$$\Delta i^*(t) = K_{Px} * e_x(t) + K_{Dx} * \frac{de_x(t)}{dt} \quad \Rightarrow \quad \Delta i^*(s) = (K_{Px} + K_{Dx} * s) * e_x(s)$$

$$G_{conx}(s) = \frac{\Delta i^*(s)}{e_x(s)} = (K_{Px} + K_{Dx} * s) \tag{48}$$

The block diagram of AMB system is drawn in Fig. 25.

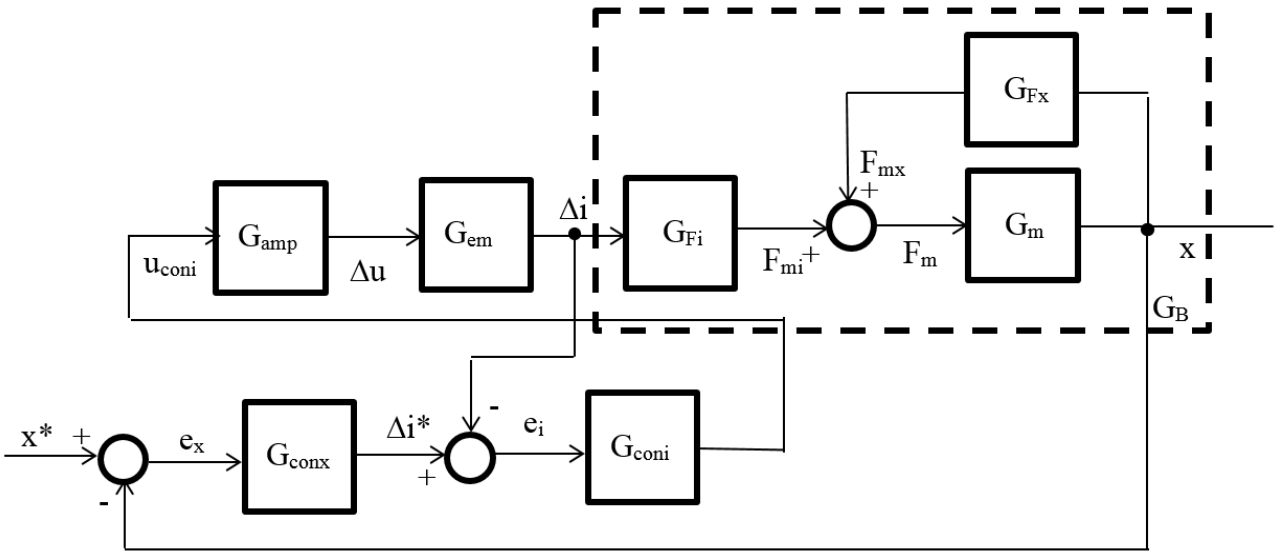

Fig. 25: Block diagram of an ABM control system

Transfer functions G_{Fi}, G_m, G_{Fx} form the transfer function of magnetic bearing G_B. It is possible to write:

$$\begin{aligned} F_{mi}(s) &= F_m(s) - F_{mx}(s) \\ K_{Fi} * \Delta i(s) &= \left(m_{shaft} * s^2 - K_{Fx}\right) * \Delta x(s) \\ G_B &= \frac{\Delta x(s)}{\Delta i(s)} = \frac{K_i}{m_{shaft} * s^2 - K_{Fx}} \end{aligned} \tag{49}$$

For open loop of the current controller it is possible to write:

$$G_{coniO} = G_{coni} * G_{amp} * G_{em} = \left(K_{Pi} + \frac{K_{Ii}}{s}\right) * K_U * \frac{1}{L_W * \left(\frac{R_W}{L_W} + s\right)} = \\ = \frac{\left(\frac{K_{Ii}}{K_{Pi}} + s\right) * K_{Pi} * K_U}{L_W * \left(\frac{R_W}{L_W} + s\right) * s} \tag{50}$$

If $\frac{K_{Ii}}{K_{Pi}} = \frac{R_W}{L_W}$ then:

$$G_{coniO} = \frac{K_{Pi} * K_U}{L_W * s} \tag{51}$$

and the transfer function of the close loop G_{coniC} is:

$$G_{coniC} = \frac{\Delta i(s)}{\Delta i^*(s)} = \frac{G_{coniO}}{1+G_{coniO}} = \frac{\frac{K_{Pi} * K_U}{L_W * s}}{1+\frac{K_{Pi} * K_U}{L_W * s}} = \frac{\frac{K_{Pi} * K_U}{L_W}}{s+\frac{K_{Pi} * K_U}{L_W}} \tag{52}$$

It is possible to write for open loop of the position controller:

$$G_{conxO} = G_{conx} * G_{coniC} * G_B = \left(K_{Px} + K_{Dx} * s\right) * \frac{\frac{K_{Pi} * K_U}{L_W}}{s+\frac{K_{Pi} * K_U}{L_W}} * \frac{K_i}{m_{shaft} * s^2 - K_{Fx}} =$$

$$= \frac{\left(K_{Px} + K_{Dx} * s\right) * \frac{K_{Pi} * K_U * K_i}{L_W}}{m_{shaft} * s^3 + \frac{K_{Pi} * K_U * m_{shaft}}{L_W} * s^2 - K_{Fx} * s - \frac{K_{Pi} * K_U * K_{Fx}}{L_W}} \tag{53}$$

The transfer function of the close loop G_{conxC} is:

$$G_{conxC} = \frac{x(s)}{x^*(s)} = \frac{G_{coniO}}{1+G_{coniO}} = \frac{\frac{\left(K_{Px} + K_{Dx} * s\right) * \frac{K_{Pi} * K_U * K_i}{L_W}}{m_{shaft} * s^3 + \frac{K_{Pi} * K_U * m_{shaft}}{L_W} * s^2 - K_{Fx} * s - \frac{K_{Pi} * K_U * K_{Fx}}{L_W}}}{1+\frac{\left(K_{Px} + K_{Dx} * s\right) * \frac{K_{Pi} * K_U * K_i}{L_W}}{m_{shaft} * s^3 + \frac{K_{Pi} * K_U * m_{shaft}}{L_W} * s^2 - K_{Fx} * s - \frac{K_{Pi} * K_U * K_{Fx}}{L_W}}} =$$

$$= \frac{\left(K_{Px} + K_{Dx} * s\right) * \frac{K_{Pi} * K_U * K_i}{L_W}}{m_{shaft} * s^3 + \frac{K_{Pi} * K_U * m_{shaft}}{L_W} * s^2 + \left(\frac{K_{Pi} * K_U * K_i * K_{Dx}}{L_W} - K_{Fx}\right) * s + \frac{K_{Pi} * K_U}{L_W} * \left(K_{Px} * K_i - K_{Fx}\right)} \tag{54}$$

We put the denominator of the transfer function G_{conxC} equal to zero for determine of AMB stability. When the behavior of the AMB system is to be stable, then the real components of the roots must be negative.

The control part could be split into control logic, measurement and communication system. Logic and control functions as well as analog to digital conversions and service or calibration

communication are provided by the DSP controller.

We can say that controlled system generally contains the magnetic part and power electric part. Inverter produces the three-phase currents according to the PWM control signals. The actual currents are measured by Hall sensors like a feedback for controllers. Magnetic field of the stator coils effects position of the rotor, which is measured by inductive sensors. Deviation of the rotor is a second feedback for the controlling part. The flow diagram in Fig. 26 shows how the system could be split into function blocks.

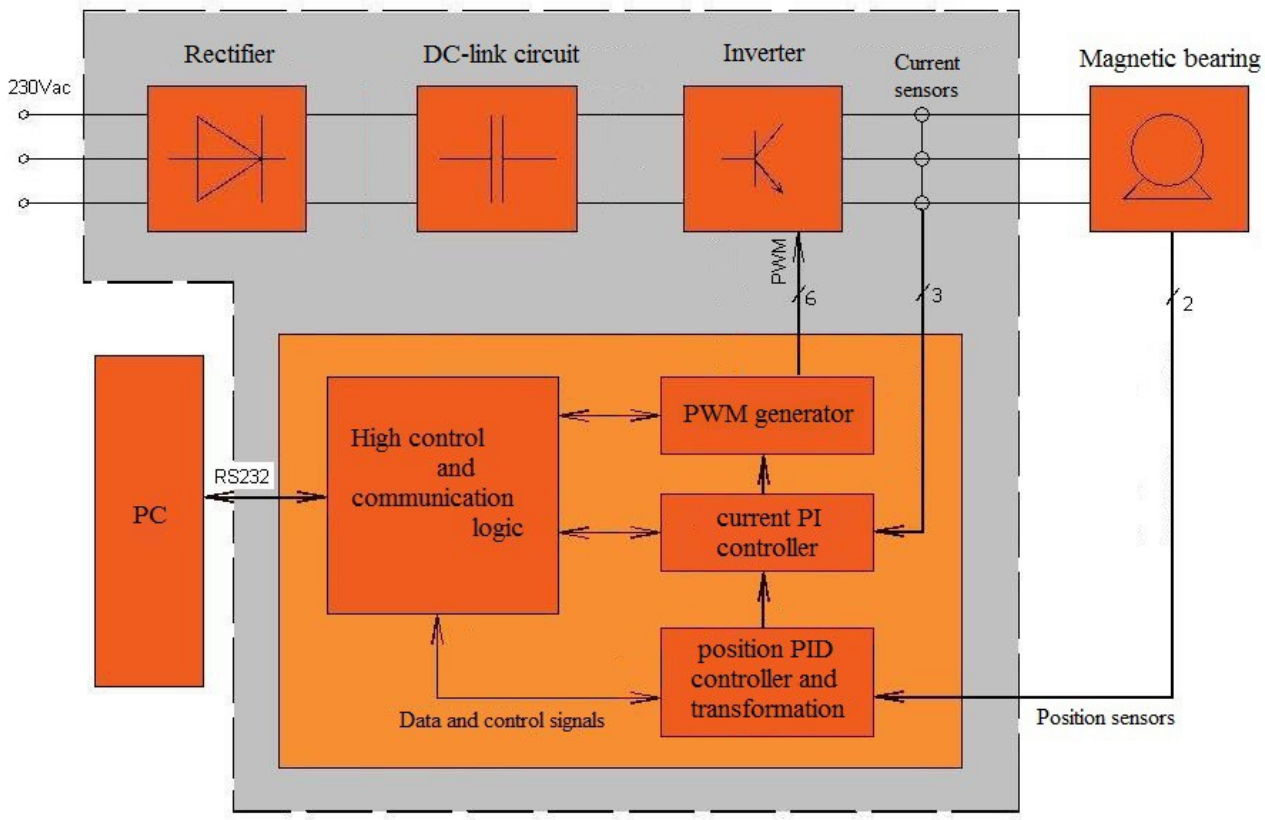

Fig. 26: Function diagram

The control winding position placement is in 3-axes configuration, but the position sensors are 2-axes. Therefore the control current has to be transformed by Park and Clarke transformation. [16]

The controlling block consists of two parts. First one, which is responsible for the position stabilization, contains two PID controllers for control of the actual rotor position in two axes. Output of those controllers, two-phase currents, is in the next step an input to the second controlling part – current controller. In this logic block the required currents have to be transformed from the two- to three-phase system, compared with the actual measured current values and controlled by two PI controllers. Third phase current is not controlled directly, but it is a result of first two controls. The reason is that the stator winding is connected to star, so the currents have to keep the Kirchhoff's first circuit law Eq. (55).

$$I_1 + I_2 + I_3 = 0 \tag{55}$$

Action signals are the output of whole controlling system affecting the inverter to produce the required phase currents. In our case, the action signals are represented by the PWM pulses on

the gate input of the inverter power semiconductors.

4 Standard ISO 14839

All active magnetic bearings, used in practical applications, should keep standard ISO14839, Mechanical vibration - Vibration of rotating machinery equipped with active magnetic bearings. It consists of four parts [7]:

- ISO 14839-1 Vocabulary
- ISO 14839-2 Evaluation of vibration
- ISO 14839-3 Evaluation of stability margin
- ISO 14839-4 Technical guidelines (FDIS)

4.1 Evaluation of vibration

Second part of the standard sets out general guidelines for measuring and evaluation rotating machinery equipped with active magnetic bearings.

As shown in Fig. 27, the displacement transducers are oriented in *x* and *y* axes at each radial bearing. Measurement should be done at the rated rotation speed. The signal from the transducers indicates the rotor journal position, consisting of the DC part (eccentricity) and AC part (vibration orbit) as shown in Fig. 28.

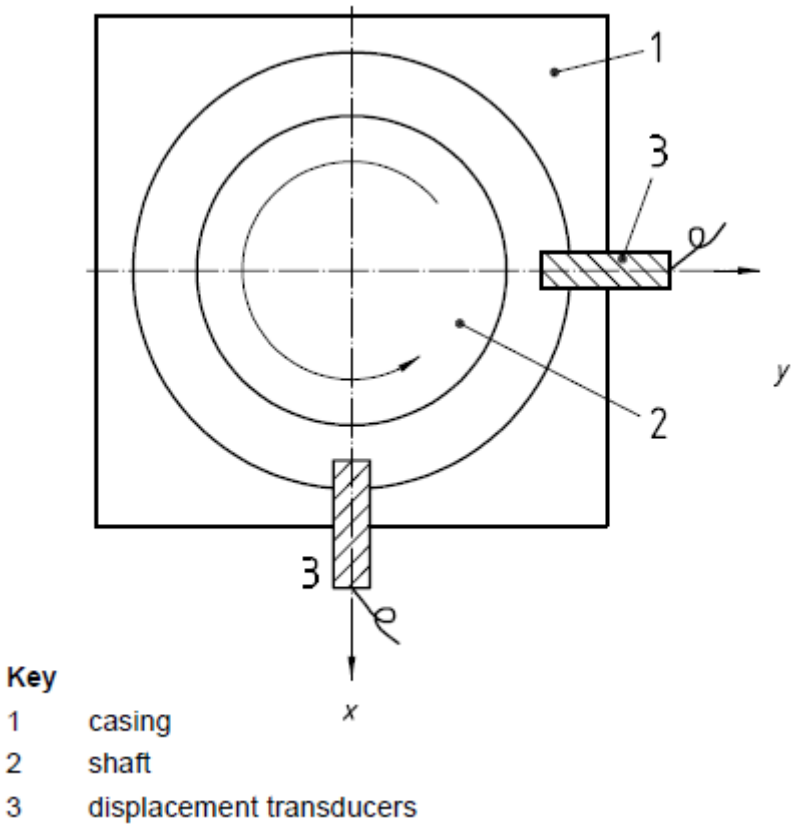

Fig. 27: Displacement transducers [7]

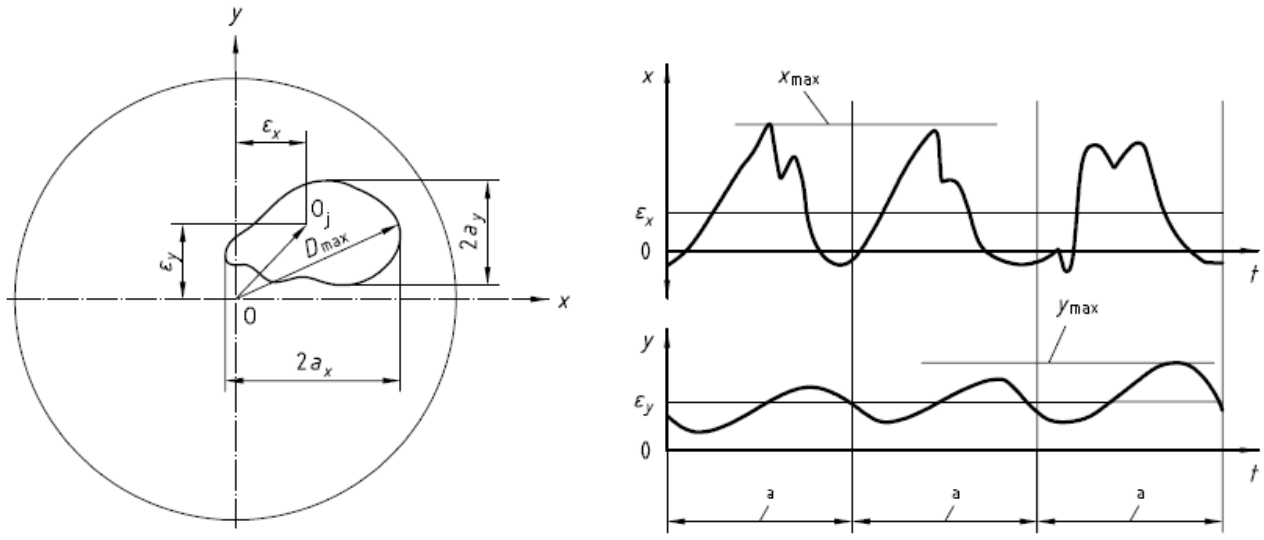

a) Orbit

b) Vibration time history

a the vibration orbit amplitude

t the time

ε the eccentricity from the clearance centre

[a] Time for one revolution.

Fig. 28: Shaft orbit and vibration time history [7]

The maximum displacement of the rotor from the clearance center of the radial AMB (desired D_{max}) can be calculated as Eq. (56).

$$D_{max} = \max\left[\sqrt{x^2(t) + y^2(t)}\right] \tag{56}$$

Reliable operation of the AMB machines requires to avoid contact between rotary and stationary parts of a machinery. The minimum radial clearance C_{min} can be defined by the minimum gap when statically moving the rotor in any radial direction. The criterion range is split into 4 zones:

Zone A: The vibratory displacement of commissioned machines would normally fall within this zone.

Zone B: Machines with vibratory displacement within this zone are normally considered acceptable for an unrestricted long-term operation.

Zone C: Machines with vibratory displacement within this zone are normally considered unsatisfactory for a long-term continuous operation. Generally, the machine may be operated for a limited period in this condition until a suitable opportunity arises for a remedial action.

Zone D: Vibratory displacement within this zone is normally considered to be sufficiently severe to cause damage to the machine.

The corresponding zone table for magnetic bearings, established from experiences of international community, is given in Tab. 3 and the corresponding graphical descriptions are provided in Fig. 29. [7]

Zone limit	Displacement D_{max}
A/B	$< 0{,}3\ C_{min}$
B/C	$< 0{,}4\ C_{min}$
C/D	$< 0{,}5\ C_{min}$
NOTE C_{min} is the minimum value of radial or axial clearance between rotor and stator.	

Tab. 3: Zone limits for vibration criteria [7]

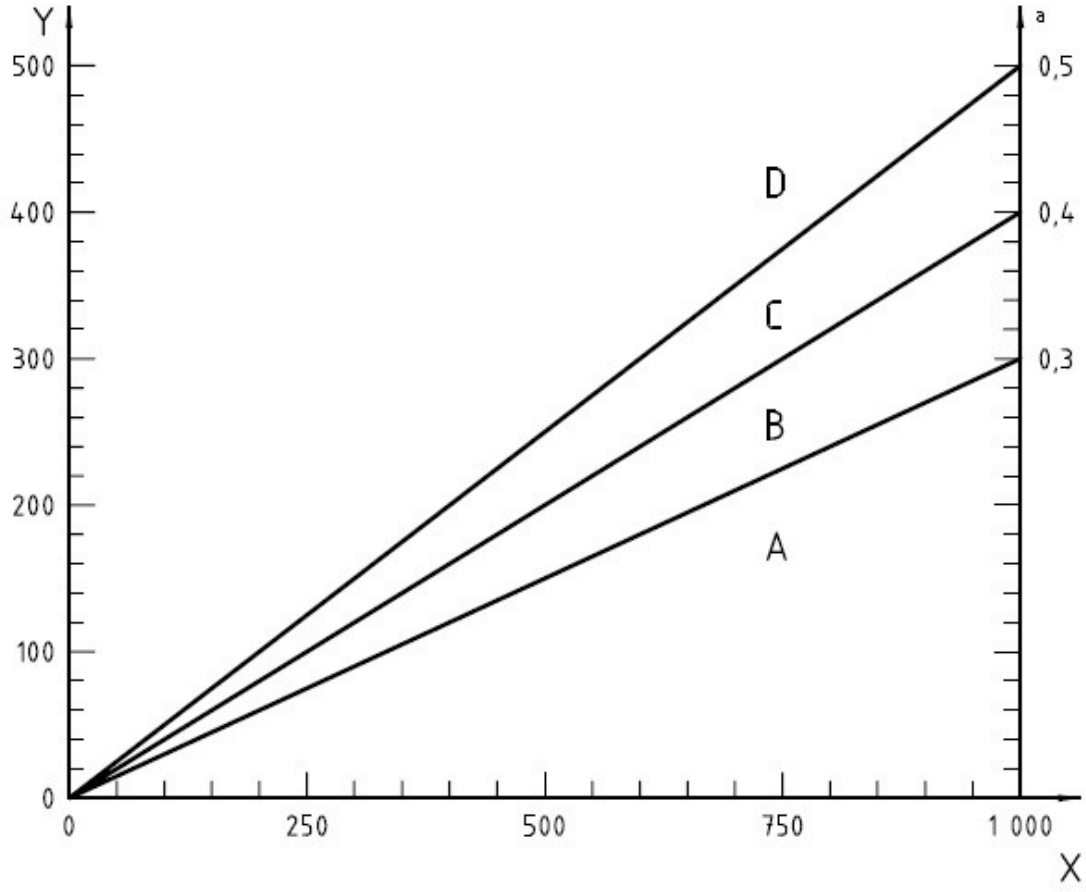

Key

X minimum radial clearance, C_{min}, in micrometres

Y maximum peak displacement, D_{max}, in micrometres

[a] Ratio D_{max}/C_{min}.

Fig. 29: Zone limits for vibration criteria [7]

4.2 Evaluation of stability margin

Third part of the ISO14839 specifies a particular index to evaluate the stability margin, delineates the measurement of this index and defines evaluation criteria. The target of measurement is to find transfer functions of the magnetic bearing system (control and controlled part) for all operation axes. The transfer function could be in general measured as a response to the unit jump (using specific hammer in our case) or by measuring the feedback of the injected error signal. Second option takes more time for measurement, but it does not really require special equipment – control unit of the magnetic bearing could be used for data logging. The data are computed later on.

This method is also described in the standard.

The closed control loop, used in our case, is similar to Fig. 30. An excitation $E(s)$ is injected into a certain point of the closed-loop network as a error signal. The signal has harmonic character and the frequency of it is defined. The response signals V_1 and V_2 are measured for each frequency directly after and before the injection point, respectively. The ratio of these two signals in the frequency domain provides an open-loop transfer function, G_O, with $s = j\omega$, as shown in Eq. (57). The closed-loop transfer function, G_C, is measured by the ratio shown in Eq. (58).

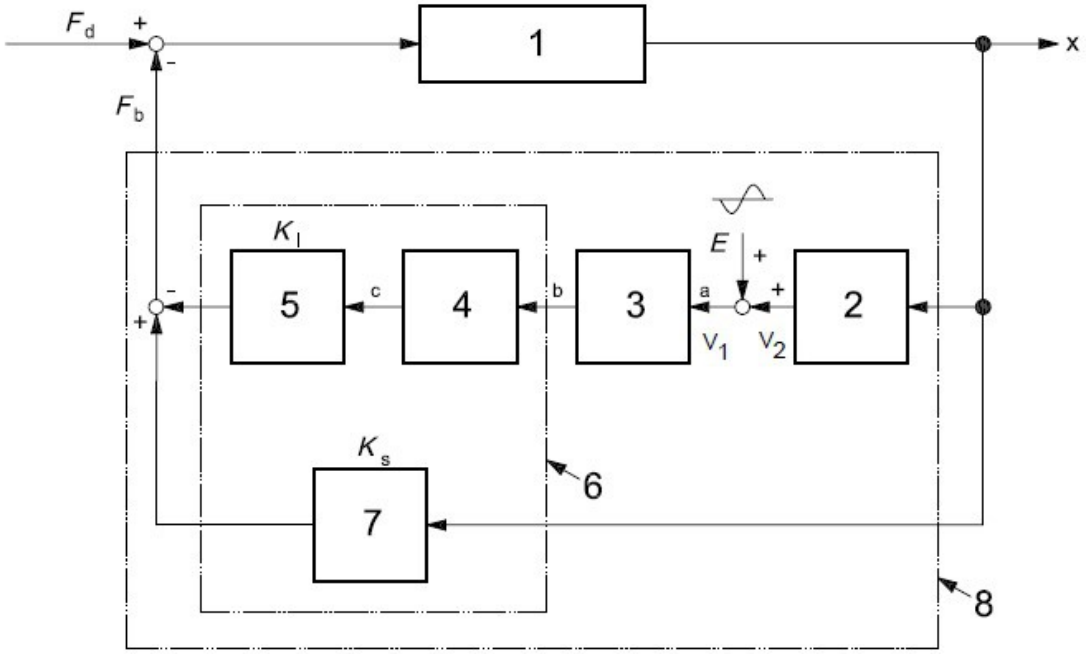

Key

1	mechanical plant rotor	E	excitation signal	a	Sensor signal.
2	position sensor, expressed in V/m	F_b	AMB force, expressed in newtons	b	Control signal.
3	AMB controller, expressed in V/V	F_d	disturbance force, expressed in newtons	c	Control current.
4	power amplifier, expressed in A/V	K_i	current stiffness, expressed in newtons per ampere		
5	electromagnet, expressed in N/A	K_s	negative position stiffness, expressed in newtons per metre		
6	AMB actuator	x	displacement, expressed in metres		
7	negative position stiffness, expressed in N/m				
8	AMB				

Fig. 30: Block diagram of an AMB system [7]

Note that this definition of the open-loop transfer function is very specific. Most AMB systems have multiple feedback loops (associated with, typically, five axes of control) and testing is typically done with all loops closed. Consequently, the open-loop transfer function for a given control axis is defined by Eq. (58) with the assumption that all feedback paths are closed during this measurement. This definition is different from the elements of a matrix open-loop transfer function defined with the assumption that all signal paths from the plant rotor to the controller are broken.

$$G_o(s) = -\frac{V_2(s)}{V_1(s)} \tag{57}$$

$$G_c(s) = -\frac{V_2(s)}{E(s)} \tag{58}$$

The sensitivity function, defined by Eq. (59), provides a simple way of the maximum magnitude construction and it is easy to calculate.

$$G_s(s) = \frac{V_1(s)}{E(s)} \tag{59}$$

Both transfer functions (open and closed loop) could be displayed in the Bode or Nyquist plots. Moreover, the Bode plot of the sensitivity function is used for stability diagnostic.

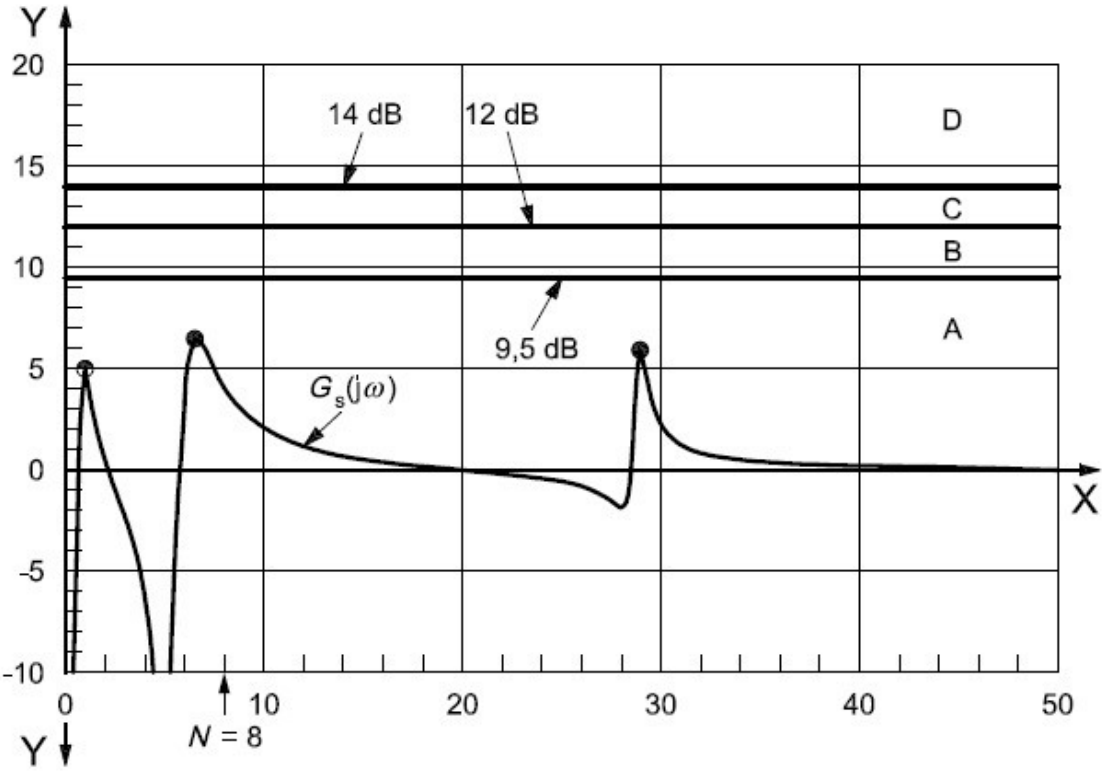

Key

X non-dimensional rotational speed

Y sensitivity gain and zone limits, expressed in decibels

A, B, C, D stability zones

N rated non-dimensional speed

Fig. 31: Evaluation of stability margin Gs [7]

For evaluation of the stability margin, zone limits are given in Tab. 4. Example of evaluation is shown in Fig. 31 as a Bode plot. The criterion range is split into 4 zones:

Zone A: The sensitivity functions of newly commissioned machines normally fall within this zone.

Zone B: Machines with the sensitivity functions within this zone are normally considered acceptable for an unrestricted long-term operation.

Zone C: Machines with the sensitivity functions within this zone are normally considered

unsatisfactory for a long-term continuous operation. Generally, the machine may be operated for a limited period in this condition until a suitable opportunity arises for a remedial action.

Zone D: The sensitivity functions within this zone are normally considered to be sufficiently severe to cause damage to the machine. [7]

Zone	Peak sensitivity	
	Level	Factor
A/B	9,5 dB	3
B/C	12 dB	4
C/D	14 dB	5

Tab. 4: Peak sensitivity at zone limits [7]

5 Realization of hybrid magnetic bearing

An important part of this project is focused to practical realization of the hybrid magnetic bearing with a new electric part and to testing it consequently. The magnetic part was already constructed in the CTU laboratory, but it wasn't really tested. Only a simple equipment was used for a basic tests – the electrical part consisted of several laboratory inverters, rectifiers and universal circuit boards and the whole system was controlled by the Freescale controller DSP56F805 on the standard evaluation board.

This chapter describes the final realization of the completed magnetic bearing. The control and power electric systems will be replaced and adapted to the existing magnetic part.

5.1 Magnetic part

The real PM magnetic bearing was intuitively designed, constructed and produced in the years 2001 – 2003. The basic parameters of this PM bearing are:

shaft diameter	d_{shaft}	*80 mm*	*i.e.*	*0,08 m*
inner diameter of PM ring	d_{in}	*165 mm*	*i.e.*	*0,165 m*
outer diameter of PM ring	d_{out}	*210 mm*	*i.e.*	*0,210 m*
length of magnet pol	l_m	*18 mm*	*i.e.*	*0,018 m*
length of PM ring	l_{PM}	*8 mm*	*i.e.*	*0,008 m*
length of air gap	δ_0	*0,5 mm*	*i.e.*	*0,0005 m*
flex density in air gap $B_{\delta 0}$	*0,5 T*			
flex density of PM B_{PM}	*0,385 T*			
coercive PM MMF	${}_BH_C$	*270 kA/m*		
PM permeability	μ_{PM}	$1{,}43*10^{-6}$ *H/m*		
vacuum permeability	μ_0	$4\pi*10^{-7}$ *H/m*		

We obtain from Eq. (15) for these real values into Eq. (60)

$$\frac{B_{PM}}{B_r} = 1 - \frac{1{,}43*10^{-6}}{4\pi*10^{-7}} * \frac{2*0{,}5}{l_{PM}} * \frac{0{,}5}{0{,}385} = 1 - \frac{1{,}47}{l_{PM}} \tag{60}$$

The diagram of the function $B_{PM} / B_r = f(l_{PM})$ is in Fig. 32. The real value of the ratio B_{PM} / B_r must be higher than the zero. Therefore the length l_{PM} must be longer than 1,5 mm.

The length of the real PM radial AMB in CTU-FEL lab is $l_{PM} = 8\ mm$. For this value we

obtain from equation (60) the value of the ratio $B_{PM} / B_r = 0{,}816$.

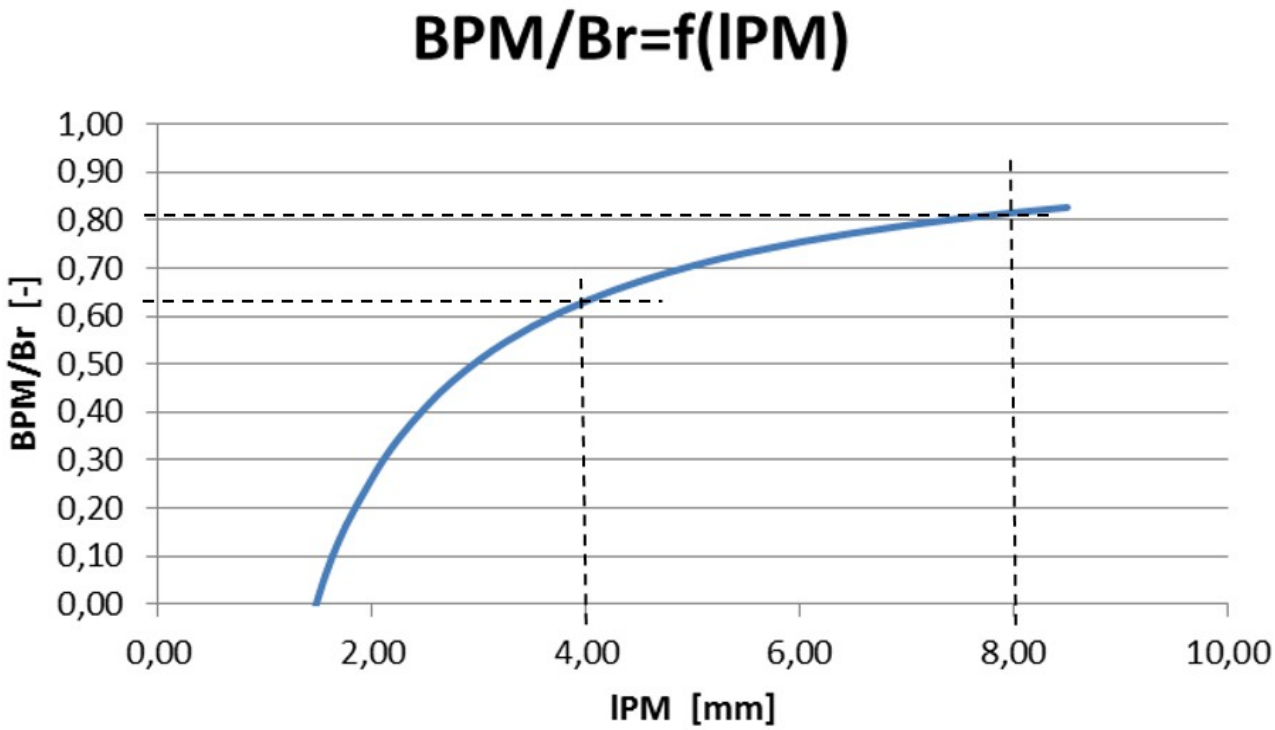

Fig. 32: Diagram of the function $B_{PM} / B_r = f(l_{PM})$

Similar diagram of the function $B_{PM} / B_{\delta 0} = f(l_{PM})$ is in Fig. 33.

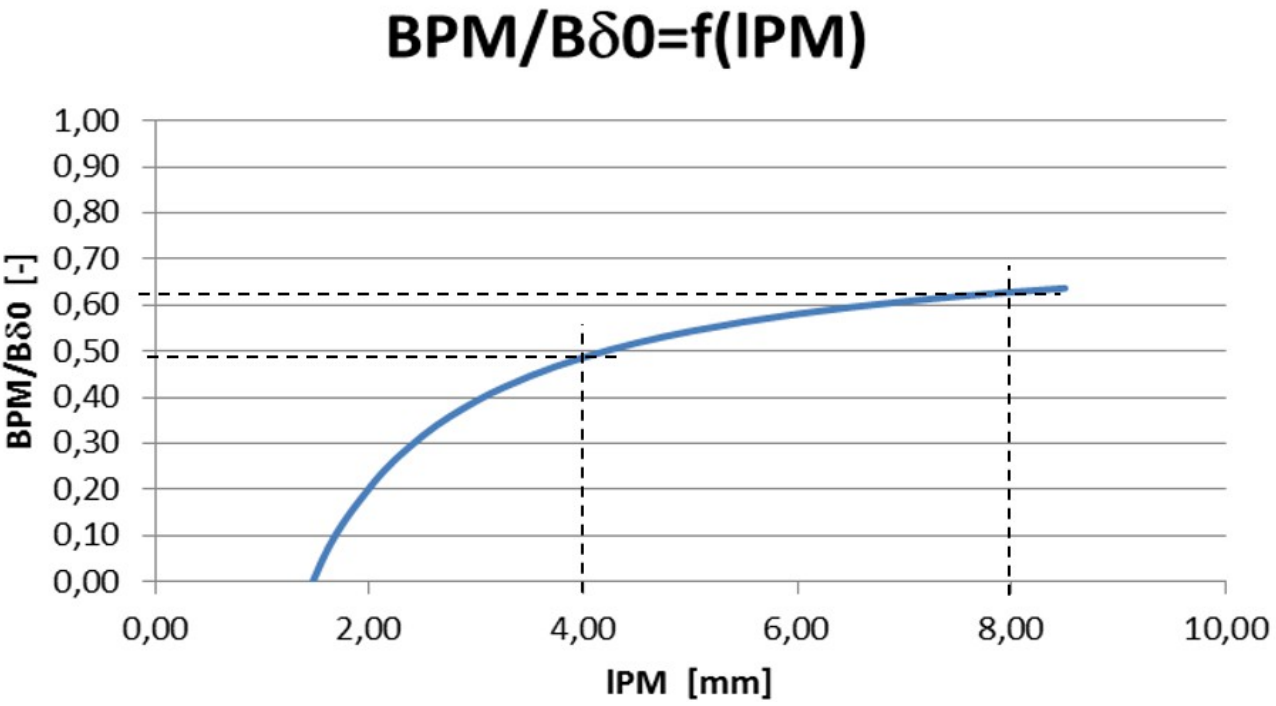

Fig. 33: Diagram of the function $B_{PM}/B_{\delta 0} = f(l_{PM})$

A recommended value of the ratio B_{PM} / B_r is about 0,6 Then the "recommended" value of l_{PM} from Fig. 31 is $l_{PM} = 4\ mm$. Then the MMF of PM is defined by Eq. (61).

$$F_{PM} = {}_B H_C * l_{PM} = 270 * 4 = 1080\ At \tag{61}$$

It is seen that the "recommended" PM ring length *4 mm* is about one half of the real length on the PM radial AMB in the CTU-FEE lab.

The inner diameter of the real PM ring d_{in} = *165 mm*. Equation (22) allows to determine the value of the PM ring height h_{PM}. We obtain for values d_{in} = *165 mm*, l_m = *18 mm*, k_m = *0,6* k_B = *0,54*, d_{shaft} = *80 mm*.

$$h_{PM} = -\frac{165}{2} + \sqrt{\left(\frac{165}{2}\right)^2 + 18 * \frac{0{,}6}{0{,}54} * 80} = 9{,}28 \text{ mm} \tag{62}$$

The diameter d_{out} is given by the following equation (63).

$$d_{out} = d_{in} + 2 * h_{PM} = 165 + 2 * 9{,}28 = 183{,}56 \text{ mm} \tag{63}$$

A real outer diameter of the PM radial AMB in CTU-FEE lab is 210 mm. It is seen that the optimal outer diameter of PM ring 183,56 mm is 27,44 mm lower as the real value.

The area of the PM ring is:

$$S_{PM} = \frac{\pi}{4}\left(d_{out}^2 - d_{in}^2\right) = \frac{\pi}{4}\left(183{,}44^2 - 165^2\right) = 5046 \text{ mm}^2 \tag{64}$$

The area of the magnet poles is defined by Eq. (65):

$$S_m = \pi * d_{shaft} * l_m * k_m = \pi * 80 * 18 * 0{,}6 = 2714 \text{ mm}^2 \tag{65}$$

Finally we calculate NI_0 of the PM ring from following Eq.(66) for $B_{0\delta}$ = *0,5 T*, δ_{g0} = *0,5 mm*.

$$NI_0 = \frac{B_{0\delta} * 2 * \delta_{g0}}{\mu_0} = \frac{0{,}5 * 2 * 0{,}0005}{4\pi * 1e-7} = 398 \text{ } At \tag{66}$$

5.1.1 Stator winding

The conventional homopolar active magnetic bearing in Fig. 4 has four separated windings each with a number of turns N_{1pol} that are located on four C core magnets. Each winding is supplied from own separated power electronic amplifier.

When PMs are used on the place of the bias current I_0 MMF then each couple of magnets in the same axis has four coils (see Fig. 16) and these coils can be connected in series and supplied with only one control current i from only one four quadrant power electronic amplifier. Two perpendicular couples of magnets produce two different MMFs of currents i_x, i_y in two perpendicular axes *x, y*. We will suppose that the maximum value of both currents i_x, i_y is equal to $\pm I_0$. One end of one couple of magnets contains two coils each with N_{1pol} turns. The maximum resulted MMF of these two coils is $2 * N_{1pol} * I_0$ and has to be equal to the value of MMF_{PM} from Eq. (54) i.e. *398 At*.

It is known from the theory of electric machines that these two MMFs Ni_x and Ni_y produce in the constant air gap only one common magnetic flux Φ. Its position in the air gap is given by instantaneous values of the currents i_x, i_y, defined by Eq. (67).

$$\left|\hat{\Phi}\right| = k_{\Phi} * \sqrt{i_x^2 + i_y^2}$$
$$\varphi = \arctan \frac{i_y}{i_x} \tag{67}$$

where k_{Φ} is factor of relation between the magnetic flux vector amplitude $\boldsymbol{\Phi}$ and the control current i.

Conventional AC electric machines use three phase winding on their stators. This three phase winding is supplied from three current sources i_a, i_b, i_c and these currents must fulfill the condition in Eq. (55) – no neutral current.

Following mathematical equations allow to transform two currents i_x, i_y that flow through two coils in perpendicular axes x, y to three currents i_a, i_b, i_c that flow through three coils in axis a, b, c. The axes are shifted by 120 degrees each other.

$$i_a = \frac{2}{3} i_x \qquad i_b = -\frac{1}{3} * i_x + \frac{1}{\sqrt{3}} * i_y \qquad i_c = -\frac{1}{3} * i_x - \frac{1}{\sqrt{3}} * i_y \tag{68}$$

The resulted current vector $\hat{I}$ is equal to Eq. (69).

$$\hat{I} = i_a + \left(-\frac{1}{2} + j\frac{\sqrt{3}}{2} \right) * i_b + \left(-\frac{1}{2} - j\frac{\sqrt{3}}{2} \right) * i_c = \frac{3}{2} * i_a + j\frac{\sqrt{3}}{2} * \left(i_b - i_c \right) =$$
$$= i_x + j * i_y \tag{69}$$

It is seen that the current vector $\hat{I}$ is the same for both axes systems.

It is known from theory of electric machine that the resulted MMF of three phase winding F_W is possible to calculate from following Eq. (70).

$$F_W = \frac{m * \sqrt{2}}{\pi} * \frac{N * I_{RMS} * k_w}{p} \tag{70}$$

where m is number of phases
N is number of one phase turns
I_{RMS} is RMS value of the current in on phase
k_w is winding factor
p is number of pole pairs

We propose to use three phase two pole winding. Then $m = 3$, $p = 1$ and

$$F_W = \frac{3 * \sqrt{2}}{\pi} * \frac{N * I_{RMS} * k_w}{1} = 1{,}35 * N * I_{RMS} * k_w \tag{71}$$

The two pole winding has long interconnections between layers in slots. Therefore, it is recommended to use short-pitch coils with a small winding Factor k_w about 0,8. Now it is possible to calculate value of *(NI)* by Eq. (72).

$$F_W == 1{,}35 * N * I_{RMS} * 0{,}8 = 1{,}08 * NI_{RMS} = 1{,}08 * N \frac{I_{\mathrm{mod}}}{\sqrt{2}} = 0{,}764 * NI_{\mathrm{mod}} \tag{72}$$

where I_{mod} is modul of the vector $\hat{I}$.

Following terms are used by a design of the stator winding:

- Number of slots N_{slot}
- Number of wires in one slot u
- Number of parallel branches a
- Number of one winding turns N
- clear cross section of one wire q_{Cu} [mm^2]
- clear cross section of wires in one slot Q_{Cu} [mm^2]
- current density of stator winding σ_{Cu} [A/mm^2]

It is valid

$$N = \frac{N_d}{2 * m} * \frac{u}{a} = \frac{N_d * u}{2 * 3 * 1} = \frac{N_d * u}{6} \tag{73}$$

$$Q_{Cu} = u * q_{Cu} \tag{74}$$

$$\sigma_{Cu} = \frac{I_{\mathrm{mod}}}{a * q_{Cu}} = \frac{I_{\mathrm{mod}}}{q_{Cu}} \tag{75}$$

By combining these definition equations, we can modify the relationship for the pure conductor cross section Q_{Cu} i to Eq. (76).

$$Q_{Cu} = \frac{6 * N}{N_d} * \frac{I_{\mathrm{mod}}}{\sigma_{Cu}} \tag{76}$$

In the next design, we will use the typical values for electric machines windings:

– We select the minimum "reasonable" number of slots per pole and phase q = 2. Then the number of slots $N_d = m * 2p * q = 3 * 2 * 2 = 12$.
– We select the typical current density value for the low intensively cooled windings $\sigma_{Cu} = 3$ A/mm^2.
– We estimate filling of the slot as $k_{fill} = 0{,}4$ for wire winding.

Then the net needed winding cross section Q_{Cu} in one slot will be:

$$Q_{Cu} = \frac{6}{12 * 3} * NI_{\mathrm{mod}} = 0{,}16667 * NI_{\mathrm{mod}} \tag{77}$$

The value of NI_{mod} can be calculated from Eq. (72):

$$NI_{\mathrm{mod}} = \frac{F_W}{0{,}764} = \frac{NI_0}{2 * 0{,}764} = \frac{398}{2 * 0{,}764} = 261\ At \tag{78}$$

The value of NI_{mod} was determined as 26*1 At.* Finally we obtain:

$$Q_{Cu} = 0{,}166667 * 261 = 43{,}4 \ \text{mm}^2 \tag{79}$$

The cross-section of the slot is:

$$Q_{slot} = \frac{Q_{Cu}}{k_{fill}} = \frac{43{,}4}{0{,}4} = 108{,}5 \ \text{mm}^2 \tag{80}$$

The width of slot b_{slot} is:

$$b_{slot} = \frac{\pi * d_{shaft}}{N_{slot}} * (1 - k_m) = \frac{\pi * 80}{12} * (1 - 0{,}6) = 8{,}4 \ \text{mm} \tag{81}$$

The height of the slot h_{slot} is:

$$h_{slot} = \frac{Q_{slot}}{b_{slot}} = \frac{108{,}5}{8{,}4} = 13 \ \text{mm} \tag{82}$$

5.1.2 Comparison of some sizes from intuitive and propose design method

Both methods use identical values of following sizes:

d_{shaft}	80 mm
d_{in}	165 mm
l_m	18 mm
δ_{g0}	0,5 mm
$B_{\delta 0}$	0,5 T
B_r	0,385 T
${}_BH_C$	270 kA/m

Results of		intuitive design method	proposed design method
outer diameter of PM ring	d_{out}	*210 mm*	*183,56 mm*
length of PM ring	l_{PM}	*8 mm*	*4,00 mm*
height of PM ring	h_{PM}	*22,5 mm*	*9,28 mm*
Volume of PM ring	V_{PM}	*424115 cm^3*	*162591 cm^3*

It is seen that new proposed design method gives reduced volume of PM ring to only (*162591 / 424115) = 0,383*.

The intuitive design method calculated with RPM values of currents, that is correct for variable currents in the stator winding and for rotated magnetic field. The PM radial AMB operates with standing magnetic field and therefore currents in coils are constant and therefore losses in different coils are different.

5.1.3 Realization

The real passive magnetic circuit consists of ferritic unites spread in the stator iron rings and rotor metal mass. It was used 18 permanent magnet elements along the stator circumference. For the material it was chosen FD25/27 with parameters:

Coercive force	${}_BH_C$	265/275	[kA/m]
Residual flux density	B_r	385-390	[mT]

Magnetic energy product BH_{max} 29 [kJ/m^3]

On the both sides of the stator magnetic circuits (both rings) a double-layer three-phase winding is placed. There are two times 70 turns with the area of the cross-section 0,25 mm^2 in each slot. According to the modified relation for magnetomotance of the multiphase winding the maximum current was calculated to 1,75 A, corresponding current density is 7,03 A/mm^2. This value is too high for the permanent flux, so the maximum current is a peak value and it should not be driven continuously. The real magnetic part is shown in Fig. 34. The maximum eccentricity is limited by the rolling bearing to ± 0,25 mm. [16]

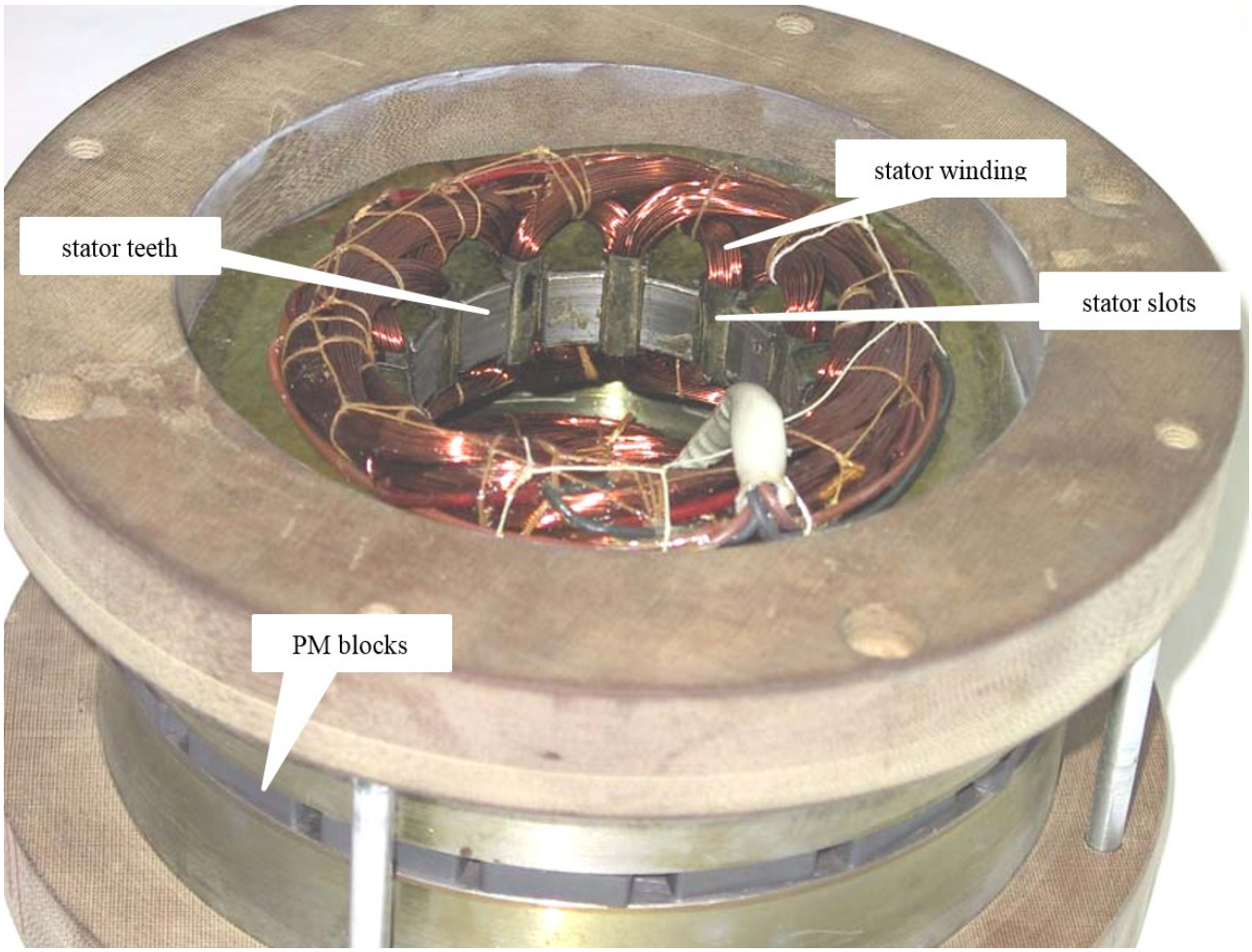

Fig. 34: View on the opened PM bearing in the CTU-FEE laboratory [15]

5.1.4 Requirements for power inputs

The stator windings are connected to star configuration, like a standard induction machine. Therefore, the power supply, which will control the bearing, has to be able to produce three-phase current. One of the additional outputs of this project will be a demonstration that the hybrid magnetic bearing could be realized similar as a real industrial product. So, the whole inverter system should be small, complex and easy to use. Electrical requirements are listed bellow.

Input voltage: 230 Vac
Maximum input power: 1 kW
Maximum output current: 3 x 2 A

5.2 Power electric part

The bridge of the action power transistors is the main part of the whole electrical circuit, but there is a lot of other devices supporting the bridge without which the system wouldn't work. The

final inverter is shown in Fig. 35. Diagrams are enclosed to this document in Appendix A and the layout and placing diagram is enclosed in Appendix B.

A power network is used for supplying the system, but operating voltage is DC. The full-wave rectification is ensured by KBU1005. This IC is designed to transfer current up to 10 A, which is more than enough for our application. The overlarge semiconductor was chosen for its unnecessity of heat sink to save place and low price. Intermediate energy is stored in one electrolytic capacitor of 450 μF which represents a DC-link circuit. The capacitance value was chosen based on the experiences – it could be also changed in production optimization. A current limitation of the first capacitor charging is ensured by a positive thermistor (PTC). The thermistor has to be bridged by relay after the capacitor is charged. The relay signal comes from the control system.

The DC-link as well as all power circuits have direct connection to the input grid. That makes work and development on this device dangerous. Especially the bridge heat sinks could be touched accidentally. Therefore it is strongly recommended to use a separation transformer for supplying the inverter during the tests.

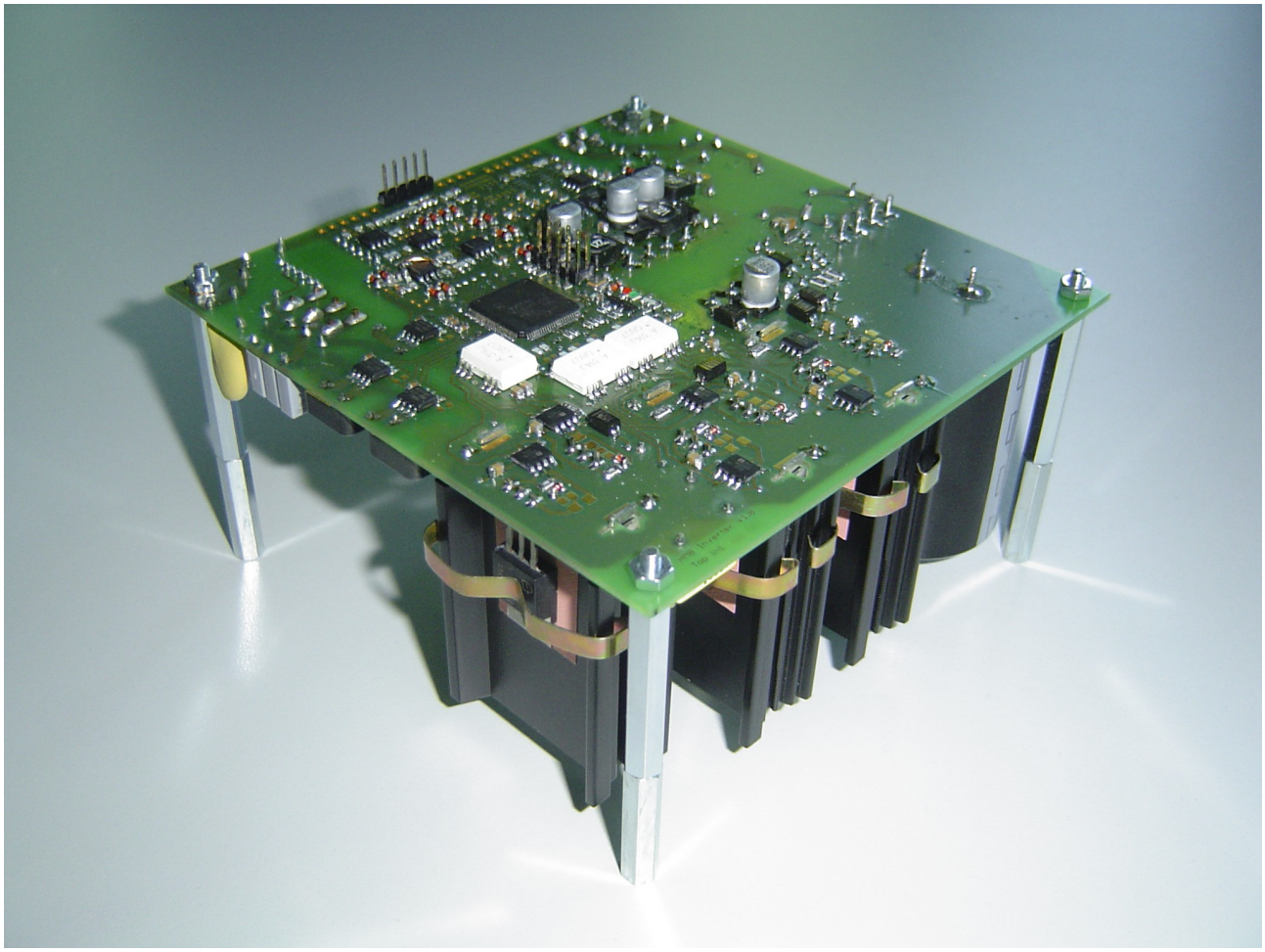

Fig. 35: Inverter [15]

The output LC filter and current measurement are also a part of the power electric circuit. Small integrated Hall current sensors are placed on the board (ACS712). Their measurement range is ± 5 A with 2,5 V offset and sensitivity 0,185 V/A. Low dimensions and price are their advantages too. Nevertheless, the output voltage range requires additional circuits for better measuring capability.

5.2.1 Bridge transistors and gate-drivers

As mentioned before, the three-phase bridge consists of 6 transistors. Infineon MOSFET type SPP20N60C3 was chosen for its power capability, construction simplicity and good price. These transistors have body diode implemented in their isolated package and they are able to transfer current of 20 A with $R_{DS(on)} = 0{,}19\ \Omega$. Of course, there is a lot of alternatives on the market in case of need in future.

The control signals, produced by DSP, are separated from the high-voltage part and the bridge by opto-couplers HCPL-314J. Here they are transformed to the driving voltage and power level by the MOSFET drivers MIC4420. These gate-drivers are fast and powerful enough to control bridge transistors. Their supplying is ensured by +15 V source on the HV side. Another trick comes for supplying higher three gate-drivers, since the high voltage difference doesn't allow 15 V to transfer the power. Therefore, the gate amplifier of the high MOSFET has to be supplied by a capacitor, which is charged by +15 V source through the low MOSFET or its body diode it the time when corresponding low part is conducting. That makes the voltage level of the bridge leg middle point equal to the ground. This charging system is called bootstraping and it requires a certain minimum value of the low part duty-cycle. In case when the low transistor is not conducting too long, the high bootstrap capacitor cannot be charged and corresponding transistor is not driven.

5.2.2 Bias power supply

A small power supply for internal logic and analog circuits is essential power electric part of all controlled electrical devices. Basically it is a DC/DC converter with a high-voltage input and several galvanic insulated low-voltage outputs.

In our case it is a small flyback converter with three separated output voltages. It is driven by the integrated circuit TOP244Y, high efficient, complex and flexible driver with integrated power transistor. Operation frequency of 132 kHz allows to use small transformer. The supply is able to produce power of around 10 W without additional cooling needs. The transformer provides galvanic separation for all control circuits, but it is still better to use the power separation transformer on the AC input for development safety purposes.

5.3 Control part

This chapter provides a complete overview of the control system. It starts with the low voltage control circuits and describes a software developed for the micro-controller and PC.

5.3.1 Control hardware

The most important device in control part is the digital signal controller TMS320F2801 produced by Texas Instruments company. This 32-bit processor was one of the first types from the family C28xx. It works on the clock frequency 100 MHz and operates with the fixed-point calculating logic. The whole controller family has also the fast 12-bit analog to digital converter (ADC), sophisticated pulse width modulator (PWM) and communication modules. Complete structure of the C28 processors is shown in Fig. 36. [17]

The requirements for two-level supplying voltage (peripheral level of 3,3 V and 1,8 V for the core) and 100-pin package make design a little more complicated. So the question of using a smaller, simpler and slower type of the same family comes up. But two important reasons for the C2801 processor was taken into consideration. At first this DSP is well known, easy to handle and to get. And opportunity of faster and more powerful controller for future possible applications is the second reason.

The rest of the control and low-power circuits are the operation amplifiers for measurement proposes, voltage controllers (3,3 V and 1,8 V) for DSP supplying, integrated circuit for CAN bus driving, small EEPROM memory and a lot of voltage dividers, current supporters and other passive

resistors and capacitors.

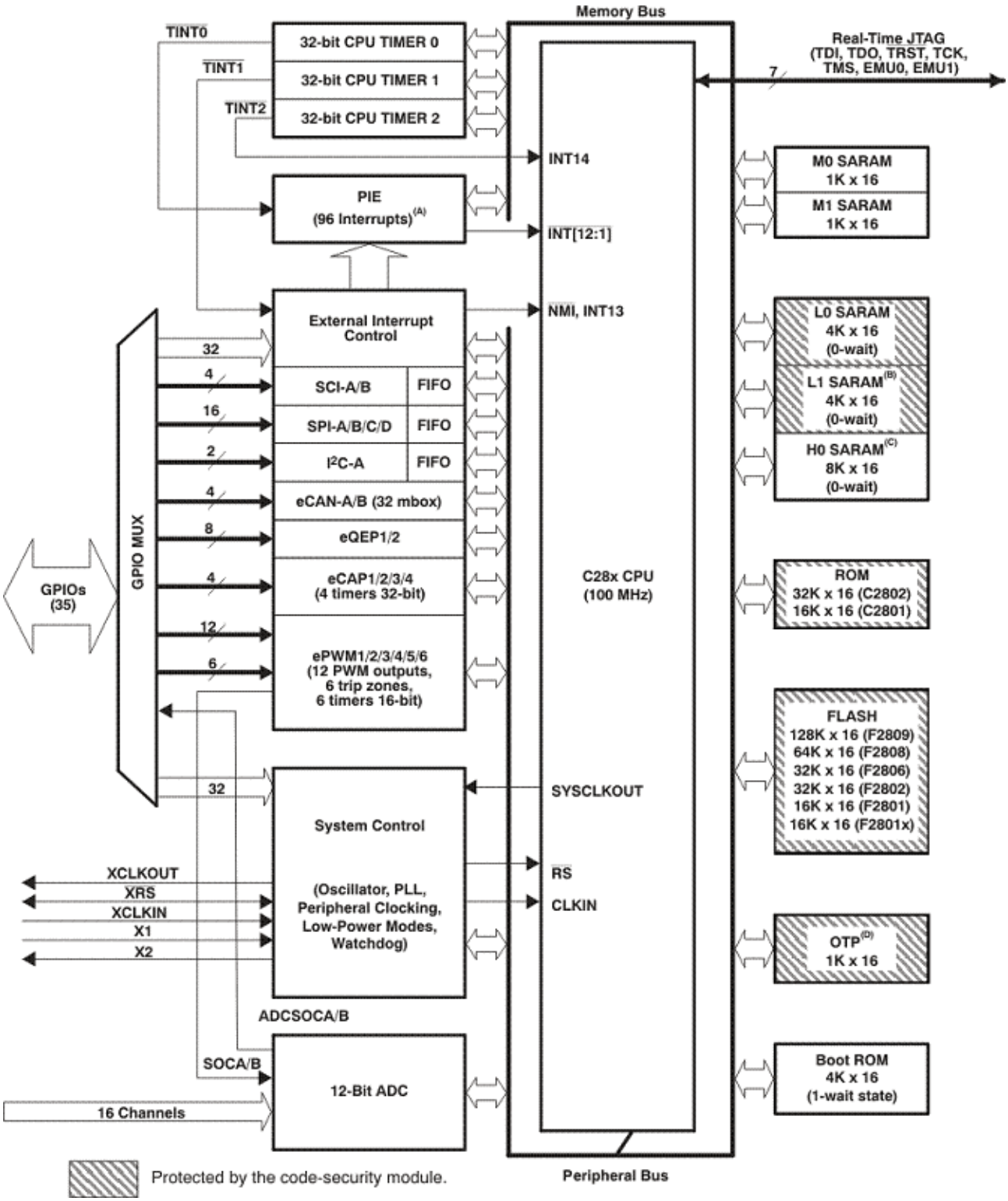

Fig. 36: Structure of C28 processor family [17]

The radial rotor stability requires real-time information about actual rotor position in x and y axes. Two inductive proximity sensors (Allen-Bradley 871C) transform information of the air gap between rotor and stator into the measurable electric voltage (Fig. 36). As shown in the figure, the resolution of the position measurement is 0,25 mm/V on the output of the sensors. The position signal connected to the AD converter of MCU has to be adapted by the voltage divider.

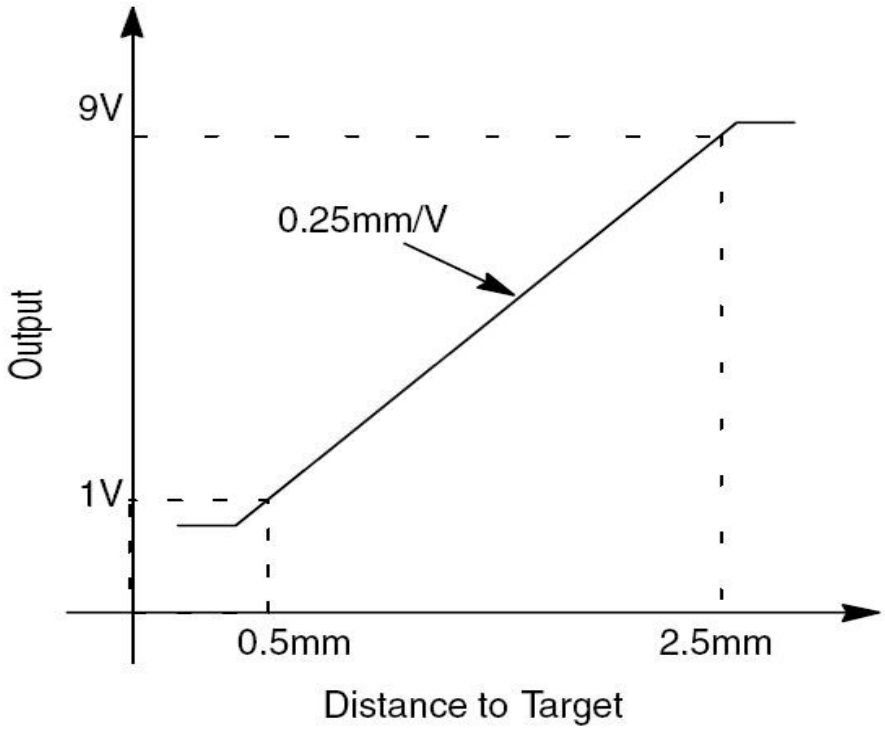

Fig. 37: Proximity sensor output relation [18]

5.3.2 MCU embedded software

An original designing tool was used for software development proposes. The Code Composer Studio v5.2 is a compiler from Texas Instruments, which provides good development interface and is available free of charge when limited used.

The software project refers to source files saved in the \HMBinv_code directory. The files could be split to two types: original controller functions and libraries (files with DSP280x_ …) and special project related files (HMBinv_ … and HMB_ComProtocol.h). Main function together with global variables definition is located in the HMBinv_main.c. The low level initialization routines are in HMBinv_init.c, interrupt service routines in HMBinv_isr.c, communication in HMBinv_com.c and special functions in the HMBinv_services.c. The file HMBinv_config.h contains configuration macros. Other macros and definitions for communication or setting and calculation purposes are located in corresponding header files.

The most important state-machine variables are called *Status_register* and *Fault_register*. Both are bit defined (the definition is set in ComProtocol.h file) and they are used for the low level control of the system. Start of the bridge could be requested only when the standby bit is set and no power operations could be enabled when any fault bit (in Fault_register) is set.

Real time variables are related to control frequency of 50 kHz. All those variables are defined as unsigned 16bit integers and their overflowing is handled by the *RealTimeUnit* function. Control variable *RT_base* is increased at each PWM cycle, that means one step is 20 µs. The variable is cleared after each 50 ms. In that moment *RT_s05* variable is increased. Limitation for 50 ms variable is 30 minutes, where *RT_30min* increases. The last timer does not have a limitation, because that long time period is not used for any measurement. So it can happily overflow after 3 years 8 months and 25 days of perfect functional running.

The control software consists of 3 basic parts: *initialization* of internal modules, slow *background loop* for calculations which are not time critical and *interrupts* for fast response functions and current control.

The doxygen commentary style is used for code documentation additionally to the in-line comments. The complete source code is enclosed to this document on CD.

5.3.2.1 Initialization

Basic initialization and configuration functions are called on the beginning of the main function. The low level chip initialization, memory setting and interrupt definitions are set at first. Next settings are listed below:

- *GPIO initialization*; digital inputs and outputs definition
- *PWM initialization*; power driving outputs are defined as three complementary pairs running on frequency 50 kHz with dead-time 500 ns
- *ADC initialization*; 13 analog inputs are periodically converted to digital value as fast as possible
- *SCI initialization*; UART communication is specified as 9600 baud, 8 bits data, 1 stop bit, no parity
- *I2C initialization*; communication with external EEPROM data memory (type 24C16) is ensured by I2C bus running at 500 kHz
- *WatchDog initialization*
- *Temperature look-up table calculation*

The temperature table mentioned in the last point is calculated after each start or restart of the controller for better variability of the resistor connection. Calculation includes the thermal dependency of NTC with relation to the connected resistors and supplied voltage based in Fig. 38 and Eq. (83).

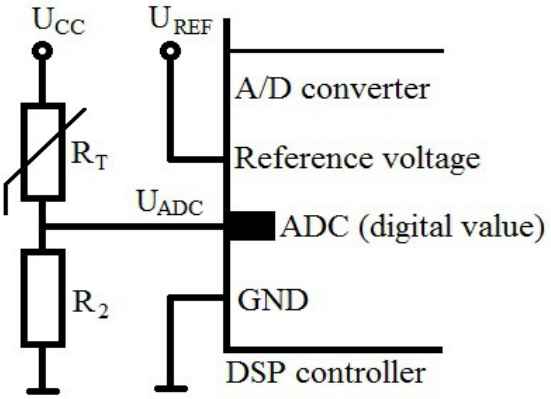

Fig. 38: Temperature sensor connection

$$R_T = R_N * e^{-B\left(\frac{1}{T_N} - \frac{1}{T}\right)} \tag{83}$$

$$T = \frac{B * T_N}{T_N * \left[\ln\frac{R_2}{R_N} + \ln\left(\frac{U_{CC}}{U_{REF} * ADC} - 1\right) + B\right]} \quad [K] \tag{84}$$

Final calculation of the measured temperature is in Eq. (84). For time-saving purposes the temperature is not calculated after each reading of the internal analog-to-digital converter register, but the register value refers to the conversion table. The table covers the whole converter range, so no other complicated calculation is necessary.

5.3.2.2 Background loop

The main function contains “endless” loop for the background logic and calculations. It is placed just after initialization and it is used for slow functions. The background loop period is not fixed, but its frequency cannot be lower than 10 kHz and most of the time it is over 20 kHz. Fast logic (50 kHz output current control) runs in the interrupt service routine independently to the background functions.

The most important functions are *Register_Observer*, where the state-machine of the system is handled (*Status_register* controlling), and *Position_controller* contains the position PID control. The position PID controller runs in 100 us period (in frequency of 10 kHz) and its input uses filtered value of the position sensors (axis X and Y). Two-axes currents alpha and beta represent the controller output. PID parameters were experimentally found and tuned in the debugging communication mode. The position controller contains a stability measurement unit, where the sinusoidal error signal (table *SM_error[]*) could be injected to the actual measured position value. The error signal has specified period by *SM_period*. This value could be changed by communication. When the stability measurement is required, one or more periods of error signal is added to control chain and result values are saved in the tables *SM_signal_V1[]* and *SM_signal_V2[]*. Both of the output tables could be transmitted by the UART interface to the computer as a result of the stability measurement for the actual error frequency (defined by *SM_period*).

The slow calculation, like the input voltage RMS measurement or filtration, is executed in the *Common_calc*() function as well as the automatic offset calibration, which takes place in the beginning of the software start (after booting).

The next function is the debug or service communication observer. Only one of those two procedures is compiled, as requires *DEBUG_TERMINAL* macro definition in *HMBinv_config.h* file. A simple hyper terminal is used for the debugging communication, but the graphical user interface is based on the communication protocol described in the *HMB_ComProtocol.h*. The PC software is described in chapter 5.3.3.

Three parameters are saved in the external data memory: the required X and Y position values and series number. The parameters are loaded after each software start (by *Parameter_Loading* function) and saving is on demand (in *Parameter_Saving* function). Both procedures run in background loop without any interruption of any other software parts (as well as other background functions). The external EEPROM memory (type 24C16) is connected to the controller by I2C bus. The internal I2C communication module is handled by *I2C_Observer* function. The bus control is provided by the bit-defined *I2C_ObsCommand* variable. Detailed description is commented in the code.

Here are last two background function: The temperature guard sets the error flag in case of an over-temperature on one of three thermal sensors. It also clears the flag when temperature on all sensors is below the error level. The *RealTimeUnit* function handles the overflow actions of time related variables.

5.3.2.3 Interrupts

Only one functional interrupt is used for the bridge driving – it is Pwm1_isr, called on each start of the PWM counter. That means, the service routine is synchronized with the gate-driver pulses and it has constant period 20 μs. The current PI control is one of the main parts in this function as well as the ADC measurement and over current protection. The float chart of the control interrupt is shown in Fig. 39.

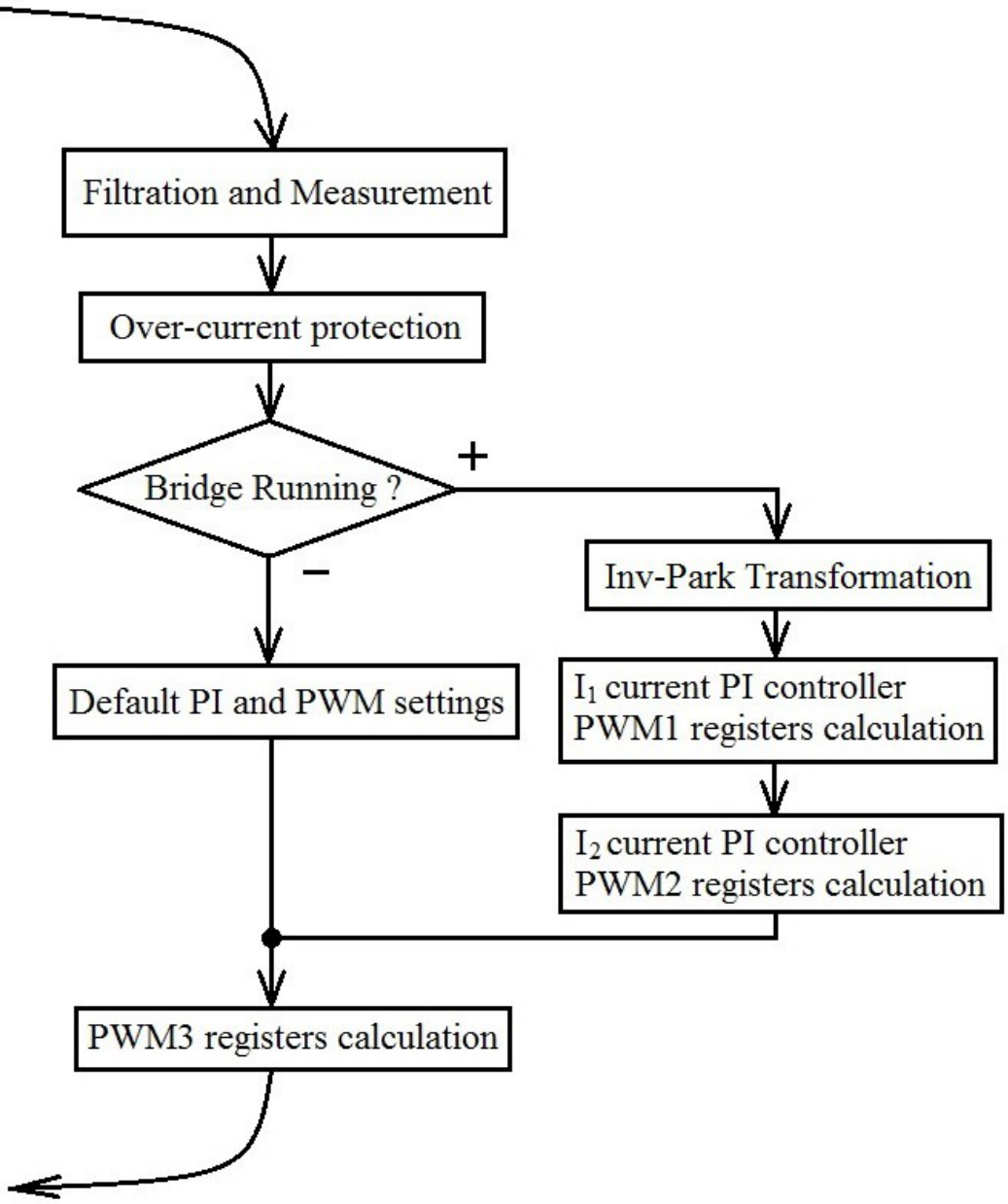

Fig. 39: Block diagram of controlling interrupt

The other interrupt routines are used for the series or I2C communication handling. They are called only when a transmission or receiving event appears.

5.3.3 PC control software

Special graphical user interface (GUI) was designed for simple and user-friendly control of the bearing electrical power part. It was written in the Borland C++ Builder platform (v10.0) and it is based on the UART communication with the DSP controller by the defined protocol (file *HMB_ComProtocol.h*).

5.3.3.1 Windows description

The control and status registers and variables are placed on the main window as well as setting boxes and command buttons. The main window in the offline state is shown in Fig. 40.

Most of the windows are used for displaying measured and calculated values, actual system identification and status or online/offline signalization.

The setting and control box is the place where the required position values and period of the injected error signal for stability measurement could be changed as well as command buttons for setting the values, starting and stopping and for stability measurement triggering.

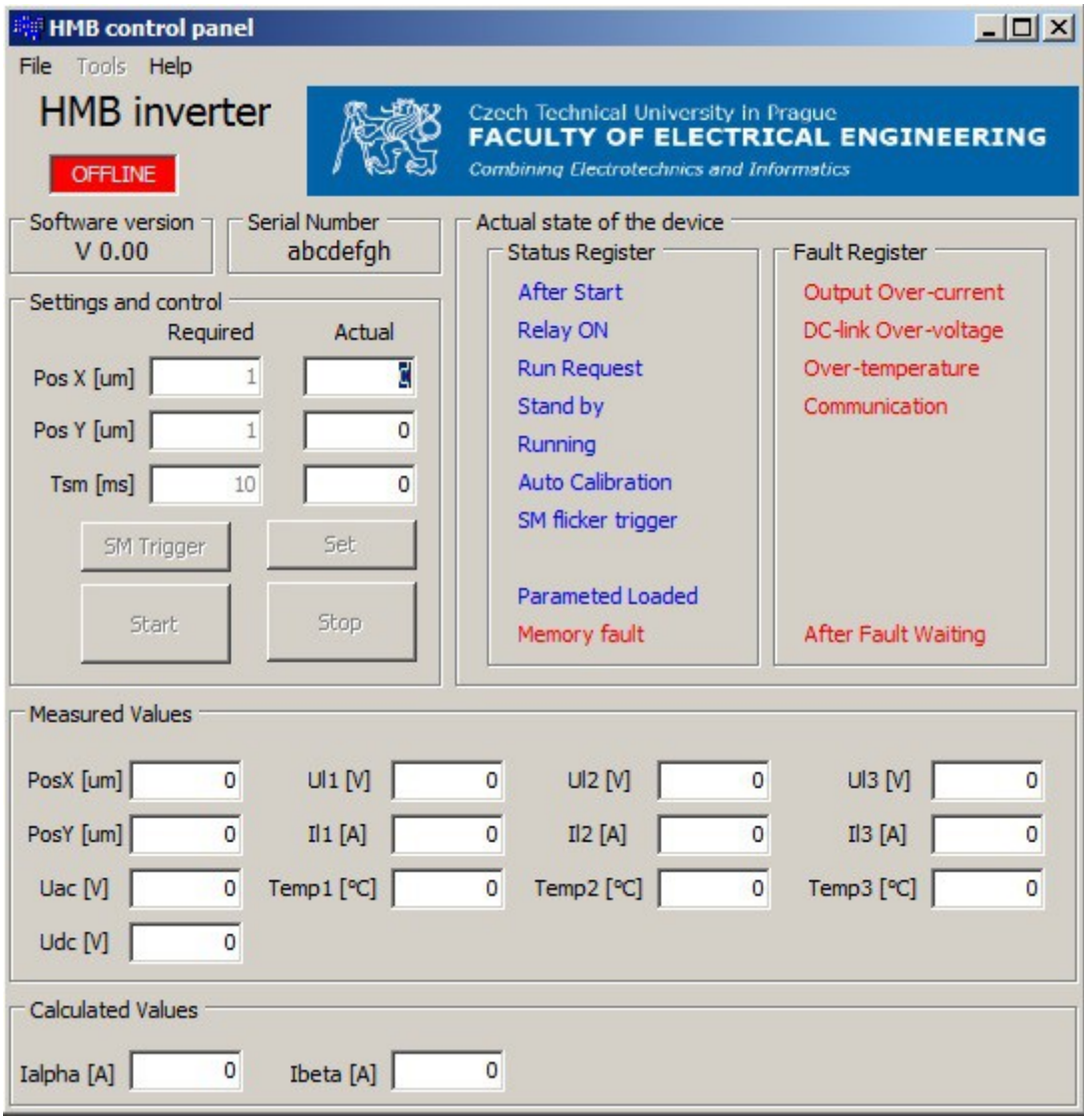

Fig. 40: GUI - Main window

The default required position values should be constant for each device and there is normally no need to change them. Therefore they are saved in the data memory on the control board and loaded after each DSP controller booting. Setting them by the GUI is possible, but it is locked as default. Unlocking or locking the setting box is provided by a command in *Tools*.

After the stability measurement function ended, if triggered, the result could be loaded from the controller by *Tools – Load measurement tables*. This command downloads the stability measurement results and saves it into text file in GUI directory. This operation could take some time, depending on the series connection.

Menu Tools also offer commands for saving and clearing the EEPROM parameters and restart of the controller.

Choosing the UART communication port is possible in the Setting window, linked in the main menu *File – Setting*. The window is shown in Fig. 41.

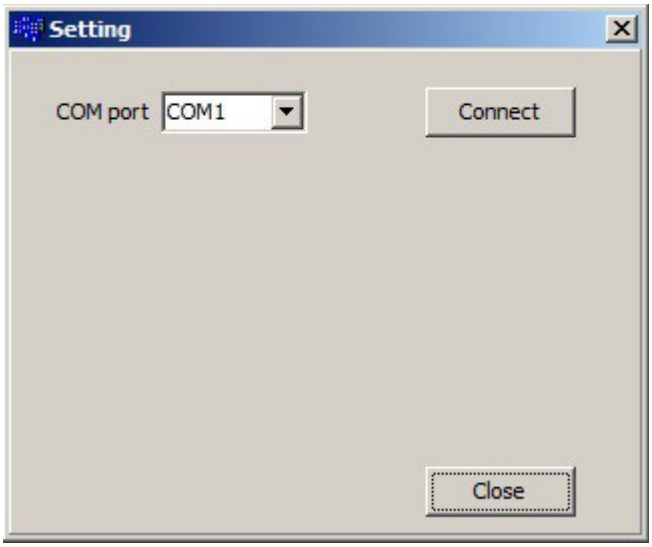

Fig. 41: GUI - Setting window

The series number of the device is used for a simple identification and it could be changed in *Tools – Serial number*. The window is shown in Fig. 42.

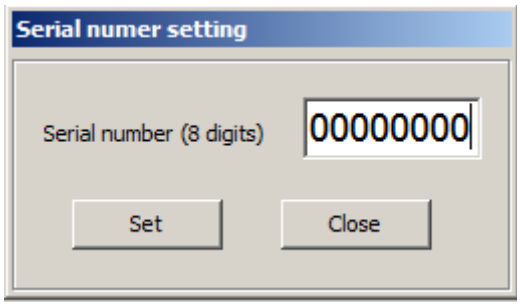

Fig. 42: GUI - Serial number setting

5.3.3.2 Code description

The GUI software project is saved as the HMB_control and it consists of 4 file groups. Each file group defines one window as a combination of the C++ code file, design specification and heather file. The list of the used windows is following:

HMB_control_mainWindow.cpp – It defines the main window of the user interface with the control and displaying part, provides communication and control by the system timer, setting variables, saving data files and it also contains global variables.
HMB_control_aboutWindow.cpp – About window is used for software information and university presentation.
HMB_control_settingWindow.cpp – UART com-port is defined here.
HMB_control_serialWindow.cpp – Series number could be changed in this window.

The doxygen commentary style is used for the code documentation additionally to the inline comments.

5.4 Circuit and PCB design

The circuit and printed circuit board (PCB) was drawn in the CadSoft EAGLE PCB design software. Output of the software are data in the Gerber file format.

The design procedure starts by drawing circuit concept and after it packages of all parts have to be defined. The diagram should be checked and over-viewed before the layout drawing starts. Complete diagram is enclosed in Appendix A. Due to the requirement of a small dimension 4-layers

35 μm board type was chosen. The final boards dimensions are 120 x 122 mm. The placing diagrams you can see in Appendix B.

5.5 Putting electrical part into operation

After board production by a PCB manufacturer and purchasing parts, the assembling and living up could start.

The proper way of putting electrical part into operation:

1. assemble SMD passive components
2. assemble parts of auxiliary power supply
3. put auxiliary power supply into operation and test it
4. assemble active SMD components including DSP and measurement parts
5. put DSP and measurements into operation and test it
6. assemble the rest of components excluding the DC-link capacitor
7. put the bridge into operation and test it with the output filter using external power supply
8. assemble the DC-link capacitor
9. test the input rectifier and charging limiter (PTC)
10. let the whole device work, check temperatures, adjust gate resistors or other components to find good performance
11. connect passive resistors to the output
12. load the debugging software version for searching PI parameters of current controller
13. tune the current controller
14. implement the current parameters into the software

Final resistance and capacitance values of unspecified components were found after living up sequence as well as some hidden mistakes on the board. The board was manufactured well, mistakes came out of design.

It is a destiny of first versions to contain most of errors and mistakes which are solved on the next development samples. They are mostly caused by wrong circuit connections and by incorrect, forgotten or unfinished layout connections. A lot of those mistakes are found and fixed during the approval procedure, but it would be a miracle to design a perfect board on the first try.

One mistake type which slipped into the inverter circuit was connection around some measuring amplifiers. Another one was misplacing of the bootstrap resistors on the high gate-drivers. The final printed circuit board contains a few layout mistakes too. All of these problems were fixed by hand soldering on the board.

First error is on page 1 (Appendix A) in the AC voltage measurement circuit. The resistor R12 is incorrectly connected to input 1 of the operation amplifier IC1A instead of pin 2. Similar problem is on page 5 on the position measurement circuits IC20A and IC20B. Here the resistors R166 and R169 should be connected to pin 2 or pin 6 respectively.

Second mistake is on page 3 (Appendix A) on the reference input of the current-measuring amplifiers IC5A, IC5B and IC6A. The reference voltage value, coming out of the voltage divider, is directly connected to all three operation amplifiers. That effects amplification and makes the whole current measurement incorrect. Solution is to insert a 750 Ω resistor between each amplifier and voltage divider or to build a reference for each op-amp.

A small mistake appears also on the gate-driving part because of the bootstrap capacitors on the higher gate-drive circuit. Using higher value of the capacitance could became dangerous for the diode because of high charging current. Therefore a small resistor (2,2 Ω) between the diode and supplying voltage has to be inserted for limiting the current. In our circuit the resistors are incorrectly placed on other side between the diode and opto-coupler. Reassembling will avoid possible problems in future.

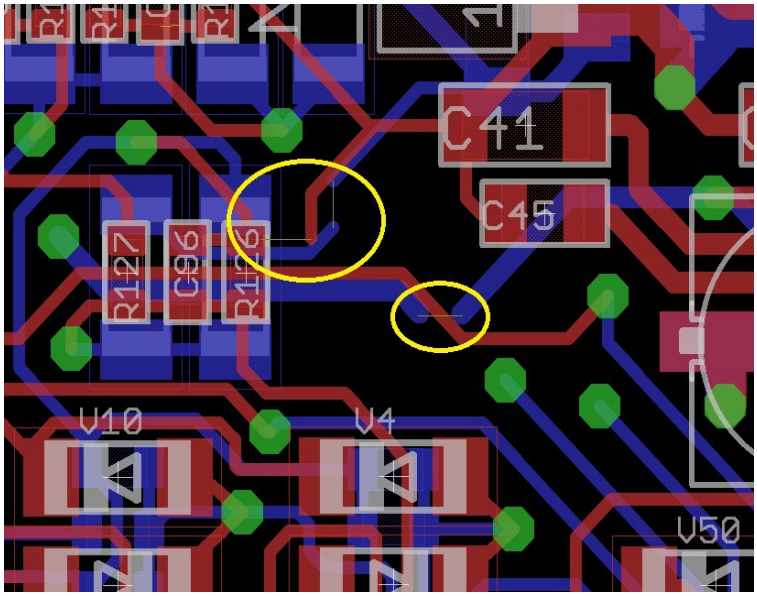

Fig. 43: Examples of layout wiring mistakes

Beside small wiring problems like forgotten or weak + 5 V connection there were more serious mistakes. At first it were forgotten + 3,3 V and GND connections around the diodes V52 and V59. Examples of those mistakes are marked by yellow circles in Fig. 43 (red lines are top wires, blues are bottom wires). Next layout issue is an incorrect gate-source driving wiring of MOSFET Q1. Part of the low gate-driver wire follows the power line. That could make driving unstable. Other transistors are connected correctly.

5.6 Running and tuning the hybrid magnetic bearing

After solving all issues on the power electric part and tuning the current PI controller, the inverter is ready to be connected to the mechanical part. The coils of active magnets were connected to three-phase power output and the position sensors to proper measurement inputs.

The proper way of start and tuning the bearing:

1. connect magnetic part and position sensors for final tests
2. check the connection between the coils and inverter and between coils themselves
3. check the position measurement – direction and polarity
4. load debugging software version for searching PID parameters of the position controller
5. tune the position controller
6. implement the position parameters into the software
7. load the final software version with correct parameters

After the tuning procedure described above is successfully finished, the bearing is ready to be tested and diagnosed. Problems, which appeared in this part of development, were connected to mechanical part. They are listed bellow.

First problem appears on the beginning of the position measurement testing. In that moment it comes up that the rotor is damaged a little. Due to probably a fall in the past manipulation at laboratory the rotor wasn't straight in the whole length. One small part was a little bent out of axis, but exactly in the point, where the position probes are sensing the air gap. So the damage was not really visible, but it made the position control impossible. The rotor had to be repaired, which extends development time of the project.

Second issue comes with the control development. The active magnetic part is split into two sections: front and back electromagnets. Both coil types are winded in three-phase configuration. According to the documentation and cable marks, corresponding axes should be connected in series

to the star as shown in Fig. 44.

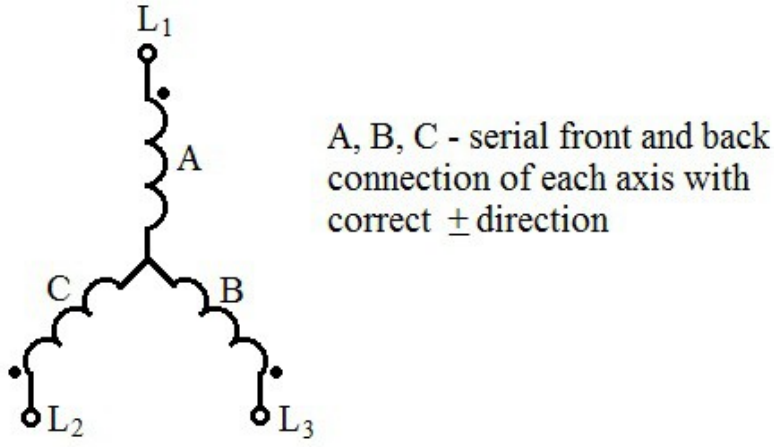

Fig. 44: The proper connection of magnetic coils

But the position control was not correct. The reason was wrong cable marking on the active magnet supplying wires. New force direction measurement explores the mistakes. The result is in Tab. 5.

Coil		Force direction		Result
Axis	Position	Expected	Measured	
A	Front	↑	↑	Correct
A	Back	↑	↑	Correct
B	Front	↓→	↑←	Opposite
B	Back	↓→	↓→	Correct
C	Front	↓←	↓←	Correct
C	Back	↓←	↑→	Opposite

Tab. 5: Force direction measurement

The force direction measurement proves that some of coil wires are marked wrong, so the power connection has to be corrected as is shown in Fig. 45. After this change, electromagnetic power excited by active part of the magnetic bearing will react to the control in right way.

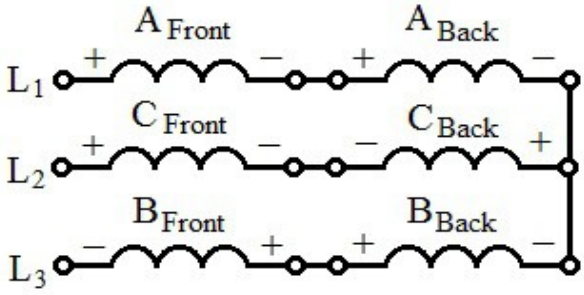

Fig. 45: Correct coil connection

6 Measurement and diagnostic

The international standard ISO14839 is intended for active magnetic bearings, but it will be used for diagnostic of our system too. The reason is to prove that final functionality of both types (hybrid and active bearings) is the same. This is one the object of this doctoral thesis.

6.1 Evaluation of vibration result

Digital oscilloscope was used for the vibration measurement. In case of our project, the position sensors are already assembled for control purposes and they can be used as displacement transducers too.

The rotor was centered to the correct position during the operation, therefore the eccentricity is almost zero and we can omit the DC part of the measurement. The orbit diagrams and vibration history display only the mechanical vibration.

According to the proximity sensors (Allen-Bradley 871C) described in datasheet, they provide distance voltage value resolution of 0,25 mm/V. The minimum radial clearance of the bearing is C_{min} = 250 µm [16], as mentioned in chapter 5.1.3. Final vibrations for several revolution periods (90 ms, 45 ms, 30 ms and 20 ms) are shown in Figs. 46 – 49.

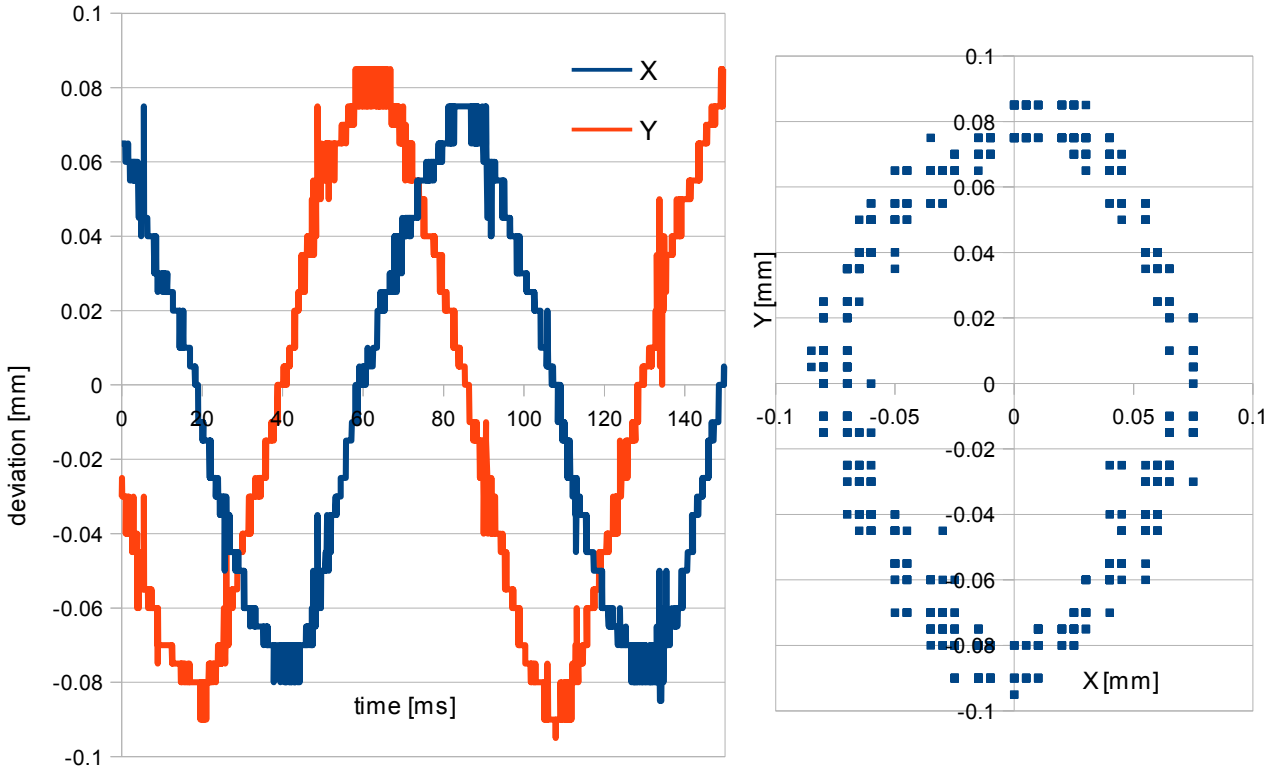

Fig. 46: Vibration history and orbit for the period 90 ms

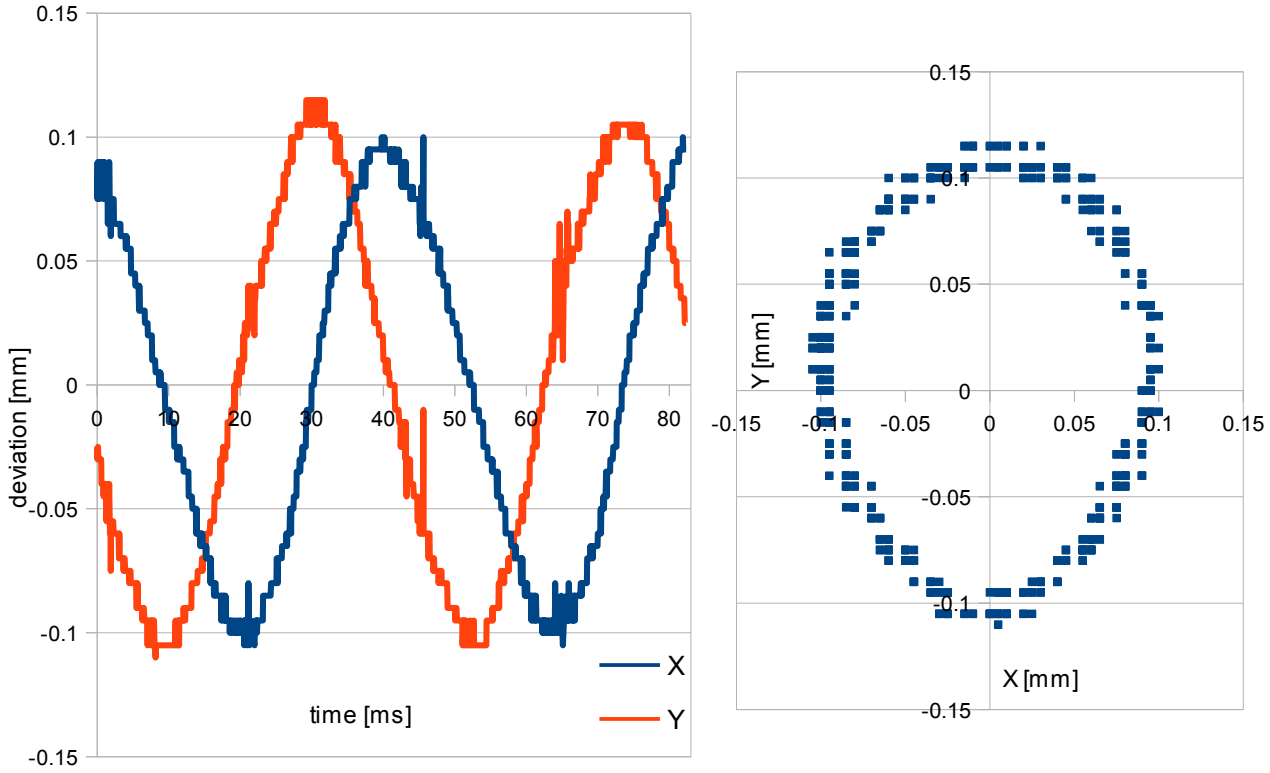

Fig. 47: Vibration history and orbit for the period 45 ms

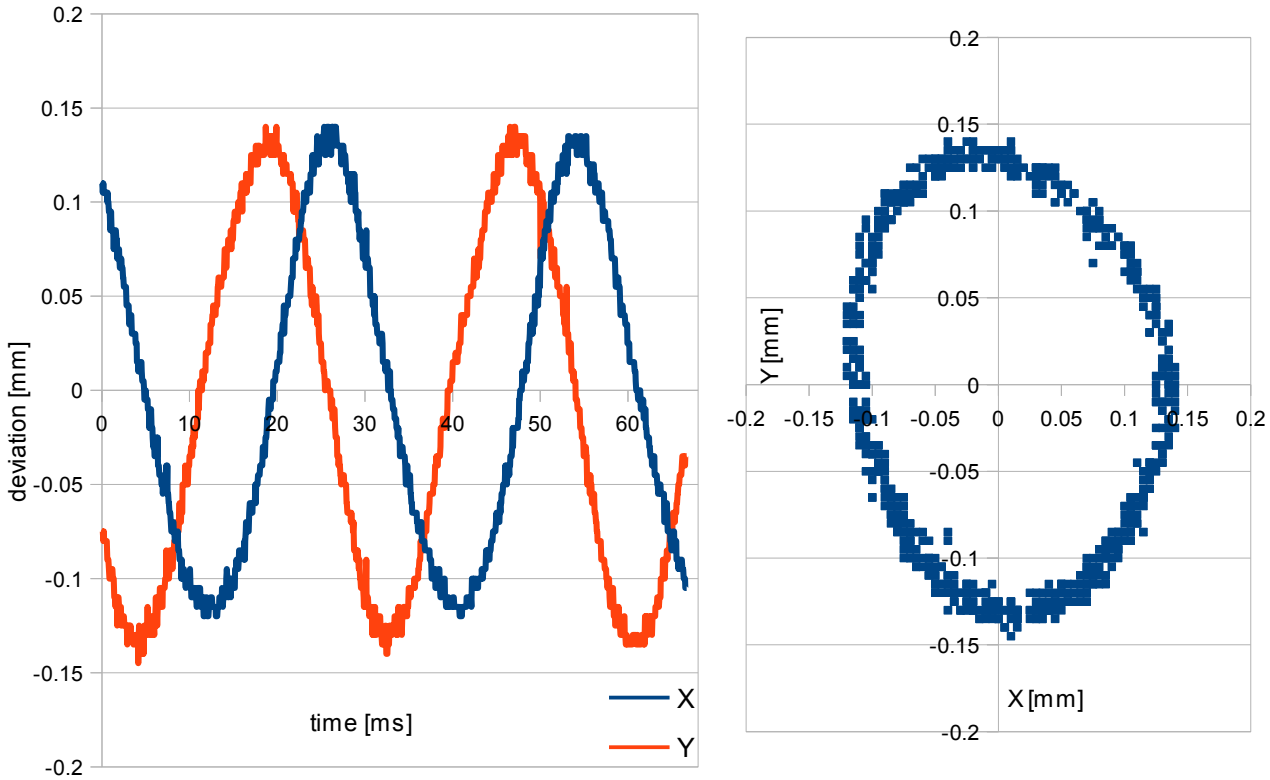

Fig. 48: Vibration history and orbit for the period 30 ms

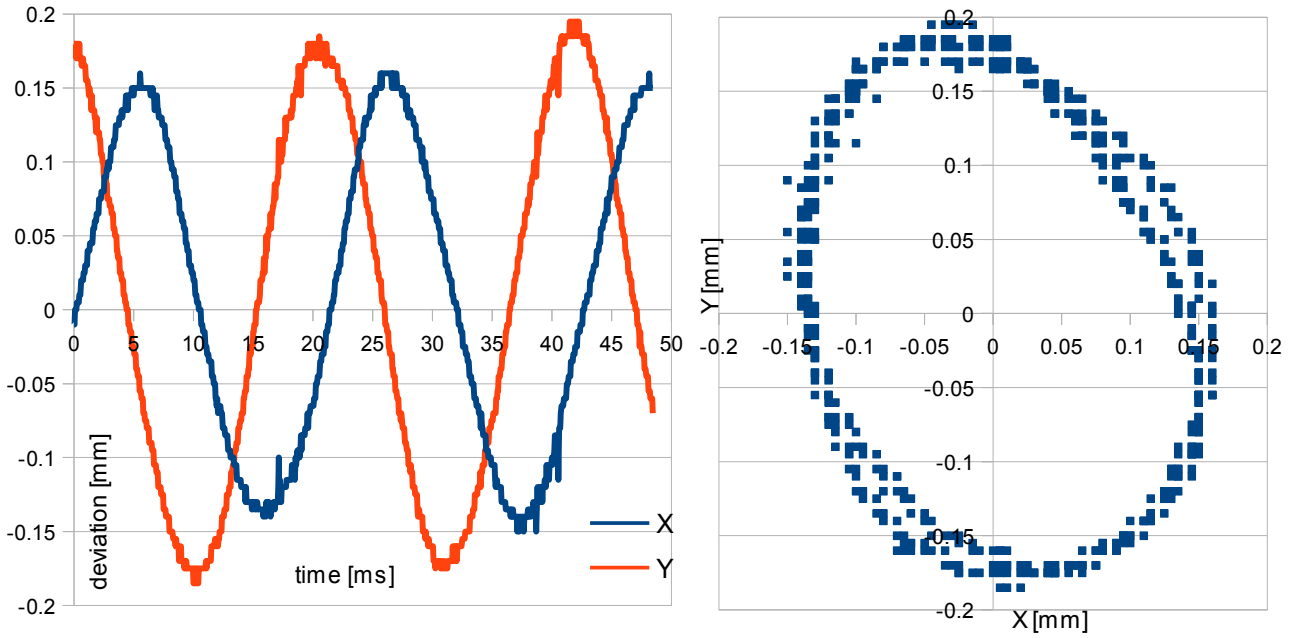

Fig. 49: Vibration history and orbit for the period 20 ms

Result of the vibration measurement in Tab. 6 shows the D_{max} / C_{min} criterion depends on rotating speed. According to the measurement, we can say that our magnetic bearing is a device in the Zone B for low rotating periods (up to 70 ms), in the Zone C for periods up to 40 ms and Zone D for higher speed. Final displacement criteria speed dependency is shown in Fig. 50.

Period [ms]	Speed [turns/min]	Dmax [um]	Dmax/Cmin [-]	Zone
90	667	95	0,38	B
45	1333	118,9	0,4756	C
30	2000	145,6	0,5824	D
20	3000	200	0,8	D

Tab. 6: Vibration measurement

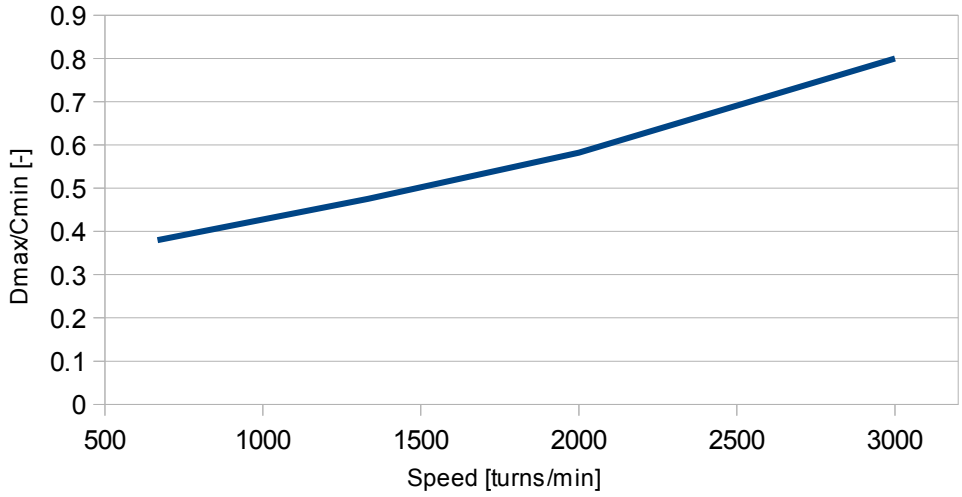

Fig. 50: Displacement speed dependency

6.2 Evaluation of stability margin result

Calculation and memory resources of the DSP controller were used for the stability measurement. The measurement procedure, described in chapter 3.2, begins with pressing the measurement trigger on the PC user interface (as mentioned in 4.3.3.1). The trigger starts injecting error signal and saving two data tables with the values V1 and V2 to the RAM in real time. The tables contain signal data for one specified frequency, so measurement has to be repeated several times to get enough values for the transfer function.

The open and closed loop frequency and phase transfer functions as well as the sensitive function are in Figs. 51 – 54. There are two functions of each graph, because of the 2-axes control. The dimensions of the frequency functions are decibels (dB), respectively degrees of the phase functions.

The stability margin is evaluated from the sensitivity frequency transfer function (Fig. 55). The graph proves, that the used magnetic bearing fulfils the category A for the most of the measured ranges. Just a part around the frequency 100 Hz exceeds the level of the zone B according to the evaluation criteria.

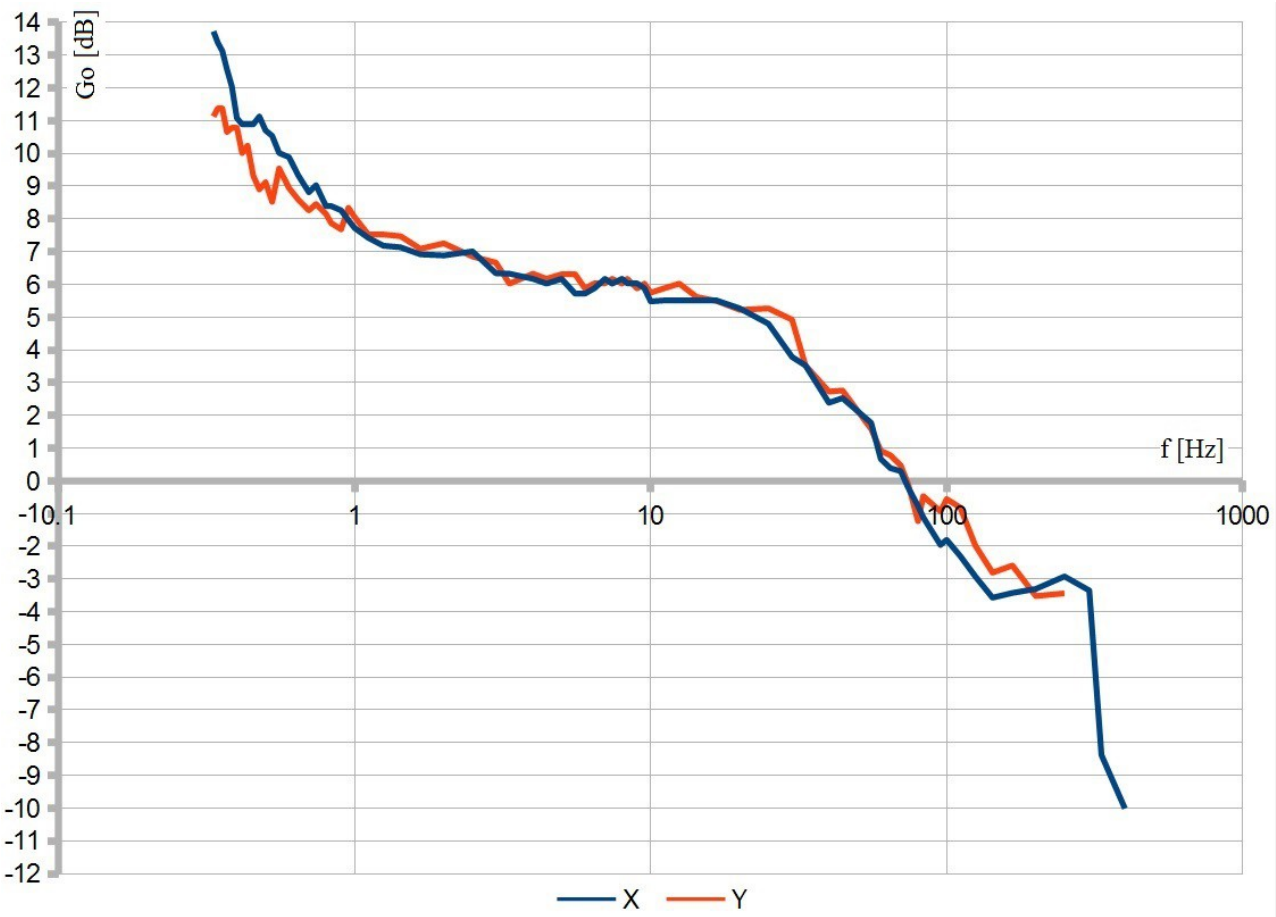

Fig. 51: Open loop frequency transfer function, G_O

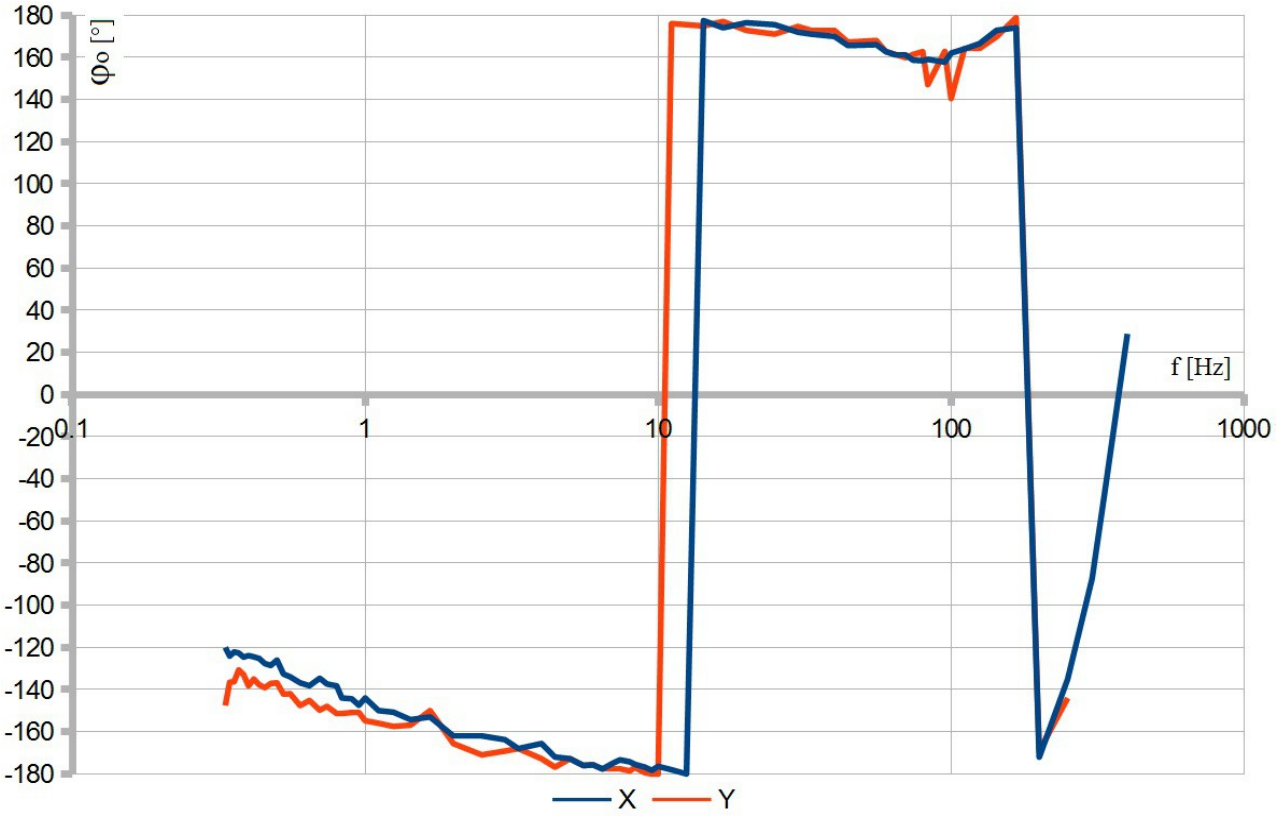

Fig. 52: Open loop phase transfer function, G_O

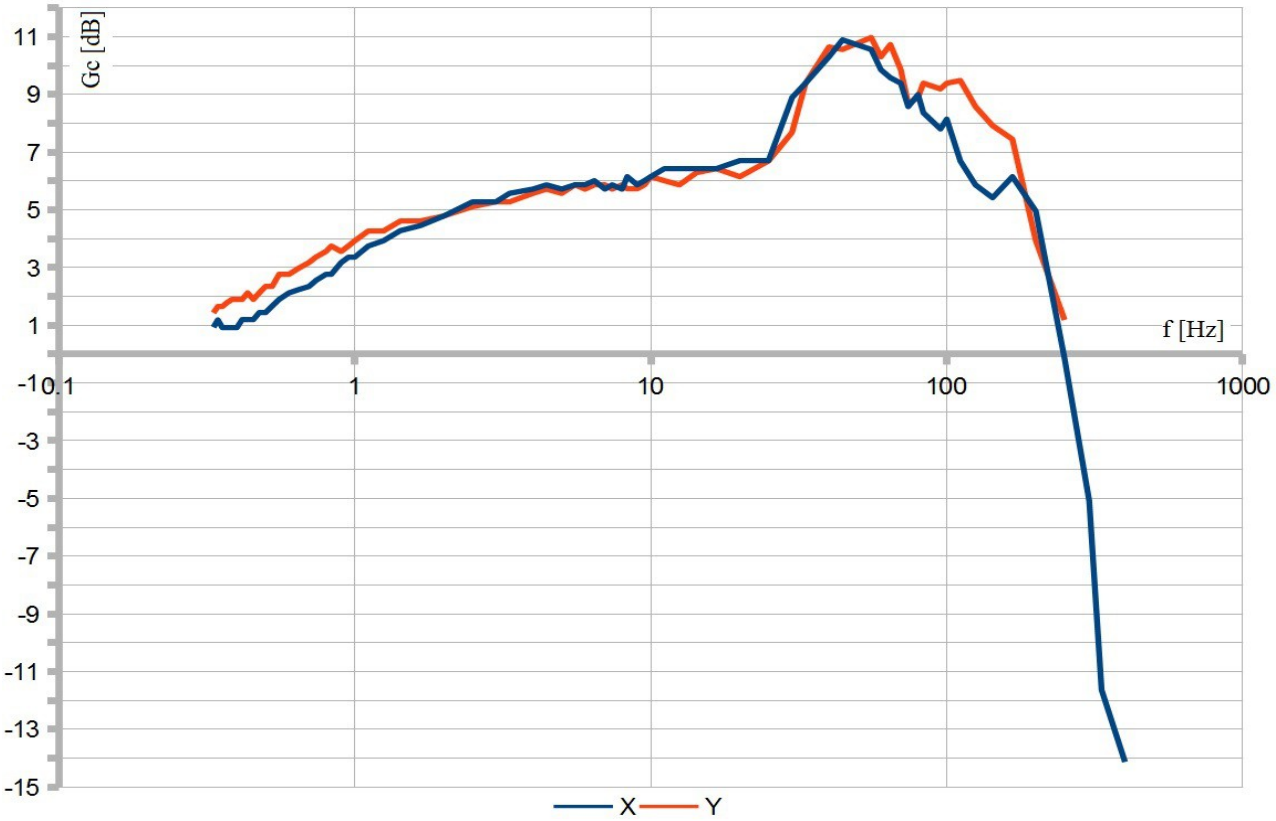

Fig. 53: Closed loop frequency transfer function, G_C

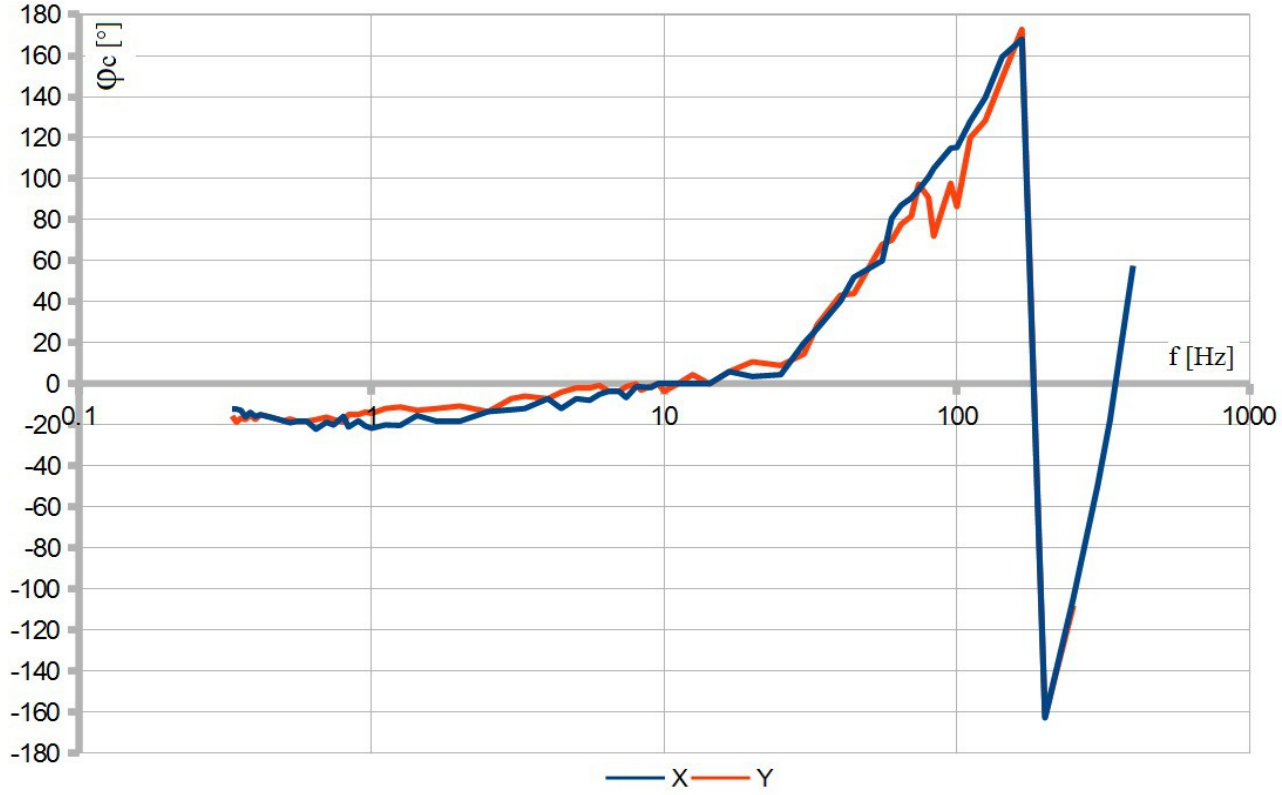

Fig. 54: Closed loop phase transfer function, G_C

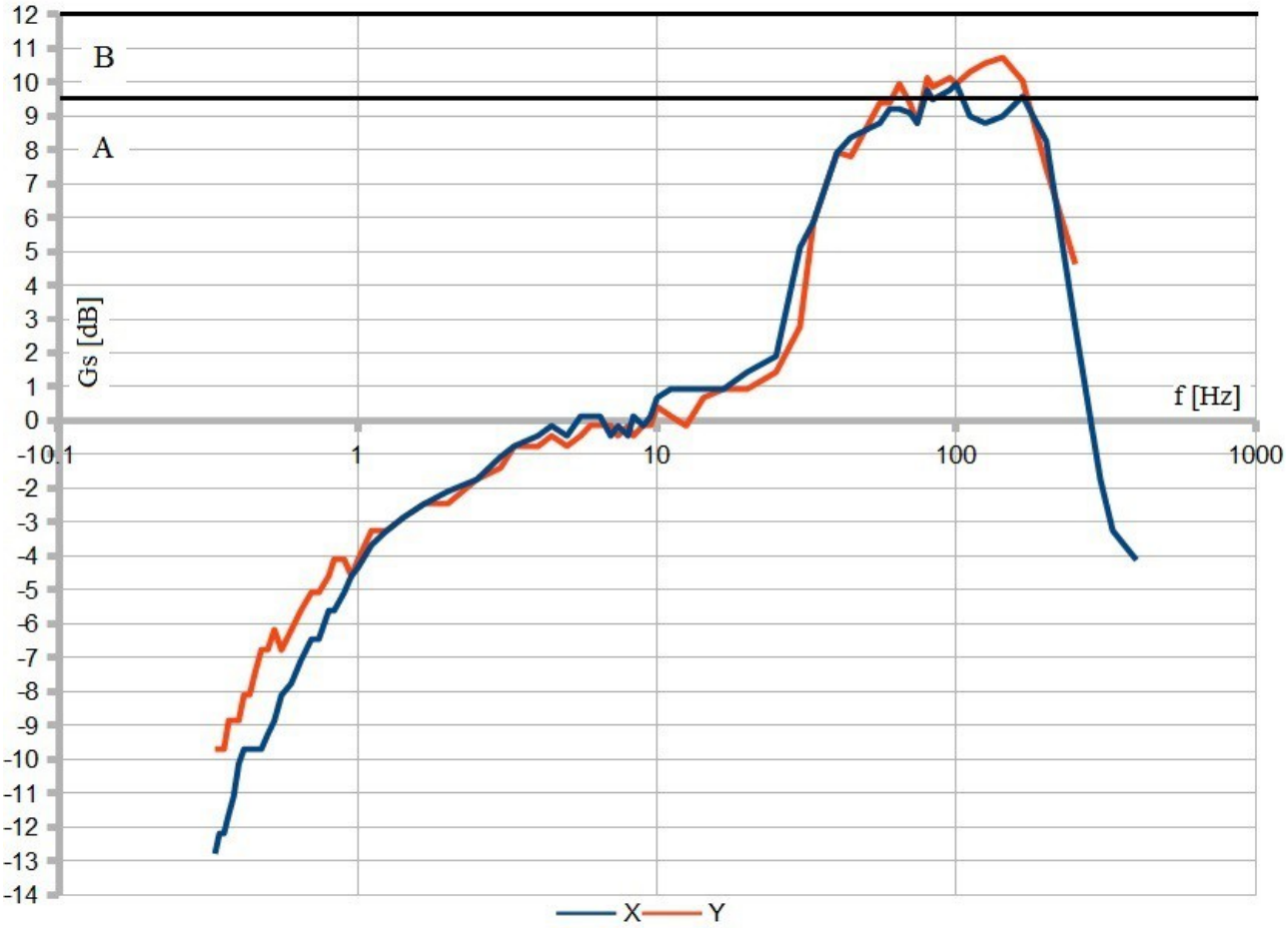

Fig. 55: Sensitivity frequency transfer function, G_S

7 Conclusion

The aim of this doctoral thesis was to analyse capability of the permanent-magnet-based active magnetic bearing with the three-phase rotor. The theoretical background was explained, new magnetic part design method was described and the real magnetic bearing was diagnosed.

For diagnostic purposes I had to design and build power electronic and control parts of a hybrid magnetic bearing, assemble it together with the existing mechanical and magnetic parts, design and optimize its control software, run the complete bearing and measure its features.

All these points, defined in chapter 2, were fulfilled and its detailed summary follows in the next chapter 7.1. The results for science or practical use improvement are following in chapter 7.2.

7.1 Results of the doctoral thesis

7.1.1 Theoretical analysis of our hybrid magnetic bearing

The basic description of magnetic bearings in chapter 1 shows the main differences between active and hybrid type. Active bearings are actually used in many specific application, but hybrid ones still represents just a tiny part of the market.

The theory described in chapter 3.1 shows that our hybrid bearings bring big advantages with low power consumption and construction is not much more complicated, because it is similar to three-phase motor.

The real PM active magnetic bearing in the CTU - FEE laboratory was designed in 2001 intuitively because at that time no professional design method was known. Therefore the theoretical analysis of conventional homo-polar active magnetic bearing was performed in the chapter 3.1.1. The theoretical analysis of a substitution of bias current MMF by MMF of permanent magnet was performed in chapter 3.1.3. and 3.1.4. The new theoretically justified design method was proposed on the base of these analyses and it was used for determination of new sizes in the chapter 5.1. Results of the some sizes comparison from the intuitive design method and from the new justified one is given in the chapter 5.1.2.

The chapter 3.2, defining power electronic requirements, shows the advantage in using common components and well-known three-phase circuit technology. The result of theoretical analysis proves that the hybrid magnetic bearing with three-phase stator should be more cost effective and space effective than the conventional active magnetic bearing for similar application.

For functional analysis it is necessary to build a real hybrid magnetic bearing system and to make the measurement and diagnostic according to the standard. The result of the realization process is written in the following chapters.

7.1.2 New power electronic development

The complex and small power electronic part was designed on the base of specification in chapter 3.2. The new power part uses components with attention to small dimensions, high efficiency and low cost. Fast and powerful MOSFET transistors were used for the output power bridge. The process of designing is described in chapter 5.4. The power part of the circuit, shown in Appendix A, could be considered as the final output of this point.

Development of my doctoral thesis started in 2010, but one of its main steps was delayed mainly because of trouble with the mechanical part, mentioned on the beginning of chapter 5.6. Therefore some components, chosen for the first sample 7 years ago, it could look a little old and slow now. But they are still much faster and younger than the parts in the previous inverters and replacing them by modern devices is not a problem in a real industrial development.

7.1.3 New control electronic development

The new control part was implemented to the same PCB as the power part. Chapter 3.3 contains description of the control system requirements and specification. The DSP controller TMS320F2801 has been chosen for the control. This chip runs at 100 MHz and provides a number of the industrial peripherals (including PWM generator, AD converter and series communication modules).

We can say that all low voltage circuits in diagram in Appendix A belong to the control system. The control part development is described in chapter 5.3.1.

7.1.4 Construction of the hardware

The final printed circuit board was manufactured and assembled with the electronic parts and tested of the basic functionality (as connections, communication, measurement, bridge control, current control or protections). The layout is shown in Appendix B. All power and control parts, required for magnetic bearing operation, are integrated on one board. Actually it is no need to use any laboratory equipment any more, but for safety reasons a separation transformer should be used as a power source, because the windings in magnetic part of the bearing may have low insulation capability.

Putting into operation is described in chapter 5.5. All problems and mistakes on the board were found and fixed. The whole electrical part has proven its functionality and it is ready to be connected to the magnetic part.

7.1.5 Running and tuning of the system

The control system development started after assembling the electrical part together with the magnetic part in the CTU laboratory. The development of the current transformation chain and tuning PID controller spent the biggest effort, because the control has to be stable in wide speed range. Especially the control current transformation from 2-axes to 3-axes system represents an improvement dedicated to the three-phase stator bearing concept. The development process is described in chapter 5.6.

Final control procedures were simplified for comfort use in future projects. The design and construction phase of the project ended by establishing communication with the graphical user interface. Final design including documentation of the micro-controller and PC software is described in chapter 5.3.2 and 5.3.3.

7.1.6 Diagnostic of magnetic bearing according to actual standard

The system measurement and diagnostic, described in chapter 6, evaluated functional features of our magnetic bearing. The measurement found a problem in a field of vibrations, but stability margin is satisfying.

The vibration diagnostic showed high maximum displacement of the rotor at higher revolution speed. According to the vibration criteria we can consider the device as the category D for the highest rotating frequency. The reason for this bad result could be for example a low difference between the DC-link and output voltage or mistakes in construction of the magnetic part. The magnetic part should be redesigned according to the new design method, which was also explored by this doctoral thesis (as mentioned in chapter 7.1.1). Then the vibration issue can be solved in a detailed research after redesign of the magnetic part.

The result of the stability measurement classified the bearing to the category B – devices able long term operation in the whole tested range. In some limited speed range it could even be classified to category A. The diagnostic procedure as well as experimental results are shown in chapter 6 too.

7.1.7 Evaluation of hybrid magnetic bearing features

PM active magnetic bearings are not present in actual market and also a research projects are not focussed to practical use so far. But as it is show in chapter 6, vibration and stability diagnostic proves that hybrid magnetic bearings could be used in the same application as active bearings, because hybrid bearing is able to fulfil the requirements for active types.

Therefore, since the magnetic part construction is not much more complicated and electric part would be even simpler (as mentioned in 7.1.1), than an opportunity to substitute active magnetic bearings in applications, where hybrid types can use their advantages, is taking place.

7.2 The improvements for science or practical application

This doctoral thesis proved theoretical bases of the PM active magnetic bearing and showed the way how the practical application can be designed. That means, the thesis provides detailed knowledge about one of undescribed, but potentially perspective, magnetic bearing types.

The main practical innovation of the actually used device is represented by control system, which was not used in previous projects. It is able to control the radial rotor position by three phase magnetic field, using current transformation functions. The control system is capable to drive hybrid magnetic bearing with similar features as the active type and with similar resources. Reserves in actual functionality were listed out above and it was described how they could be improved in a further development.

The next step in development should be redesign of the magnetic part, because some of important features, like magnetic forces or insulation distances, were not considered enough in the last design from 2001 and knowledge and experiences in magnetic and mechanical construction are much better now. This doctoral thesis also provides the new magnetic part design method, mentioned in 7.1.1, which should be used for the redesign. The new design method is the important theoretical innovation.

This doctoral thesis presents practical know-how for next research at CTU in future as well as for a possible cooperation with industrial partners. The hybrid magnetic bearing, used by this doctoral thesis, is a good base for future university studies in the field of magnetic bearings. Documentation of the hardware and software allows any other developer to start quickly working on the bearing.

References

[1] T. KUPKA: "*Vibrace točivých strojů s magnetickými ložisky"*; In: Elektro – Magazine of Electrical Engineering, 05/2017

[2] SYNCHRONY MAGNETIC BEARINGS: *www.synchrony.com*

[3] WAUKESHA BEARINGS: *www.waukbearing.com*

[4] CALNETIX TECHNOLOGIES: *www.calnetix.com*

[5] LEVITRONIX: *www.levitronix.com*

[6] MECOS: *www.mecos.com*

[7] International standard: *ISO 14839, Mechanical vibration – Vibration of rotating machinery equipped with active magnetic bearings*; 2012

[8] E. MASLEN and G. SCHWEITZER: *Magnetic Bearing, Theory, Design and Application to Rotating Machinery*; Springer 2009; ISBN 978-3-642-00496-4

[9] J. PAVELKA, K. BUHR: "*Návrh kombinovaného radiálního ložiska"*; CTU in Prague, FEE; 2001

[10] A. CHIBA, T. FUKAO, O. ICHIKAWA, M. OSHIMA, M. TAKEMOTO, D. DORELL: *Magnetic Bearings and Bearingless Drives*; Elsevier 2005; ISBN 0 7506 5727 8

[11] J. SYNEK: "*Vývojové trendy v řízení magnetických ložisek"*; CTU in Prague, FEE; 2004

[12] P. KOMÁREK: "*Vysokootáčkový bezložiskový motor"*; CTU in Prague, FEE; 2004

[13] J. JÁRA: "*Identifikace magnetického ložiska"*; CTU in Prague, FEE; 1997

[14] L. SYNEK: "*Aktivní magnetické ložisko"*; CTU in Prague, FEE; 2010

[15] T. KUPKA, J.PAVELKA: *Realization of Hybrid Magnetic Bearing*; EPE-PEMC 2012 ECCE Europe; 2012

[16] J. VITNER, J. PAVELKA: "*Činnost na kombinovaném magnetickém ložisku v roce 2004"*; CTU in Prague, FEE; 2004

[17] Texas Instruments: *TMS320F28xx fixed-point series*

[18] Allen-Bradley: *Inductive Proximity Sensors 871C*

Appendix A: Diagrams of Inverter board

1st page – input filter, power electronic part and voltage measurement
2nd page – internal power supply
3rd page – output filter, current and voltage measurement
4th page – bridge gate-drivers
5th page – DSP supply circuits
6th page – DSP digital connection and communication
7th page – DSP analog connection and EEPROM

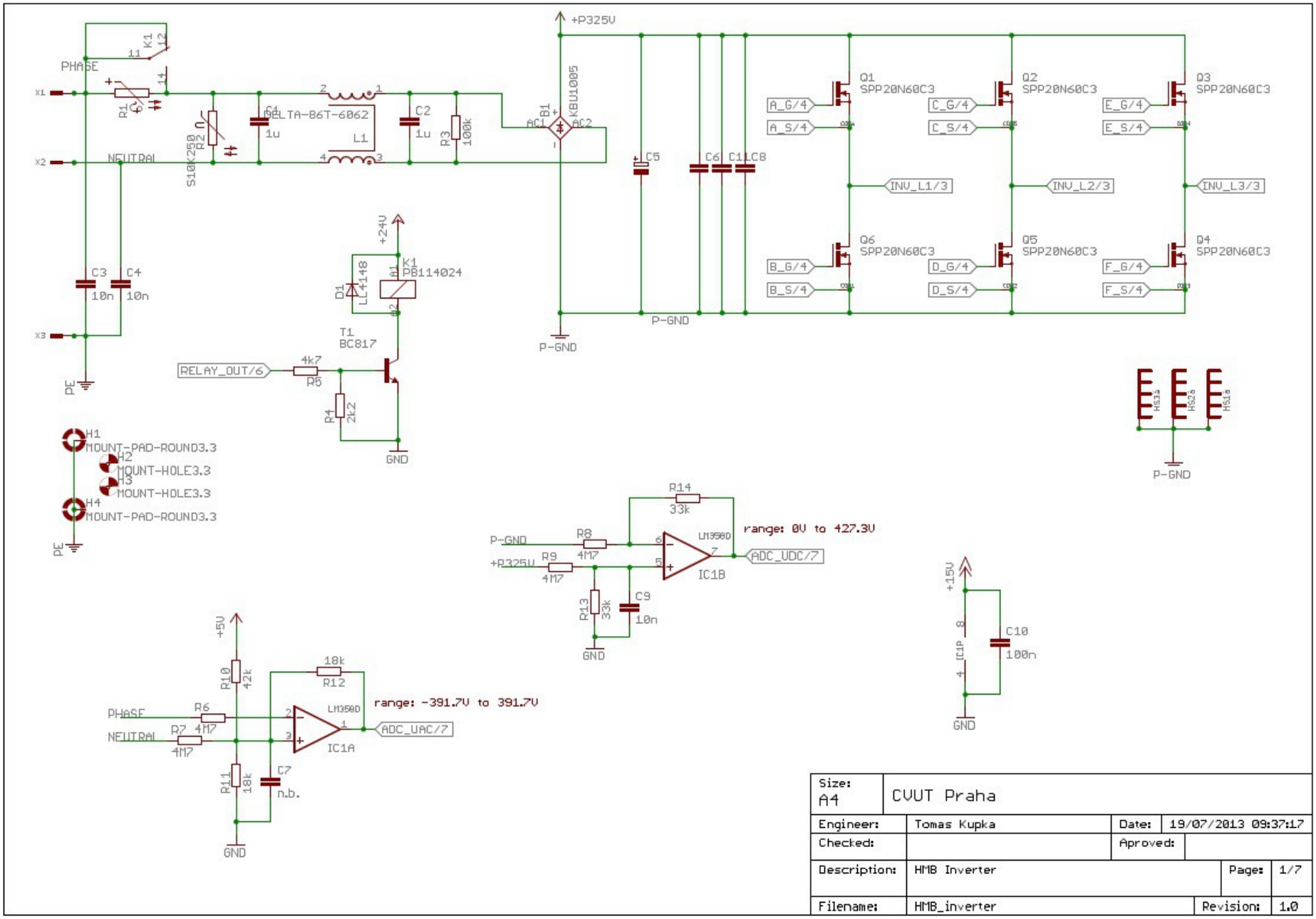

Size: A4	CVUT Praha		
Engineer:	Tomas Kupka	Date:	19/07/2013 09:37:17
Checked:		Aproved:	
Description:	HMB Inverter	Page:	1/7
Filename:	HMB_inverter	Revision:	1.0

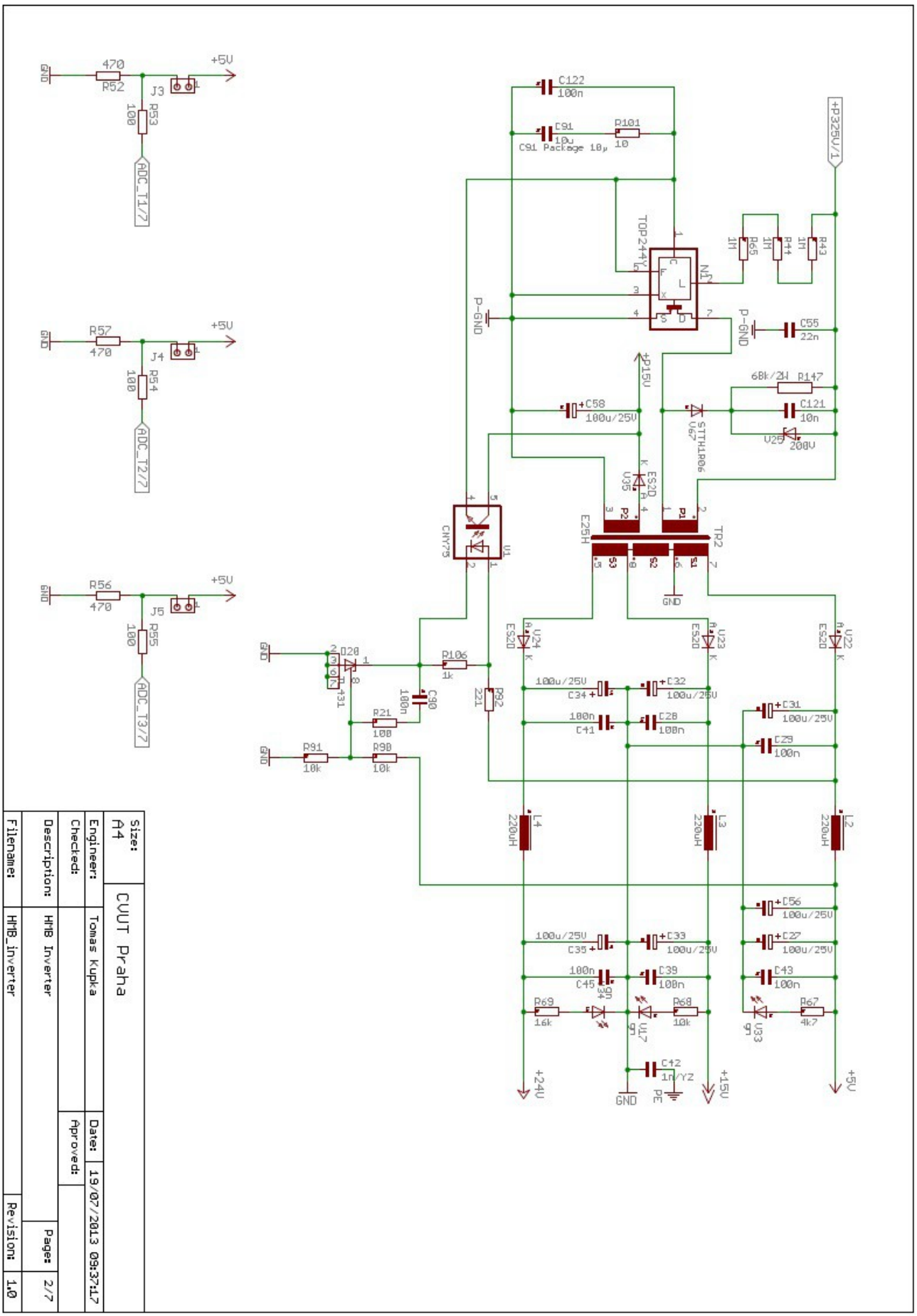

Size: A4	CVUT Praha		
Engineer: Tomas Kupka		Date:	19/07/2013 09:37:17
Checked:		Aproved:	
Description: HMB Inverter			Page: 2/7
Filename: HMB_inverter			Revision: 1.0

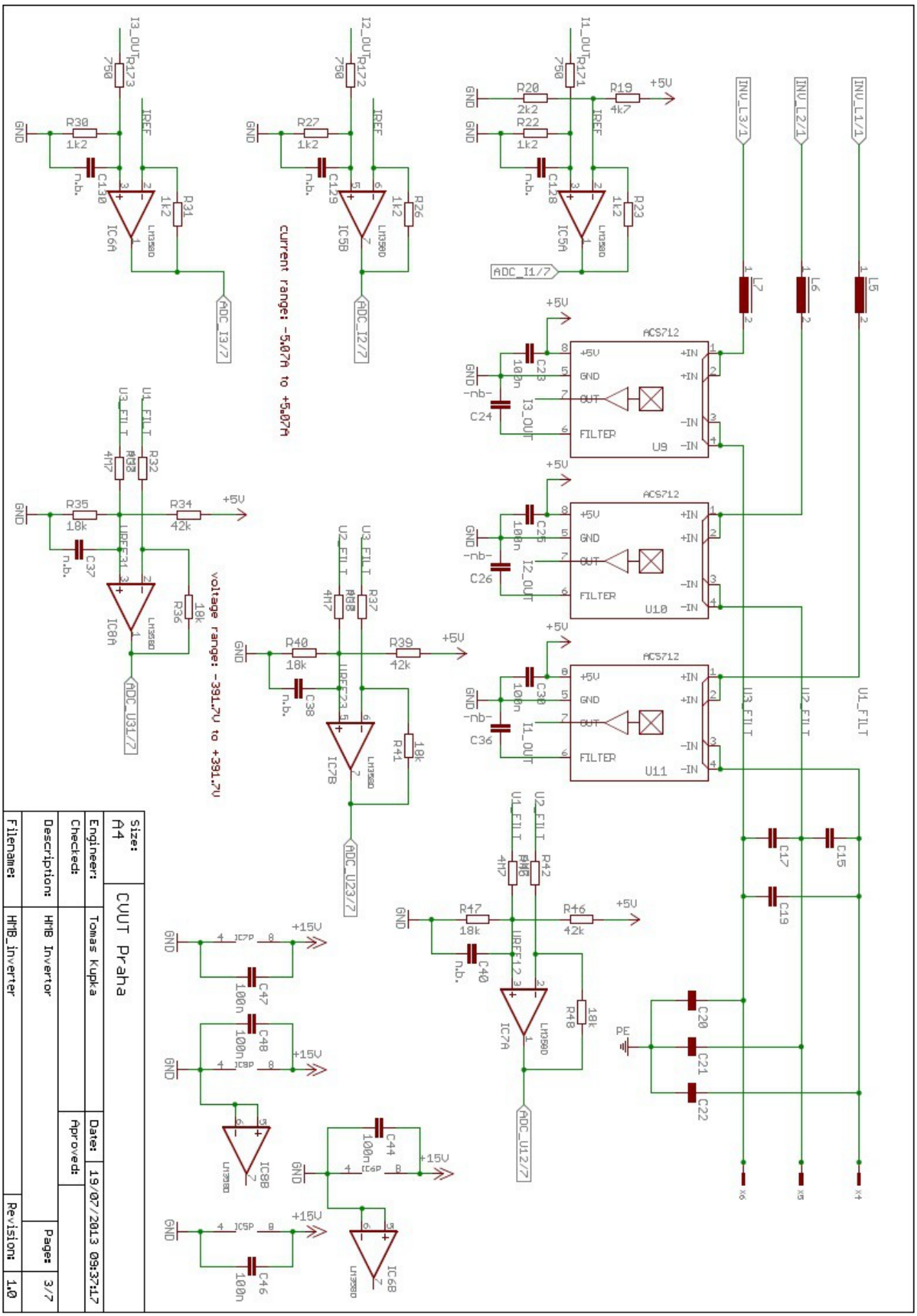
INV_L1/1
INV_L2/1
INV_L3/1
L5
L6
L7
U1_FILT
U2_FILT
U3_FILT
ACS712
U9
U10
U11
FILTER
I3_OUT
I2_OUT
I1_OUT
ADC_I1/7
ADC_I2/7
ADC_I3/7
current range: -5.07A to +5.07A
ADC_U12/7
ADC_U23/7
ADC_U31/7
voltage range: -391.7V to +391.7V
IC5A
IC5B
IC6A
IC7A
IC7B
IC8A
IC8B
IC6B
LM358D
C15
C17
C19
C20
C21
C22
PE
Size: A4
CVUT Praha
Engineer: Tomas Kupka
Checked:
Aproved:
Date: 19/07/2013 09:37:17
Description: HMB Invertor
Page: 3/7
Filename: HMB_inverter
Revision: 1.0

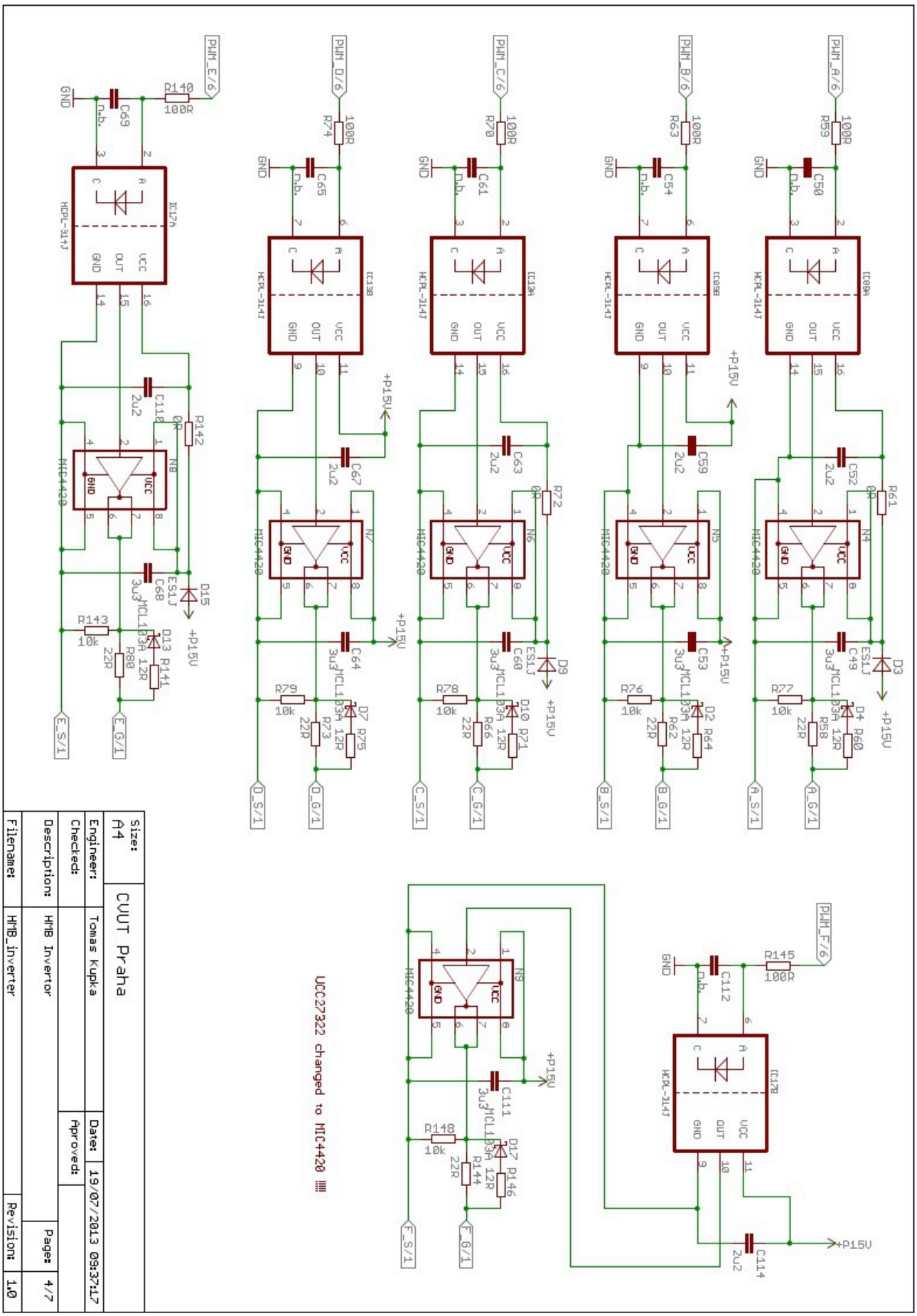
PWM_A/6
PWM_B/6
PWM_C/6
PWM_D/6
PWM_E/6
PWM_F/6
HCPL-314J
MIC4420
+P15V
GND
A_S/1
A_G/1
B_S/1
B_G/1
C_S/1
C_G/1
D_S/1
D_G/1
E_S/1
E_G/1
F_S/1
F_G/1
UCC27322 changed to MIC4420 !!!!
CVUT Praha
Size: A4
Engineer: Tomas Kupka
Checked:
Description: HMB Invertor
Filename: HMB_inverter
Date: 19/07/2013 09:37:17
Aproved:
Page: 4/7
Revision: 1.0

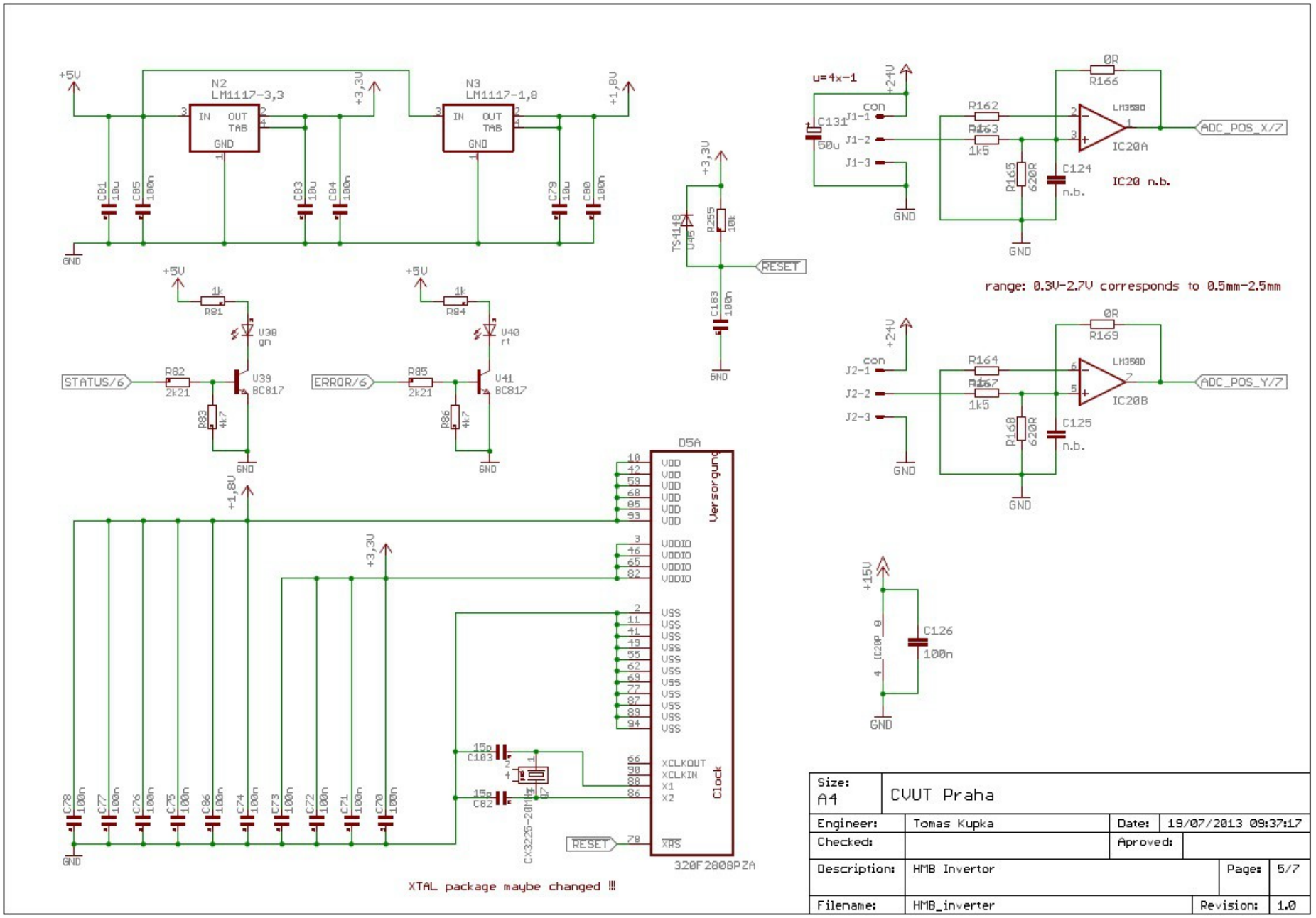

Size: A4	CVUT Praha		
Engineer:	Tomas Kupka	Date:	19/07/2013 09:37:17
Checked:		Aproved:	
Description:	HMB Invertor	Page:	5/7
Filename:	HMB_inverter	Revision:	1.0

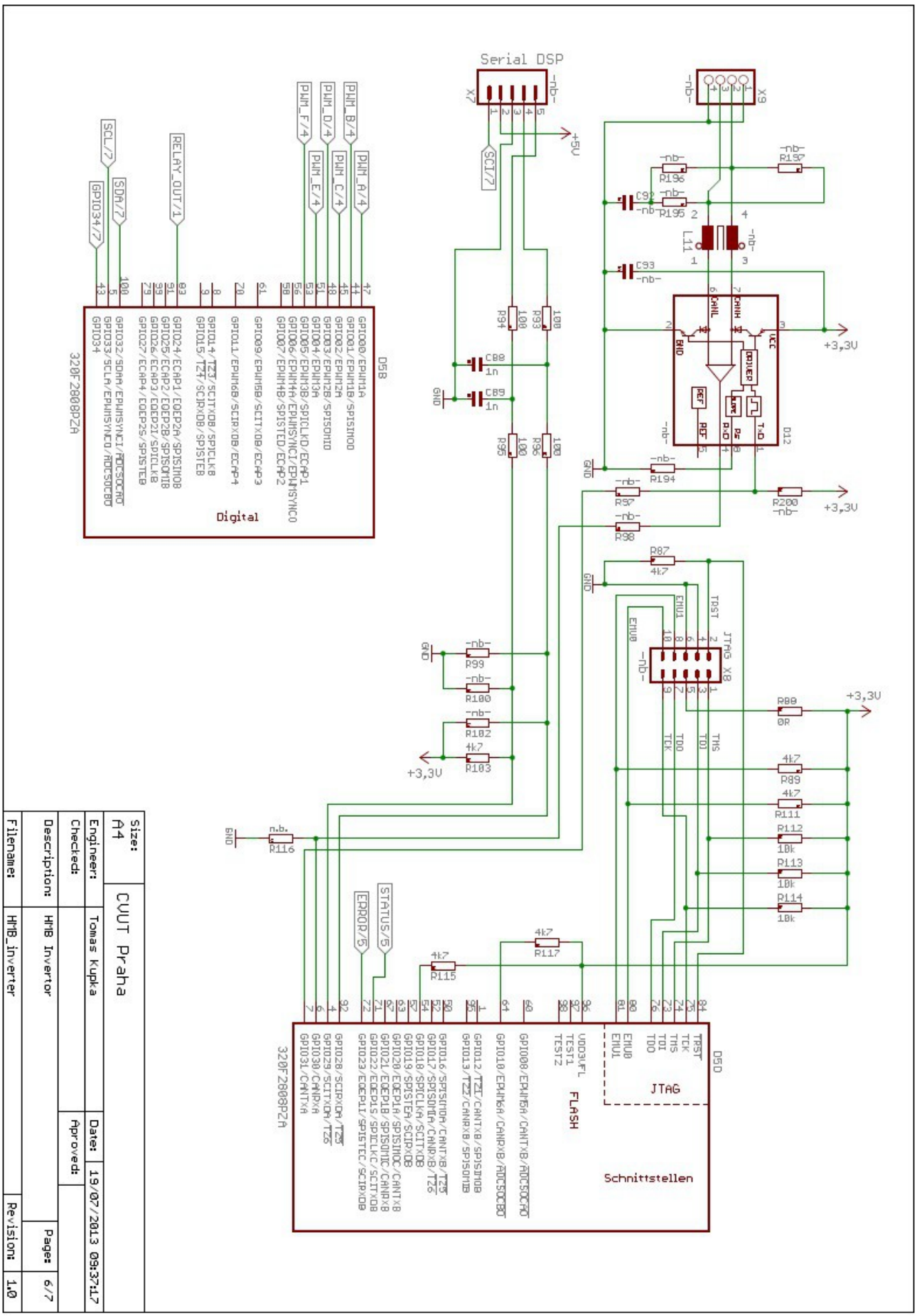

Size: A4	CVUT Praha		
Engineer:	Tomas Kupka	Date:	19/07/2013 09:37:17
Checked:		Aproved:	
Description:	HMB Invertor	Page:	6/7
Filename:	HMB_inverter	Revision:	1.0

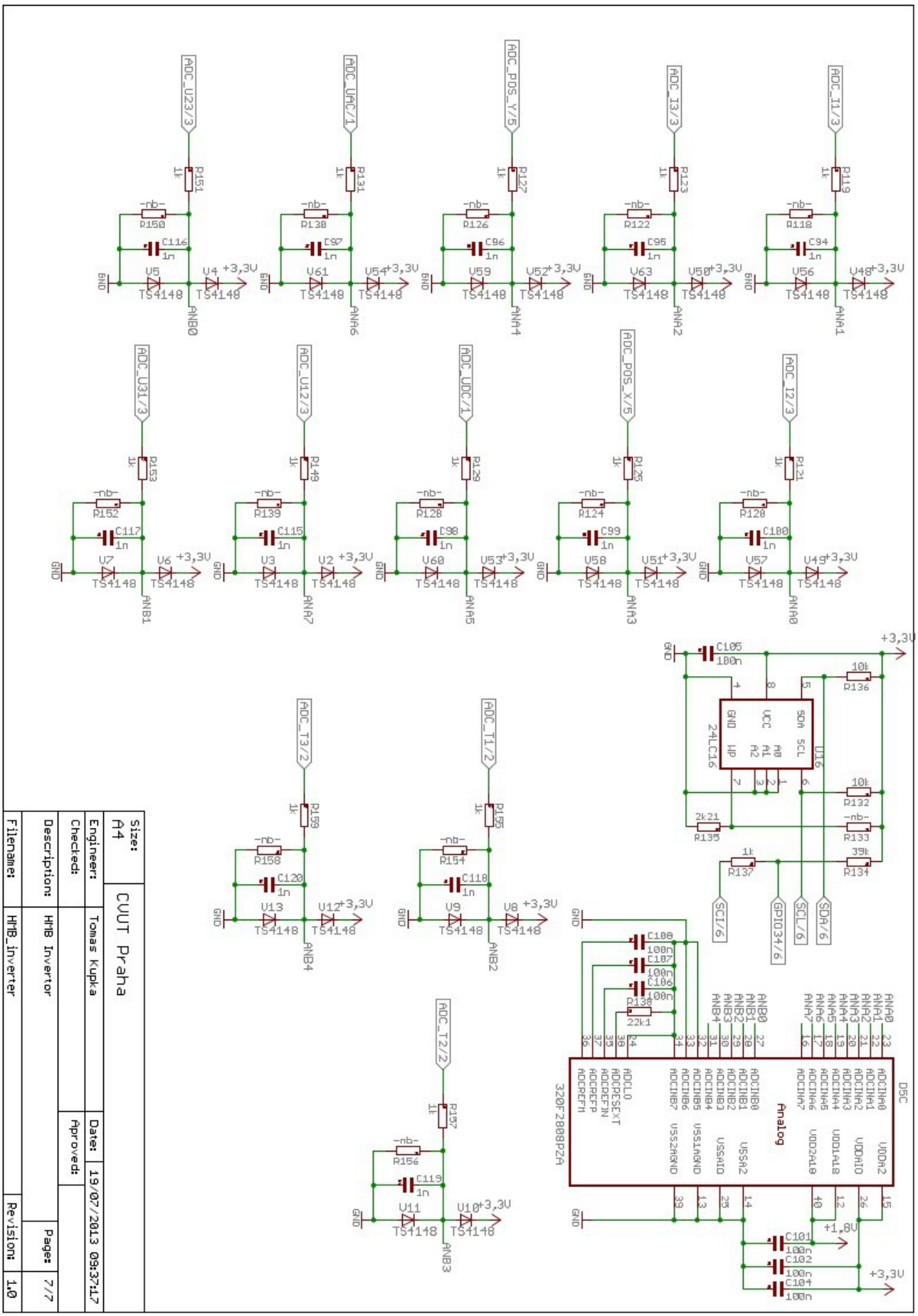
ADC_I1/3
ADC_I3/3
ADC_POS_Y/5
ADC_UAC/1
ADC_U23/3
ADC_I2/3
ADC_POS_X/5
ADC_UDC/1
ADC_U12/3
ADC_U31/3
ADC_T1/2
ADC_T3/2
ADC_T2/2
+3,3V
+1,8V
GND
SCI/6
SCL/6
SDA/6
GPIO34/6
24LC16
dsPIC33FJ128MC802
Analog
CVUT Praha
Size: A4
Engineer: Tomas Kupka
Checked:
Description: HMB Invertor
Filename: HMB_inverter
Date: 19/07/2013 09:37:17
Aproved:
Page: 7/7
Revision: 1.0

Appendix B: Layout of Inverter board

B1 – Placing diagram: Front side

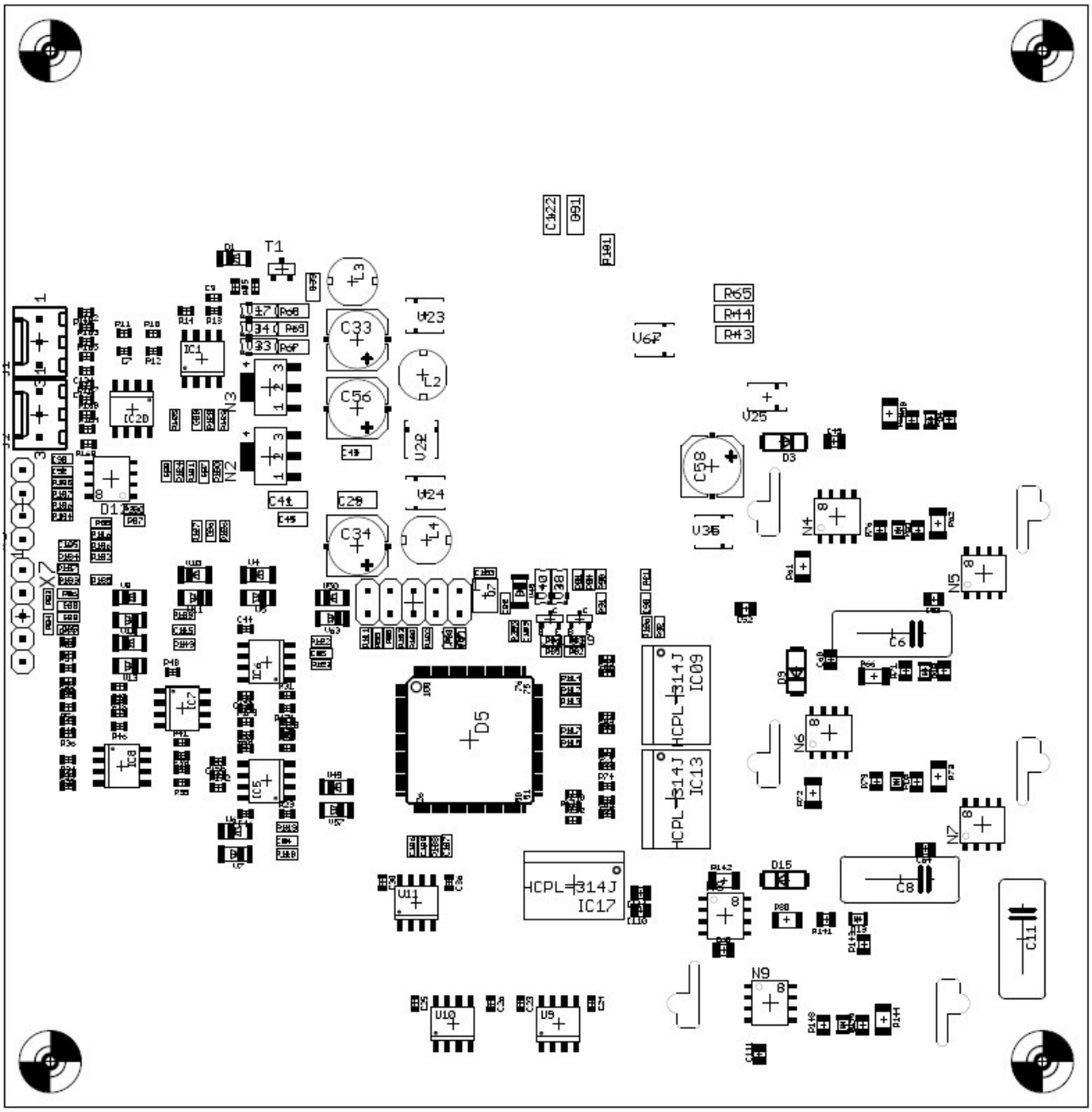

B2 – Placing diagram: Bottom side